

MARINE DEEP SEISMIC SOUNDING
OFF THE COAST OF BRITISH COLUMBIA

by

Stanislav Kníže

Eng. of Technical and Nuclear Physics
Czech Technical University, Prague, 1961

A THESIS SUBMITTED IN PARTIAL FULFILMENT OF
THE REQUIREMENTS FOR THE DEGREE OF
DOCTOR OF PHILOSOPHY

in the Department

of

Geophysics and Astronomy

We accept this thesis as conforming to the
required standard

The University of British Columbia

May, 1976

© Stanislav Kníže, 1976

In presenting this thesis in partial fulfilment of the requirements for an advanced degree at the University of British Columbia, I agree that the Library shall make it freely available for reference and Study.

I further agree that permission for extensive copying of this thesis for scholarly purposes may be granted by the Head of my Department or by his representatives. It is understood that copying or publication of this thesis for financial gain shall not be allowed without my written permission.

Department of Geophysics and Astronomy

The University of British Columbia
Vancouver 8, Canada

Date May 31, 1976

ABSTRACT

A marine seismic system for recording near-vertical incidence to wide-angle reflected waves and refracted waves with penetration to the bottom of the crust (deep seismic sounding or DSS) has been developed. In a two ship-operation, signals from six individual hydrophones are recorded in digital form on the receiving ship. To provide origin times and facilitate subsequent processing, signals from a single hydrophone are recorded in FM mode on the shooting ship.

During 1973, DSS profiles about 20km in length were recorded in three regions off the west coast of Canada: the Hudson '70 survey area, west of the Queen Charlotte Islands near 51°N , 133°W ; off Queen Charlotte Sound; and in Cascadia Basin west of central Vancouver Island. The recorded data were processed with various digital techniques such as autopower spectrum analysis, band-pass filtering, deconvolution, velocity spectrum analysis, and stacking.

After compilation in record sections, the data were interpreted in terms of velocity-versus-depth models of the oceanic crust. Two kinds of models were derived. For the refraction data, models are based on a traveltime and amplitude interpretation made by comparing the observed data with synthetic seismograms. For the reflection data, the

models are based on a T^2-X^2 analysis of seismic phases. The crustal models derived from the two approaches indicate the same basic crustal layers, but the reflection models show detailed velocity changes within these layers.

The models show the complexity of the structure of the oceanic crust and relate to regional geology. The crustal model of the Hudson '70 area shows thin sediments over the basement which consists of either two layers or a layer with a velocity gradient. The model compares well with the results obtained in the same area by Keen and Barrett (1971). The model for the region off Queen Charlotte Sound indicates six sedimentary layers of different velocities, basement at a depth of 2.4 km sub-bottom, and the oceanic layer at a depth of 4.5 km sub-bottom. Velocity reversals within the sediments possibly show the influence of Pleistocene glaciation on the deposition of sediments underneath the continental slope. The model for northern Cascadia Basin shows four layers within the sediments of thickness 1.9 km, a velocity transition between the sediments and the basement, the basement at a depth of 2.7 km sub-bottom, and the oceanic layer at a depth of 4.2 km sub-bottom. Proposed interbedding of volcanic material with high velocity sediments at the top of the basement correlates with geological formative processes observed at the crest of the near-by Juan de Fuca Ridge.

The results have shown that the marine DSS system is an efficient technique for detailed investigation of the oceanic crust and is an inexpensive alternative to the multichannel common depth point techniques used in the oil industry.

Contents

1	INTRODUCTION	1
1.1	Why Deep Seismic Sounding at Sea	1
1.2	Review of the Seismic Work at Sea	4
1.3	Project History and Areas of Recording	11
2	DATA ACQUISITION	17
2.1	Field Techniques	17
2.2	Instrumentation and Procedure	19
2.3	DSS Profiles and Their Locations	27
2.4	Examples of Observed Data	31
3	DATA PROCESSING AND ANALYSIS	44
3.1	Field Data and Corrections	44
3.2	Autopower Spectra	47
3.3	Band-pass Filtering	50
3.3	Deconvolution	55
3.4	Stacking of Refraction Data	71
3.5	Velocity Analysis of Reflection Data	76
4	INTERPRETATION	83
4.1	Methods of Interpretation	83
4.2	Velocity-depth Models	88
4.3	Discussion of the Results	130
4.4	Relation to Regional Geology	131
5	CONCLUSIONS	137

List of Figures

Figure 1.1 Location Map for the Areas of Recording	14
Figure 2.1 Schematic Diagram of the DSS System Using Two Ships	18
Figure 2.2 Schematic Diagram of the Instrumentation on the Shooting Ship	22
Figure 2.3 Schematic Diagram of the Seismic Recording System on the Receiving Ship	25
Figure 2.4 Detailed Maps of the Locations of the Seismic Profiles	29
Figure 2.5 A Typical Source Wavelet	33
Figure 2.6 Example of a Seismic Reflection Trace	36
Figure 2.7 Example of Five Refraction Traces Recorded Simultaneously	39
Figure 2.8 Example of a Record Section from the Expanding Profile in AREA 3	41
Figure 3.1 Amplitude Normalized Autopower Spectra of Characteristic Parts of Seismic Traces	49
Figure 3.2 Examples of the Effect of Various Bandpass Filters	52
Figure 3.3 Effects of the Spectral Divisional Deconvolution on a Reflection Trace	60
Figure 3.4 Characteristics of the Shaping Operator for	

Spike Deconvolution	64
Figure 3.5 Example of the Application of Spike Deconvolution to a Reflection Seismogram	66
Figure 3.6 Example of the Application of Deconvolution with Variable Wavelet to Seismograms	69
Figure 3.7 Record Sections of the Unstacked and Stacked Data of the Refraction Profile 73-1	73
Figure 3.8 Velocity Spectrum for Six Seismic Traces of the Expanding Reflection Profile 73-5	80
Figure 4.1 Traveltime-Distance Plot of the Refraction Profile 73-1 from AREA 1	90
Figure 4.2 Reduced Traveltime-Distance Plot of the Refraction Profile 73-5 from AREA 3	94
Figure 4.3 Comparison of the Observed and Synthetic Seismograms of the Refraction Profile 73-5	98
Figure 4.4 Record Section of the Expanding Reflection Profile 73-5 from AREA 3	101
Figure 4.5 Record Section of the Quasi-Continuous Subcritical Reflection Profile 73-6 from AREA 3	103
Figure 4.6 T^2-X^2 Graph for the Expanding Profile 73-5	107
Figure 4.7 Velocity-Depth Model for AREA 3	109
Figure 4.8 Reduced Traveltime-Distance Plot of the Two Reversed Refraction Profiles 73-2,3 from AREA 2	113
Figure 4.9 Comparison of the Observed and Synthetic Seismograms of the Refraction Profile 73-2	116

Figure 4.11 Record Section of the Expanding Reflection Profile 73-2 from AREA 2	118
Figure 4.11 T^2-X^2 Graph for the Expanding Reflection Profile 73-2	121
Figure 4.12 Velocity-Depth Model from the Base of Continental Slope in AREA 2	123
Figure 4.13 Quasi-continuous Subcritical Profile 73- 4 from the Continental Slope in AREA 2	126
Figure 4.14 Structural Model of Sediments on the Continental Slope and Its Correlation with a CSP Profile	128

ACKNOWLEDGMENTS

I would like to thank Dr. R.M. Clowes for initiating this challenging project. Because we were both previously inexperienced with work at sea, on many occasions the project demanded great endeavour and mutual personal encouragement.

Considerable assistance was necessary during the field operations and for this I sincerely appreciated the cooperation of the officers and crews of CFAV Laymore, Endeavour and St. Anthony, who participated in the operations during the project. My particular thanks go to Captain M. Dyers and officers W. Frame and A. Reid for their personal involvement and friendship. I also appreciated the helpful assistance of my fellow mates, Paul Somerville, Larry Lines, and others from the Department of Geophysics and Astronomy, who shared some of the tough moments at sea with me.

The suggestions of Dr. R.A. Wiggins in the data analysis were constructive and together with the practical help of my friend Rob Clayton during computer programming, were very much appreciated.

During part of this project, the author was supported

by a Graduate Research Fellowship from the University of British Columbia. Financial support for the project was provided by National Research Council equipment grant E3235 and operating grant A7707. Additional funds were contributed by Mobil Oil Canada Limited.

1 INTRODUCTION

1.1 Why Deep Seismic Sounding at Sea

In recent years, increased research efforts have been made toward studies of the ocean. From a geophysical viewpoint, two principal areas of investigation have evolved, one of a more economic, the other one of a more academic importance.

An area of future economic importance is the location and recovery of natural resources beneath the sea. It appears possible that within the next decades the acquisition of minerals and petroleum from the regions of the deep oceans will be feasible and economically profitable. An example of such a promising area is the Gulf of Mexico where salt domes with petroleum indicators have been found in deep water regions (Watkins et al., 1975).

The second area of interest concerns the study of tectonic processes and the geological history of the earth. For the development of geotectonic theories, a detailed knowledge of the structure of tectonically active areas at sea and of the transition zones from the oceans to the continents is of prime importance. However, even this more

academic research pursuit cannot be separated from its evident economic aspects as discussed recently by Hammond (1975). Volcanism associated with subduction zones and mid-oceanic ridges or other active centers such as hot spots are now thought to give rise to characteristic types of ore deposits. The clearest examples are the copper sulfide ore occurring in the Troodos area of Cyprus and porphyry copper ores in the Andes of South America.

Progress toward the solution of such practical and theoretical problems requires an extensive knowledge of the structure and physical characteristics of the earth's crust and upper mantle under the oceans. Of the many geophysical techniques available, the seismological method provides the most detailed information. In university and governmental research, two standard techniques have been applied: continuous seismic profiling (CSP) and seismic refraction profiling. The principal advantage of the CSP method is its excellent resolution due to the high frequency content of the reflected signal; the principal disadvantage is its relatively shallow penetration due to low energy sources with a high frequency content. The CSP method has been used for more than a decade for obtaining detailed information about the uppermost parts of the crust, mainly the sedimentary layers. On the other hand, the penetration of the seismic refraction method as used at sea is

theoretically unlimited but its resolution is poorer. The lower frequency content of the seismic signals limits the precision of the method for distinguishing fine structures. Since the signal usually travels long distances, only averaged parameters along the horizontal ray path can be obtained. In addition, velocity gradients and inversions cannot be detected without additional analysis including the use of both traveltimes and amplitudes; even then this can be difficult.

In the petroleum exploration industry, another technique of investigation has been developed. The multichannel common depth point (CDP) procedure has the capability of providing good resolution with deep penetration. The cost of the equipment required for this procedure is so high that its use in university research is unrealistic.

However, it was believed that a technique which would combine the advantages of the seismic refraction technique and the industry's multichannel CDP technique might be established on a limited budget. Using the name established by Russian seismologists (Zverev, 1967), this compromise technique has been called marine 'deep seismic sounding' (DSS). Marine DSS refers to a marine seismic procedure for recording near-vertical incidence to wide-angle reflected and refracted waves with penetration from the ocean bottom

to the upper mantle. Higher frequency signals than with the usual refraction method are recorded at the near distances, thus allowing detailed changes in structure to be distinguished even in the deeper layers of the crust. At greater distances, the seismic refraction signals provide average characteristics along the profiles and are used to check the information obtained from the reflection data.

Several factors played important role in the decision to initiate the marine DSS program within the Department of Geophysics and Astronomy at U.B.C. The dominant ones among these were the necessity for detailed information throughout the oceanic crust and the successful use of the DSS method for detailed crustal studies on land. As well, the location of the University on the west coast, continuing marine studies of the upper crust by the Department of Geological Sciences and complementary work by the Marine Geosciences Group of the Geological Survey of Canada in Vancouver, all contributed to the initiation of the project.

This thesis concerns the establishment of the marine DSS technique , methods of data analysis and interpretation, examples of interpreted velocity-depth structures in representative areas off the west coast of Canada, and a discussion of their geological significance.

1.2 Review of the Seismic Work at Sea

During the last decade our knowledge of the structure of the crust and upper mantle under the oceans increased remarkably. Much of the information is due to the use of new seismic recording techniques at sea and the development of more sophisticated methods of analysing recorded data.

The original seismic model of the oceanic crust was based on the results obtained with well established refraction techniques (Hill, 1952; Officer et al., 1959; and Shor, 1963) using unreversed, reversed and split profile recording. These techniques are a reliable source of information in normal oceanic regions such as deep basins. The model consists of three layers with a sediment layer at the top, a basement or secondary layer beneath, and an oceanic or third layer at the bottom. The velocities and thicknesses of the layers can vary widely. The average model for the Pacific Ocean basin (Shor et al., 1970) shows that the velocity for the sediments varies in the range from 1.9 to 2.5 km/sec and the thickness from 0 to 1.6 km. The basement velocity varies from 4.5 to 5.8 km/sec and its thickness from 0.5 to 2.5 km. For the oceanic layer the velocity is in the range from 6.7 to 7.0 km/sec with varying thickness from 3.3 to 5.9 km.

Abnormal oceanic regions such as ridges and continental

margins are characterized by a more complex crustal structure. Several difficulties are encountered when one tries to obtain reliable data with the use of refraction techniques in such areas. Interfaces distorted by folding or broken by faulting give complex travelttime curves which are undulating or broken into short segments. The most reliable seismic arrivals are the first ones. For operational reasons it has been difficult with refraction techniques using explosives to provide spacing close enough to detect structural features or layers that appear as first arrivals on the records only over a limited distance interval. Thus thin sedimentary layers or a thin basement lying at greater depth can be difficult to detect (Shor and Raitt, 1969). For second or later arrivals the coincidence of two or more phases makes the analysis difficult, unless there is an appreciable difference in the characteristic frequencies.

New techniques of marine recording and shooting have solved some of the problems. Recording of variable-angle reflection data from closely spaced series of shots fired at shorter ranges (M. Ewing, 1963; J. Ewing and Nafe, 1963) together with records of vertical reflection profiles (Hersey, 1963) provide valuable assistance in the analysis and interpretation of the travelttime curves. Such data enable determination of the velocities and thicknesses of sedimentary layers , a result which is not possible with the

CSP method. The vertical incidence reflections provide apparent dip and topographic corrections for the variable-angle reflection data (Le Pichon et al., 1968). Reliable measurements of the thickness of basement are obtained by comparing the reflected wave results with the position of the top of the deeper oceanic layer as determined from refraction measurements (Zverev, 1970).

Another technique with increased structural resolution uses expendable sonobuoys and precision echo-recording equipment (Maynard et al., 1969; Ewing and Houtz, 1969). The shot spacing was decreased significantly through the use of a repetitive air gun as a signal source. With this technique a previously undetected layer in the deep parts of the oceanic crust was identified. This high velocity basalt crustal layer with an average seismic velocity of 7.3 km/sec under the normal oceanic layer was discussed by Maynard (1970) and by Sutton et al. (1971).

Variations in velocities and velocity gradients within the oceanic layer and upper mantle have been investigated, particularly by Russian researchers. In their work, which was one of the earliest applications of the DSS technique for this purpose, they used both the traveltimes and amplitude information from long expanding profiles with dense explosion spacing. In such a study near the Southern Kurile Islands near Kamchatka, running profiles up to the

distance of 160 km with shot spacing of about 6 km, they were able to identify velocities of 8.6 to 9.0 km/sec at a depth of 12 km below the Mohorovičić (M-) discontinuity (Zverev, 1970).

With the realization of the greater complexity of the crust and upper mantle under the oceans, new shooting procedures and instrumentation for the study of specific problems in the investigation of seismic structures have been developed. For example, orthogonal and ring surveys have been conducted to detect lower crust and upper mantle anisotropy (Raitt et al., 1971; Keen and Barrett, 1971; Whitmarsh, 1971). In instrumentation, ocean bottom seismometers with explosion and air gun sources to detect both compressional and shear wave velocities directly have been tested (Hussong et al., 1969; Francis and Porter, 1973; Carmichael et al., 1973; Lister and Lewis, 1974; Prothéro, 1974; Orcutt et al., 1975, 1976). The comparison of their exact values with the results of laboratory tests made on rock samples from deep sea drilling would greatly help in the interpretation of oceanic structure in terms of petrology.

Attempts to investigate detailed structure of the deep crust and upper mantle with the use of the near-vertical incidence reflection technique have been reported during the last decade. In a two ship operation in the Skagerrak area

north of Denmark, vertical incidence reflections from the M-discontinuity at a depth of 30 km below the sea surface were observed (Aric, 1968). The results were compared with previous refraction observations and exhibited good agreement. A vertical incidence profile recorded at the Great Meteor Bank near the Canary Islands (Aric et al., 1970) indicated arrivals from a depth corresponding to 10 sec (two-way) traveltime. The results when compared with refraction data recorded with geophones located on the sea bottom at depths between 300 and 800 m showed good agreement. Perkins (1970) observed near-vertical incidence reflections from the deep parts of the crust north of Puerto Rico. Data were recorded in a single ship operation with the use of sonobuoys and 0.8 kg charges as a source of energy. Stacked data show reflection arrivals from within the basement, oceanic layer and possibly from the M-discontinuity.

Some special applications of the multichannel CDP procedure with the use of repetitive sources to obtain deep crustal and upper mantle reflections have recently been realized. Limond et al. (1972) reported mantle reflections at near-vertical incidence in the Bay of Biscay north of Spain. Threefold stacked data indicate vertical incidence arrivals of 9.2 to 9.4 sec (two-way) traveltime. The results agreed well with wide-angle reflection and refraction data

previously recorded in the area. Watkins et al. (1975), using a similar method, recorded deep reflections in the Gulf of Mexico. Their multifold data recorded digitally clearly show a deep reflector (possibly upper mantle) at 6.5 sec (two-way) traveltime after the first water bottom reflection.

In the interpretation of marine refraction data, the usual method used was the slope-intercept method described by J. Ewing (1963). It is relatively straightforward, but such deviations as velocity gradients and inversions were not usually incorporated in the interpreted seismic structures. Thus it can lead to major errors, particularly in the determination of layer thicknesses.

As new recording procedures and methods were applied new techniques of data analysis were developed to obtain more information from recorded data. For example, a method using the amplitude and waveform information developed by Helmberger (1968), and by Helmberger and Morris (1969, 1970) has enabled identification of velocity gradients and inversions from refraction data. Orcutt et al. (1975, 1976), analyzing seismic refraction profiles recorded digitally by an ocean bottom seismometer on the East Pacific Rise, show the occurrence of a low velocity layer of 4.8 km/sec underlying a high velocity layer of 6.7 km/sec. In the analysis of the seismograms both traveltime and amplitude

studies were used.

Recent detailed studies indicate that the model of the oceanic crust is much more complex than was originally assumed. Successfully recorded subcritical reflections from the deep parts of the crust suggest that the method of reflection seismology should be developed further and used to a greater extent as one of the principal means for detailed investigation of the oceanic crust.

1.3 Project History and Areas of Recording

In 1971, the marine deep seismic sounding research program was initiated at the Department of Geophysics and Astronomy, University of British Columbia. The purpose of the project was to:

- 1) develop and test the instrumentation in the laboratory and at sea;
- 2) use the technique for recording in tectonically and economically interesting areas off Canada's west coast;
- 3) apply data processing techniques such as bandpass filtering, stacking and deconvolution to the digitally recorded data to improve the quality of the seismograms;

- 4) analyse the recorded data in terms of velocity structure;
- 5) interpret the structure to give a geological understanding; and thus
- 6) determine the feasibility of the technique for detailed seismic studies of the oceanic crust.

Two basic factors, a limited budget, and availability of two ships for the operation, strongly influenced the decisions concerning the marine technique to be used. A design similar in concept to that used by Scripps Institute of Oceanography and described by Shor (1963) was chosen. However, the data acquisition was improved with multiple sensors and digital recording. Section 2.1 of this thesis describes the system in detail.

During the first half of 1971, the instrumentation was assembled and tested in the laboratory. The first test of recording with the designed technique at sea in July 1971 was unsuccessful. Any possible seismic information was lost due to high noise background caused by water wave motion. After a few changes in the seismic data acquisition system to compensate for this, another cruise was undertaken in November 1971. During an experiment carried out 150 km west of Los Angeles an expanding seismic profile was successfully recorded. The sea operation had to be suddenly terminated due to a serious accident on one of the ships. In this

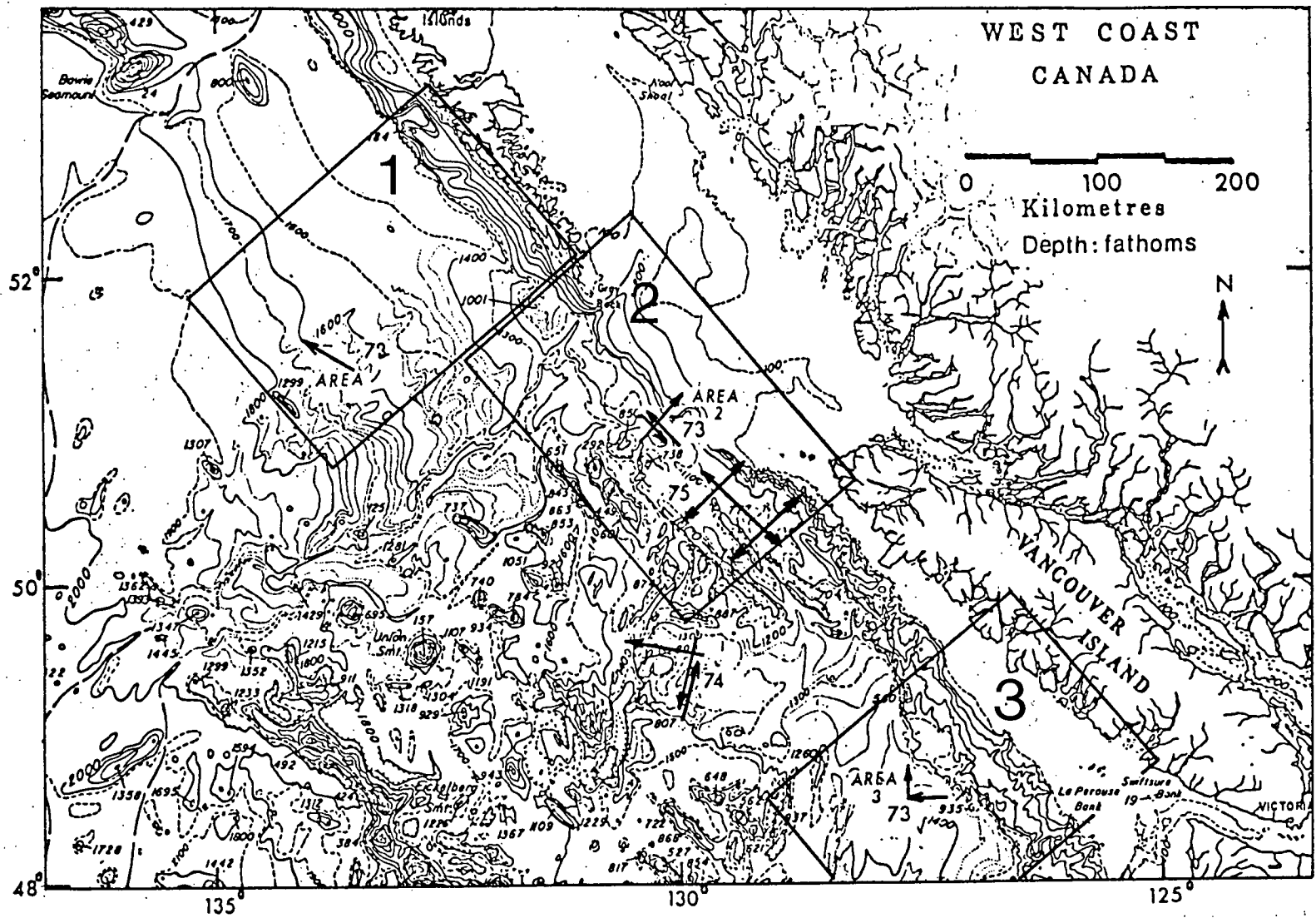
experiment analog FM magnetic tape recording was used. Electrical firing of charges enabled recording of the exact shot instants. The disadvantage of this shooting procedure was that it significantly slowed the operation. Much of the recorded data showed a low signal/noise ratio, although some indication of deep reflections was noted. However, the timing signal was often unreadable because of poor radio reception. For these reasons the interpretation of the data was not considered. However, a record section of the subcritical reflection data was made to ascertain its overall quality and provided enough encouragement to continue the development. In 1972, no ship time was available. In the meantime the method of tape recording was changed from analog FM to multichannel digital. Concurrently, the hydrophone suspension was improved by the introduction of additional mechanical damping against the pull of sea waves. In the summer of 1973, the final sea experiment was planned for three areas off the coast of British Columbia (Fig. 1.1). AREA 1 is located west of the southern tip of the Queen Charlotte Islands. It was the area of the 'HUDSON 70' experiment where the anisotropy of the upper mantle was investigated by Keen and Barrett (1971). By choosing this area the results of our recording could be compared with the seismic model determined from previous refraction work.

AREA 2 lies at the entrance to the Queen Charlotte

Figure 1.1 Location Map For the Areas of DSS Recording

Area 1:	51° 24'	-	51° 32' N
	133° 30'	-	133° 53' W
Area 2:	50° 58'	-	51° 12' N
	130° 04'	-	130° 21' W
Area 3:	48° 31'	-	48° 34' N
	127° 21'	-	127° 25' W

The boxes outline the regions which are shown in more detail in Figs. 2.4a and 2.4b. The numbers 74 and 75 designate profile lines for recording in 1974 and 1975. Map after Chace et al., 1970. Contours are in fathoms.



Sound and includes a part of the continental slope. It is a tectonically complex area. In such a region, information about the deeper structures would assist in the understanding of the ocean-continent transition zone and the tectonic history of the region. Deep seismic data from this area would also complement the CSP work on the continental shelf and slope being done by marine geoscientists of the Geological Survey and U.B.C.

AREA 3 is located in the northern Cascadia Basin west of the southern part of Vancouver Island. This region is a deep sedimentary basin where previous CSP profiles did not show sufficient penetration to reach the basement. Because of the thick sediments and therefore a lack of information about the depth and form of basement, some interest in this region had been indicated by the oil industry and by the Geological Survey of Canada. In addition to providing data of interest to other groups, the region would be a good area for testing the penetration and resolution of the DSS technique. Also, determination of the velocities of the sedimentary layers would enable an estimate of their thicknesses.

In July 1973, seismic profiles as indicated in Fig. 1.1 were successfully recorded. The data acquisition, and their analysis and interpretation, are presented in the remainder of the thesis.

2 DATA ACQUISITION

2.1 Field Techniques

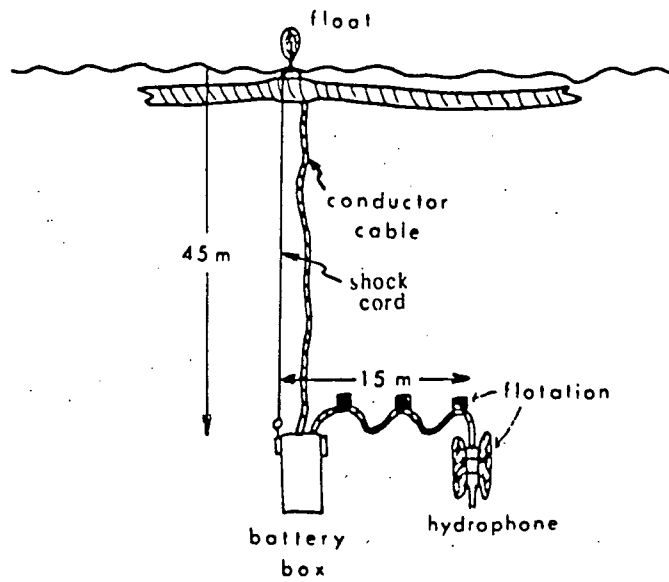
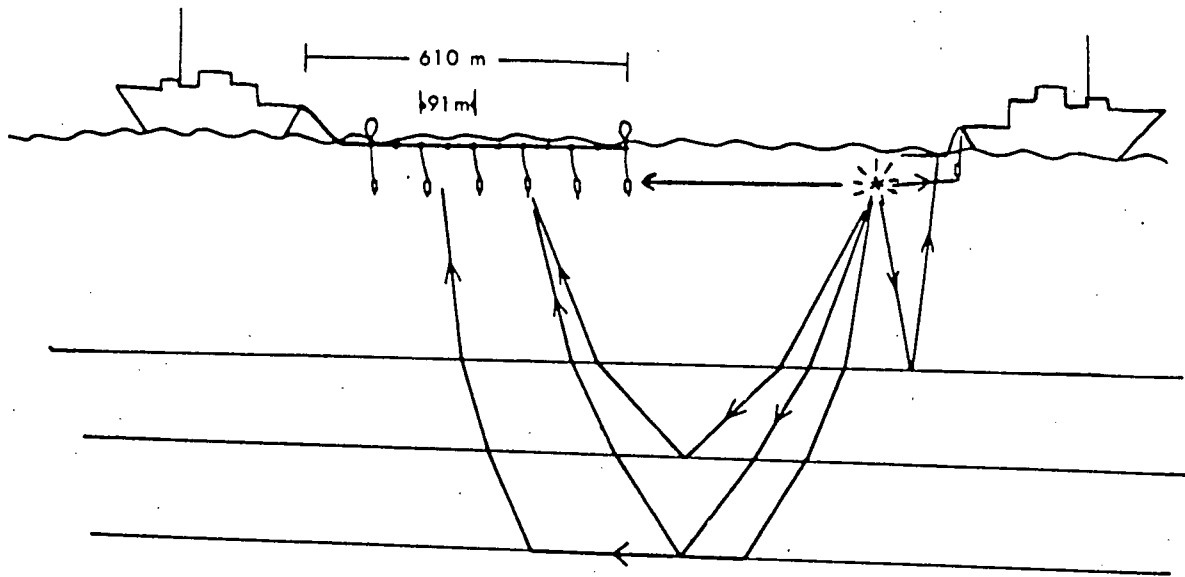
The DSS technique which was developed requires two ships . During this project CFAV ENDEAVOUR served as the receiving vessel and CFAV LAYMORE as the shooting vessel.

Fig. 2.1 illustrates the general features of the field technique. During a profile run the receiving ship drifts freely while trailing the neutrally buoyant main cable. Six individual hydrophone systems suspended from this cable were used for recording the direct water wave and seismic signals. The shooting ship proceeds along a chosen course and detonates charges at predetermined distances. The locations of the profile lines were determined with an accuracy of about 2 km from Loran A fixes and checked every 2 km. Ship-to-ship distances were determined by radar readings on both ships. Water depths were recorded with echo-sounding systems operating continuously on both ships during the profile run.

Figure 2.1 Schematic Diagram of the DSS System Using Two Ships

Top - The two ship procedure with direct water wave, reflected and refracted wave ray paths indicated.

Bottom - Sketch of one of the six hydrophone systems suspended from the main cable. The battery box contains 4 6-volt Gel-Cel rechargeable batteries to provide power for the preamplifiers. Flotation is attached to make the 15 m cables with hydrophones neutrally buoyant at depth. The S-shapes of these cables plus the shock cord minimize the effects of the surface sea waves.



2.2 Instrumentation and Procedure

SHOOTING SHIP

As a source of seismic energy, Nitrone SM Super commercial explosive was used. This blasting agent gives high seismic energy per unit and was developed specifically for marine seismic shooting. It was used in the form of 0.45 kg cans which were easy to handle on the ship. Charges up to 8.1 kg were assembled for shots at the greatest distances. The shooting procedure was relatively simple and similar to that outlined by Shor (1963). Charges were prepared for detonation with a timed-fuse/Seismocap assembly and Primacord (Malecek, 1976). After the charge was fastened to a line which had one or more balloons tied to the end of it, the fuse was lit and the charge was dropped overboard. A four minute fuse allowed time for the charge to sink to the required depth and gave the shooting ship time to sail a safe distance ahead of the shot. After the shot was detonated, the distance of the balloon from the ship was estimated by visual sighting.

The optimum depth for detonating charges with respect to the minimum loss of energy depends on the charge size

(Raitt, 1952), and for TNT is given by the empirical formula

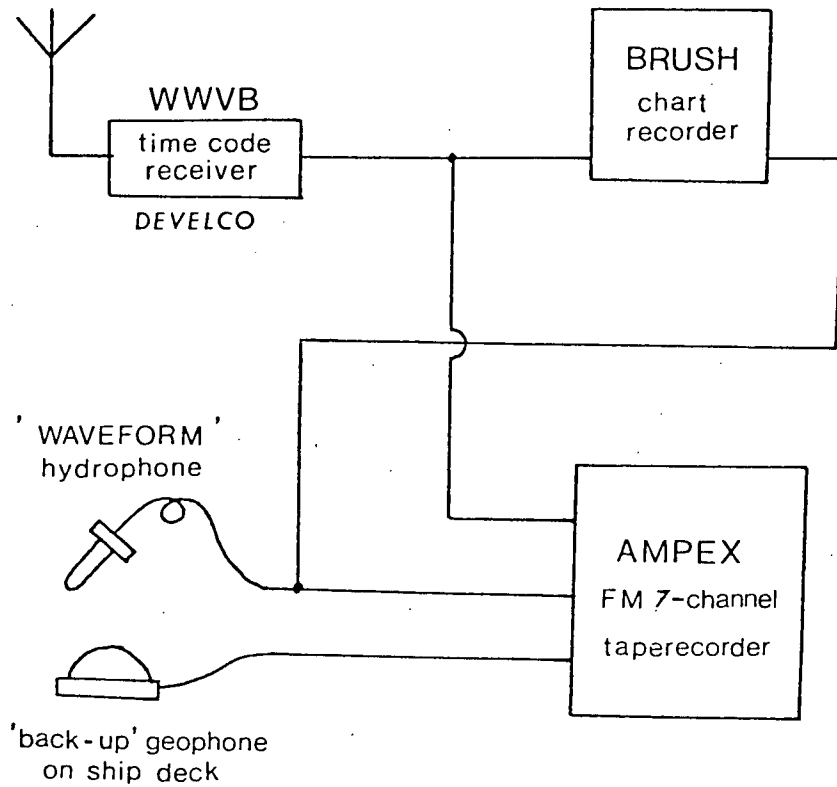
$$H(H+10)^{5/6} = 4.43 C_0 W^{1/3} \quad (2.2-1)$$

where H is the depth (m) of the charge from the sea surface, C_0 is the sound velocity (km/sec) in sea water, and W is the weight (kg) of the charge. This formula is based on a curve relating frequency of bubble oscillations to charge weight and the criteria that the detonation depth should equal a quarter of the wavelength for the bubble pulse frequency. For the Nitrone SM Super charges (60% TNT) of sizes from 0.45 to 8.1 kg the formula gives the optimum depths in the range of 30 to 52 m. A preliminary testing at sea confirmed these values, and it was decided to shoot all charges at a uniform depth of 45 m.

In order to time the direct wave arrivals, each detonation was received by a single hydrophone located 30m behind the shooting ship. As a back up for the hydrophone, a geophone was placed on the deck of the ship. These signals, together with the WWVF time code signal, were recorded on an FM tape recorder for subsequent playback. A two channel chart recorder was used to monitor signals being recorded. The instrumentation on the shooting ship is illustrated schematically in Fig. 2.2.

Figure 2.2 Schematic Diagram of the Instrumentation on the
Shooting Ship

SHOOTING SHIP INSTRUMENTATION



GOULD - CLEVITE
CH - 24 hydrophone

BRUSH - 220
chart recorder

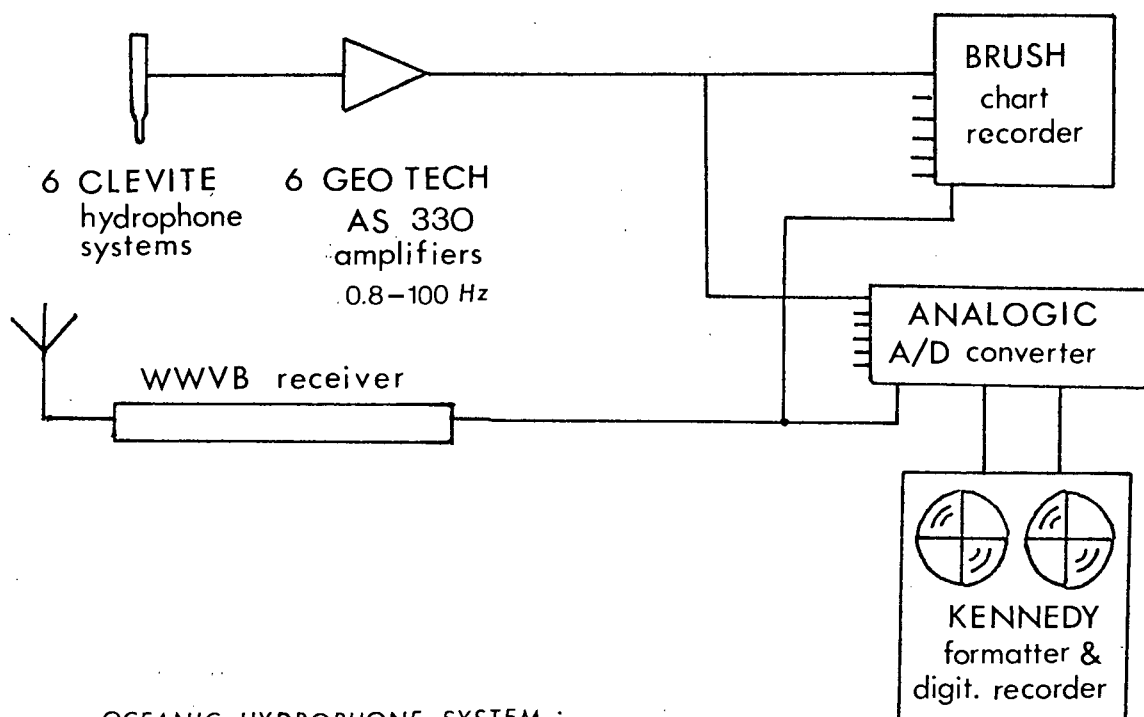
RECEIVING SHIP

During the running of a profile, the receiving ship drifted freely with engines stopped and the main cable stretched behind. The effects of the motion (due to sea waves at the surface) of the main cable on the hydrophone systems were reduced by means of rubber shock cords extending from the main cable to the battery cases. Additional mechanical damping of the movement of the hydrophones due to water disturbances was effected by attaching sufficient flotation to the hydrophones and 15 m cables such that they were approximately neutrally buoyant at depth (Fig. 2.1, lower part).

The instrumentation used on the receiving ship is shown in Fig. 2.3. Pressure waves incident on a piezoelectric crystal in the CH-2A hydrophone produce an electrical signal which is preamplified and transmitted to an amplifier system aboard ship. In the latter, the signal is bandpass filtered between 0.8 and 100 Hz, and then amplified with the gain set manually for each shot. The outputs from the six amplifiers plus the WWVB time code signal are recorded on magnetic tape with an IBM-compatible, 14 bit, multichannel digital acquisition system. Five seismic data channels and the WWVB time signal are monitored on a six-channel chart recorder. This enables one to check data quality and make decisions

Figure 2.3 Schematic Diagram of the Seismic Recording System on the Receiving Ship

SEISMIC RECORDING SYSTEM



OCEANIC HYDROPHONE SYSTEM :

CH-2A sensor &
GOULD CE-25 L preamplifier
(20db, 2 Hz - 40 kHz)

ANALOGIC SERIES AN - 5800
14 bit conversion system :

AN 2814 digital convertor &
16 channel multiplexor

KENNEDY MODEL 8108
synchr. digital taperecorder.
(9 track IBM compatible) &

BUFFER FORMATTER 8208
(sampling interval 40 μ sec)

concerning changes in gain settings of the amplifiers or changes in charge sizes with increasing distance between ships.

2.3 DSS Profiles and Their Locations

Two kinds of seismic lines were recorded: expanding profiles and near-vertical incidence profiles. For the former, the shooting ship detonated charges at increasing distances from the receiving ship. Shot spacing was 0.2 km for small charges (0.9 kg) at distances where near-vertical incidence reflections were anticipated, 0.5 km for intermediate charges (1.4-2.3 kg) where wide-angle reflections were recorded, and approximately 1 km for the large charges (3.2-8.1 kg) used in refraction recording. For the near-vertical incidence profiles the shooting ship detonated 0.9 kg (2 lb) charges at 1.1, 0.9, 0.7 and 0.5 km behind the stationary receiving ship. After each set of four detonations the receiving ship moved along the recording line and the procedure was repeated.

In AREA 1, a single expanding profile 20 km long was recorded. Because of the direction of drift of the receiving ship and the desire to have the shots detonated in line with the hydrophone cable, the profile was run oblique to the

refraction lines of the 'HUDSON 70' experiment as shown in Fig. 2.4a, upper. In AREA 2, two parallel reversed profiles of the lengths 18 and 15 km respectively were recorded. They were run along the base of the continental slope to determine the velocity structure and possible sloping of layers in the area. As well, a single quasi-continuous near-vertical incidence profile, 36 km long, was recorded across the expanding profiles in order to follow stratigraphic changes of the structure up the continental slope (Fig. 2.4b). In AREA 3 two profiles were recorded. An expanding profile over the sedimentary basin near the continental slope was run to determine layer velocities, and a short near-vertical incidence profile perpendicular to it (Fig. 2.4a, lower). The latter one was recorded in order to investigate uniformity of the local stratigraphy.

2.4 Examples of Observed Data

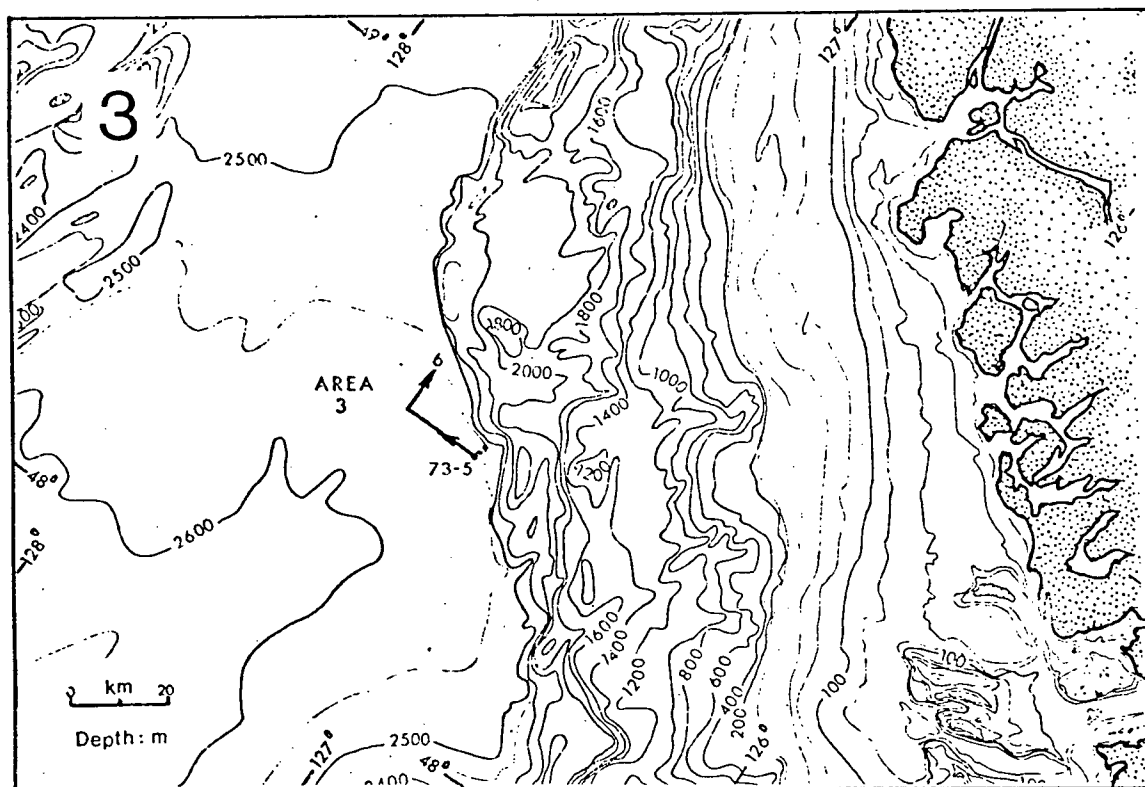
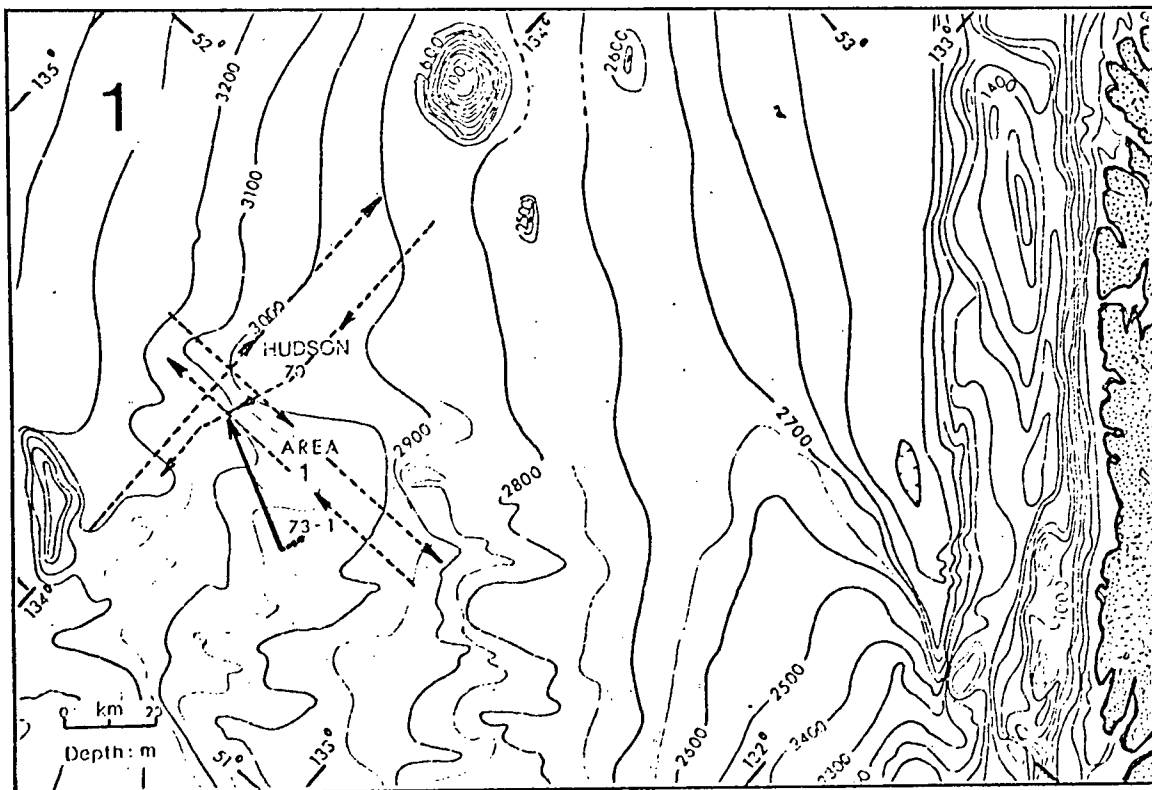
During the 1973 cruise, source wavelets and seismograms from 240 shots were recorded. The quality of the acquired data varied depending upon the physical conditions for recording.

Figure 2.4 Detailed Maps of the Locations of the Seismic Profiles

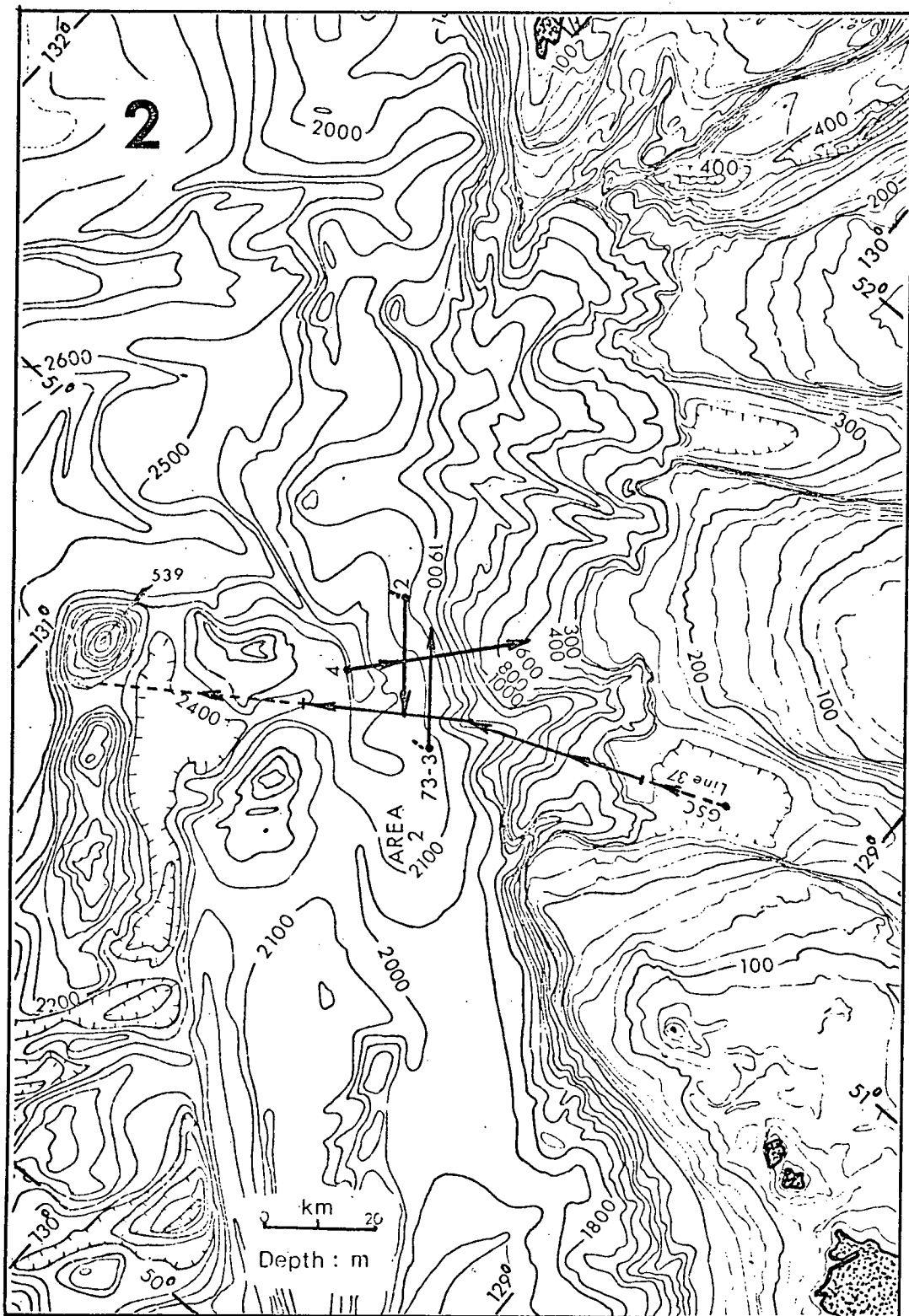
a) Top - The seismic profiles of recording in AREA 1. The solid line designated with 73-1 is the expanding profile. The dotted lines are refraction profiles from HUDSON '70 experiment. Drift of the receiving ship is shown by the solid dots.

Bottom - The seismic profiles of recording from AREA 3. Number 5 designates the expanding profile, number 6 the near-vertical incidence profile.

b) The seismic profiles of recording in AREA 2. Number 2 and 3 designate the reversed expanding profiles, number 4 the near-vertical incidence profile. Line 37 is CSP profile recorded by the Geological Survey of Canada in 1975. (The map sections are parts of the Bathymetric Map of the Continental Margin of Western Canada, Tiffin and Seeman, 1975. Contours are in meters.)



a)



b)

SHOOTING SHIP

An example of a typical source signature showing the sequence of bubble pulses is given in Fig. 2.5. This signature was recorded during the 1971 cruise when firing was done electrically and exact shot instants were known. As shown in the diagram, the direct wave from the explosion arrived 64 msec after the shot instant. The second large peak of opposite polarity and delayed by 7 msec, followed immediately by high frequency reverberations of decaying amplitudes, corresponds to the wave from the explosion which was reflected into the hydrophone from the sea surface. After an explosion, a gas bubble rapidly forms and expands until it reaches its maximum diameter, depending on the charge size and the ambient pressure, and begins collapsing (Kramer et al., 1968). When it reaches its minimum diameter and starts expanding again it sends a signal. The period (sec) of the first bubble cycle is given by an empirical formula

$$T_B = 2.1 W^{1/3} (H+10)^{-5/6} \quad (2.4-1)$$

where W is the charge weight (kg) of TNT, and H is the depth (m) of the charge detonation (Wielandt, 1975). The first bubble pulse is observed in the figure 133 msec after the

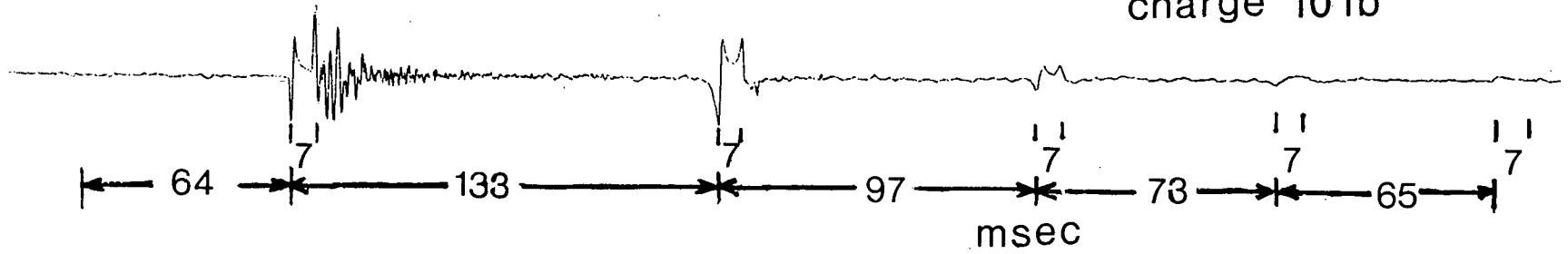
Figure 2.5 A Typical Source Signature

The top trace: a source waveform followed by a sequence of bubble pulses.

The bottom trace: shot instant signature recorded in electrical charge firing in 1971. (Both traces are recorded simultaneously on a two channel chart recorder.)

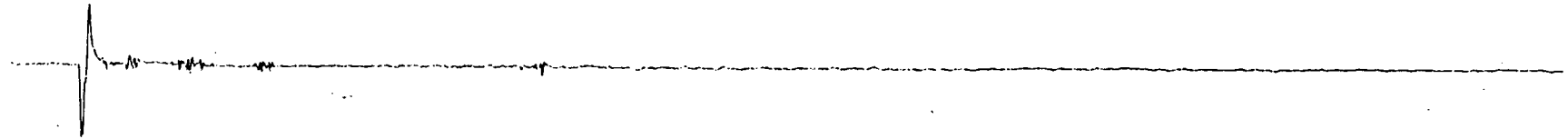
BUBBLE PULSE TRAIN

charge 10 lb



SHOT TIME BREAK

depth : 45 m
distance : 90 m



direct wave arrival. The cycle of expansion and collapse repeats a few times. However in each of the subsequent periods, the difference between the maximum and minimum diameter is smaller due to the energy loss in the gas bubble. The bubble pulsates faster and faster, and the signal amplitude decreases rapidly until the gas bubble, migrating upwards, reaches the water surface, and the remaining energy is released into the air (Kramer et al., 1968). A whole train of such events can be observed in Fig. 2.5.

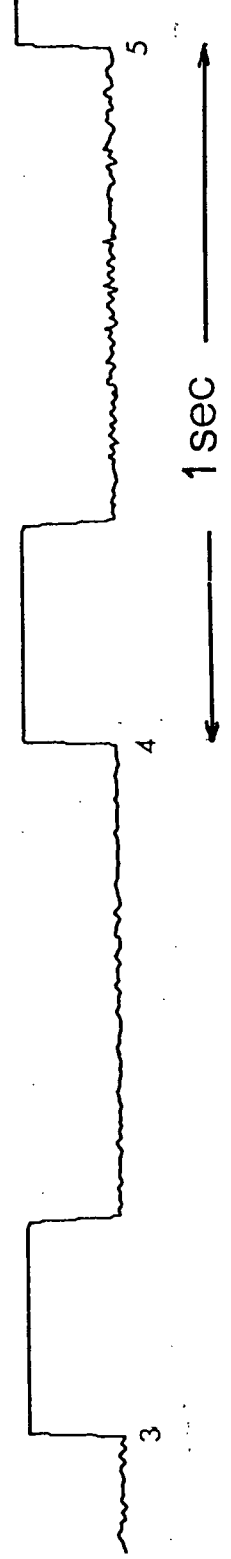
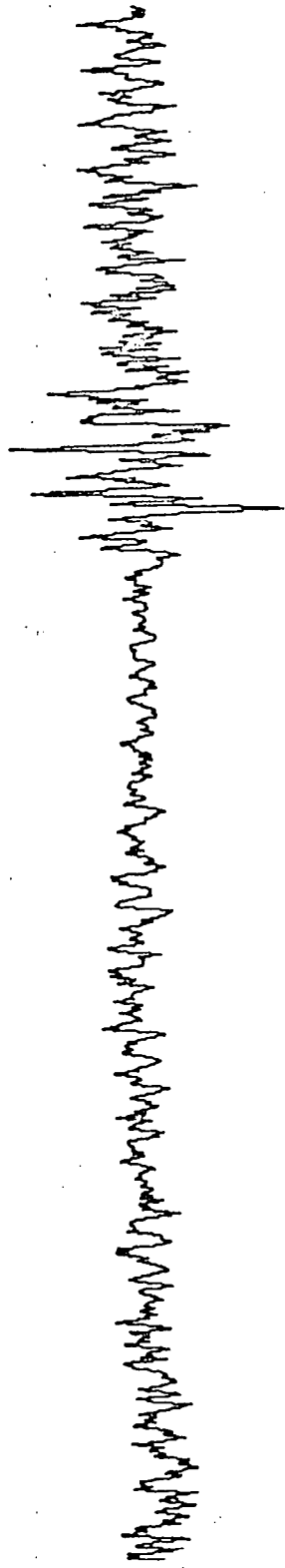
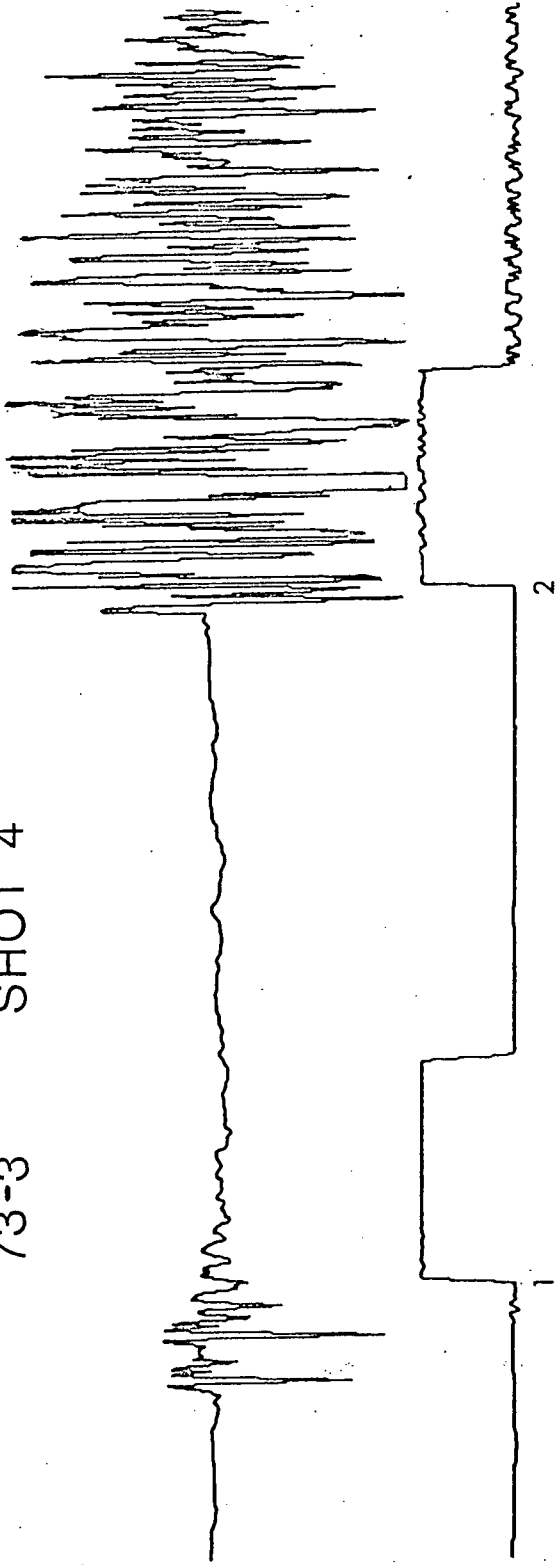
RECEIVING SHIP

As an example of the quality of the near-vertical incidence reflection seismograms, a single trace together with the WWVB time code signal is shown in Fig. 2.6. It can be seen that the signal/noise ratio is very good. The direct water wave arrives first; the complexity of the waveform is due to bubble oscillations. The water bottom reflection arrives a little more than 1 sec later. It is followed by a high frequency train of large amplitudes which correspond to reflections from within the sediments. Any reflections from beneath the sediments would arrive after second 3; they are difficult to identify from a single trace record. Toward the end of the trace, first order multiple reflections from the

Figure 2.6 Example of a Seismic Reflection Trace

The trace was recorded at the distance of 2.5 km from the detonation in water of depth 2.1 km. The first arrival is the direct water wave, the second major wave train is composed of reflections from the water bottom and beneath, and the third train (after second 4) is due to first-order multiple reflections. (The trace below the seismic line is the WWVB time code signal.)

73-3 SHOT 4



sea bottom and beneath give the train of reverberations which give rise to a sudden increase in amplitude.

Fig. 2.7 shows a section of five refraction traces recorded simultaneously for one shot. The signal/noise ratio varies very little with different channels. A few seismic events can be clearly correlated over all the traces. In Fig. 2.8 a complete record section from the expanding profile in AREA 3 is shown to demonstrate the quality of seismic data which has been obtained. Fig 2.8a shows mainly the reflection part of the profile while Fig. 2.8b illustrates the refraction part. Amplitudes of reflected waves from the upper sedimentary layers (Fig. 2.8a) are overloaded as a result of amplifier gain settings chosen to enhance reflections from deeper horizons. Coherent reflection arrivals for at least 2 sec after the bottom reflection are clearly observed on the recorded data. The first order multiple reflections from the bottom and beneath are obvious at a time of about 7 sec and later. At distances from 7 to 10 km (Fig. 2.8a) the transition from reflection arrivals to refraction arrivals is clearly shown for a strong reflector as indicated in the figure. The latter extend to nearly 22 km (Fig. 2.8b), but the quality of the data deteriorates due to the use of small charges and to poorer physical conditions at sea.

Figure 2.7 Example of Five Refraction Traces Recorded Simultaneously

Charge of 6.8 kg detonated at the distance of 18 km. Darkened wavelets indicate the correlation of possible seismic arrivals. The direct water wave and first bottom reflections can be identified clearly by their high frequency content toward the end of each trace.

SEISMIC REFRACTION TRACES

73-2 SHOT 23

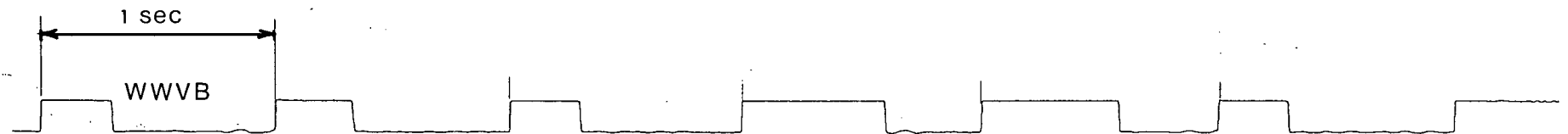
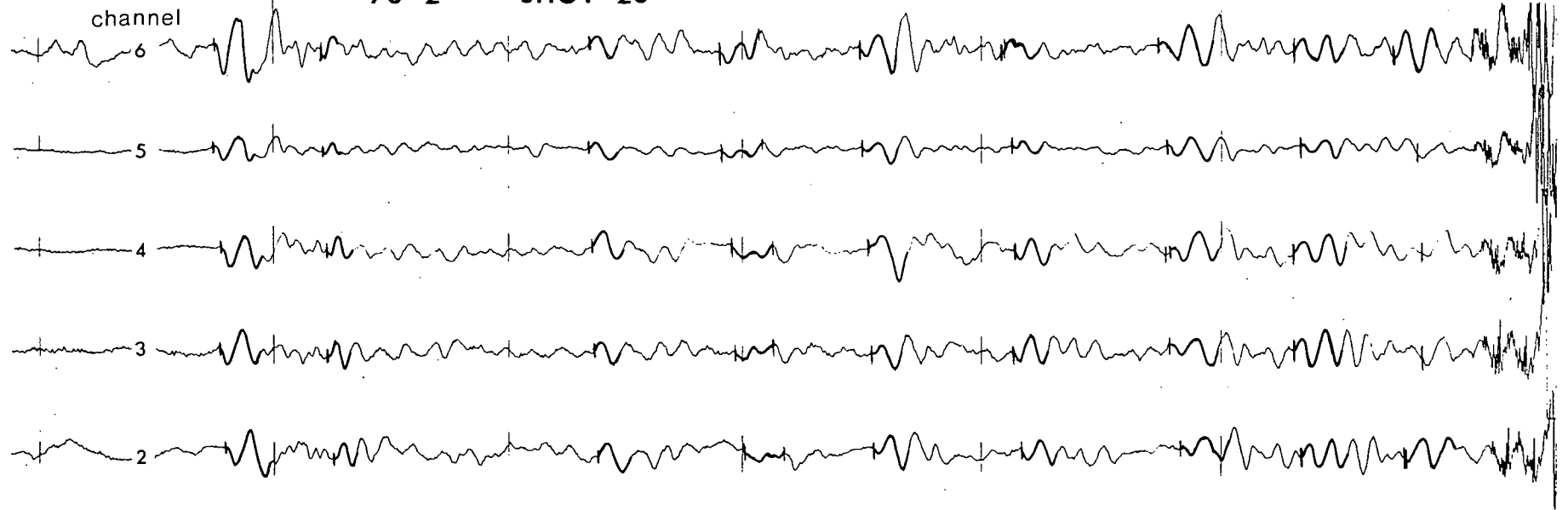


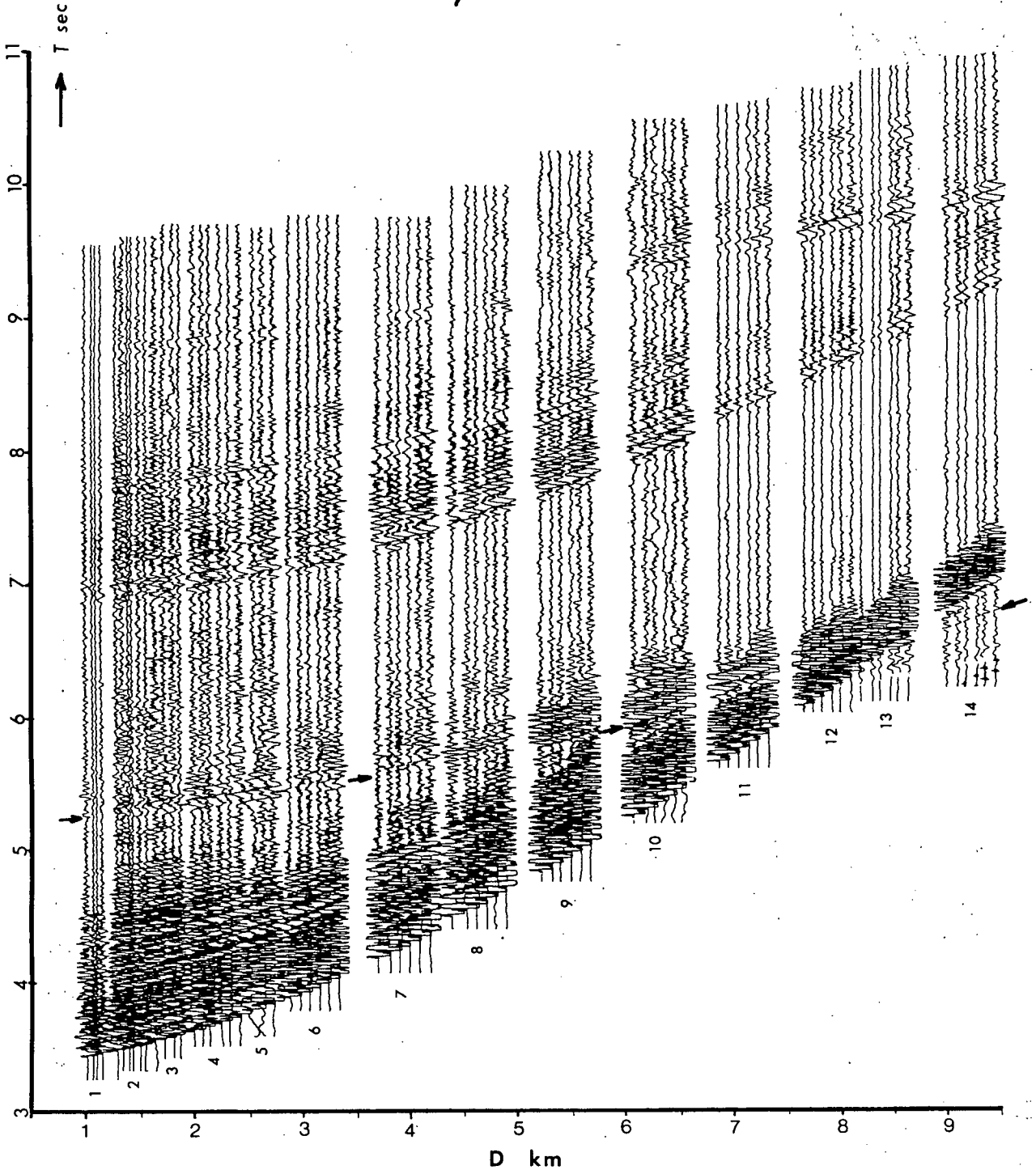
Figure 2.8 Example of a Record Section from the Expanding Profile in AREA 3

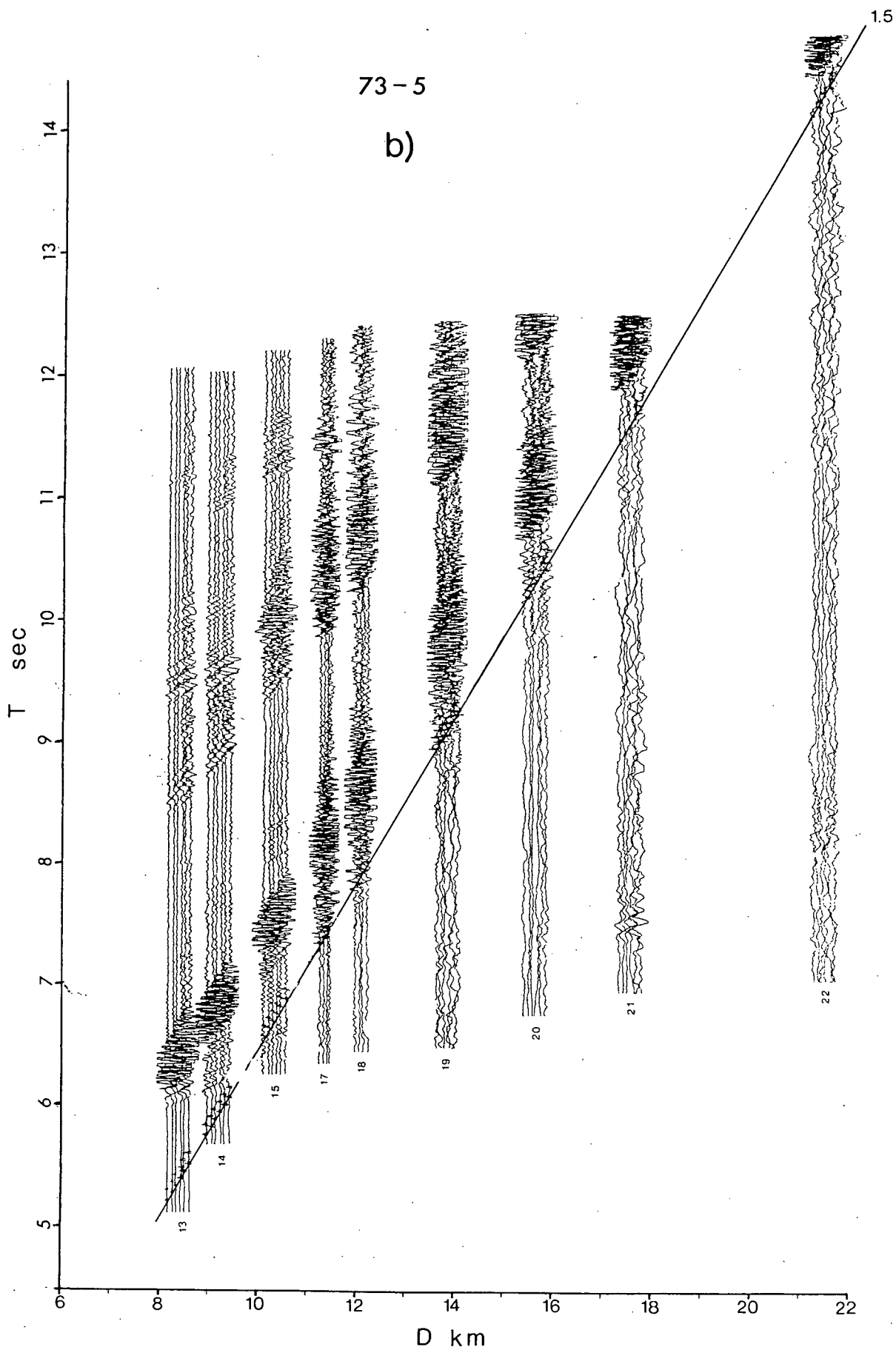
a) Reflection part: seismic data shown from the arrival of the first bottom reflections to beyond the time for most first-order multiples (7 sec and later).

b) Refraction part: the straight line connects the direct water wave arrivals and its slope gives the velocity of sound in water of about 1.5 km/sec. Numbers near the traces refer to shot numbers. Arrows point out the continuity of the deep crustal seismic arrivals across the record section. They can be followed from near-vertical incidence through wide-angle to refraction distances. Note the change in the distance scale between a) and b).

73-5

a)





3 DATA PROCESSING AND ANALYSIS

Procedures for handling the field data and for its digital processing are discussed in this chapter. By applying traveltimes and amplitude corrections, normalized record sections can be displayed for interpretation. The application of digital processing techniques improves the quality of the data. This in turn enables a clearer resolution of the seismic phases and their correlation throughout the record sections.

3.1 Field Data and Corrections

The data recorded on the field tapes were in an impractical form for immediate processing and storing. The multichannel data had been multiplexed, written in very short blocks of 512 half-words, and more than a minute of data for each shot had been recorded to ensure a complete WWVB time code. Furthermore, the recording density was 800 bytes per inch (BPI) rather than the more standard 1600 BPI. For the above reasons, the field data were edited, demultiplexed, and written on new tapes in a convenient blocking format with the higher recording density. The IBM

370/68 computer, operating under the Michigan Terminal System (MTS) at the University of British Columbia, was used for all the digital processing operations.

ORIGIN TIME CORRECTIONS

The data required corrections before they could be displayed for analysis. Origin times of the shots, obtained from an FM playback of the single hydrophone and WWVB signals onto a two-channel chart recorder, had to be corrected for the shot-to-ship distances. Although the shot instants could be timed to better than 5 msec on the chart recorder, an additional error of up to 15 msec was introduced by the application of the shot-to-ship distances since these were 'eyeball' estimated. The maximum resultant error in determination of the origin times was about 20 msec for larger detonation distances (600 to 900 m).

Shot-receiver distances for each shot and hydrophone were calculated using direct water wave (DWW) traveltimes and assuming a constant DWW velocity of 1.48 km/sec as recorded for the depth of about 45 m at the regular west coast Ocean Station P by Minkley et al. (1970). The error associated with these calculated distances is less than 3%.

TOPOGRAPHY CORRECTIONS

In most cases, topographic corrections were not required since there were no substantial topographical changes along the profile lines as was shown by the continuous fathometer records. The single exception was the 73-4 profile running up the continental slope. However, in this case also, the topographic corrections were not applied in order to be able to follow the rising topography of the bottom and the shape of the layers beneath on the record section.

AMPLITUDE CORRECTIONS

As it was intended to do an interpretation based on both traveltime and amplitude information, corrections were necessary for variations in amplifier gain settings, charge sizes, and geometrical spreading.

In order to keep the magnitude of amplitudes within a definite range during recording along a profile, signals from different distances were amplified with different gains. To get true relative amplitudes, a reference gain level was chosen and all amplitudes were normalized to it.

The corrections for charge sizes were calculated using

an expression based on studies of underwater explosions by O'Brien (1960). He has shown that first seismic arrival amplitudes are proportional to $W^{2/3}$, where W is the weight of the charge (kg). The correction equal to $1/W^{2/3}$ was applied to all shots in each profile.

As the energy travels away from the explosion, the amplitudes of the seismic arrivals decrease. With increasing epicentral distance (r) the wide-angle reflection amplitudes decrease as $1/r$ (Braile and Smith, 1975), and the head wave amplitudes for refractions as $1/r^2$ (Červený and Ravindra, 1971). The record sections of wide-angle reflection data (for distances from 4 to about 8 km) were corrected using a correction factor equal to r , and the sections of refraction data (for greater distances than 8 km) using a correction factor equal to r^2 . Amplitude corrections were not applied to the near-vertical incidence reflection data since amplitude information was not used during their interpretation.

3.2 Autopower Spectra

In order to determine the frequency content of the recorded waveforms and seismic signals, necessary for further data processing, autopower spectra were computed

with the use of a fast Fourier transform algorithm.

Fig. 3.1 shows amplitude normalized autopower spectra of some characteristic parts of seismic traces. The frequency content of the background noise, the refraction part of a seismic trace, reflections from beneath the sediments, and first-order multiples from the water bottom and beneath are displayed. The main frequency content of the background noise (Fig. 3.1a) is in the interval from 0 to 20 Hz with the maximum amplitude at 2 Hz. The refraction trace (Fig. 3.1b) has the maximum amplitude at about 10 Hz, and both reflection traces (Fig. 3.1c,d) show maxima between 20 and 30 Hz. Autopower spectra of primary reflections from within the sediments were not investigated because of amplitude overloading as mentioned earlier.

3.3 Band-pass Filtering

Since the frequency content of the reflected and refracted energy is confined to a certain band of frequencies, digital band-pass filtering was applied as a signal enhancement technique. A zero-phase shift, fourth order, recursive, Butterworth band-pass filter (Kanasewich, 1973) was applied to the data.

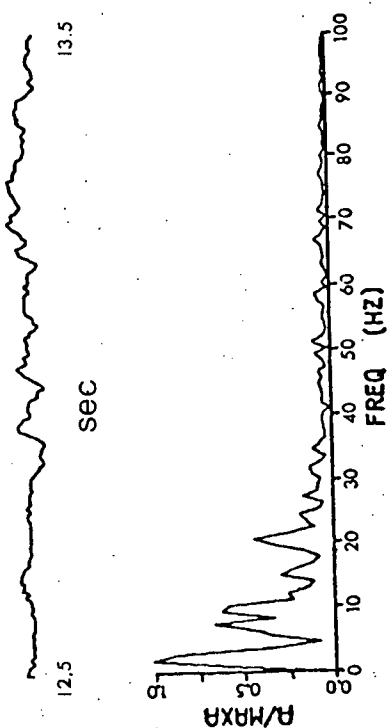
Effects of the filter for different frequency bands on

Figure 3.1 Amplitude Normalized Autopower Spectra of
Characteristic Parts of Seismic Traces

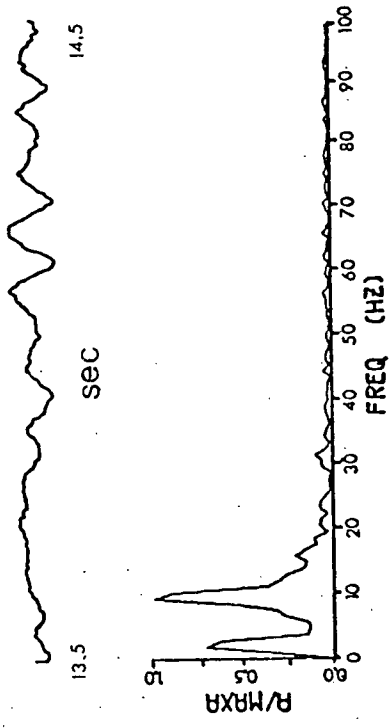
- a) Background noise,
- b) refraction trace,
- c) reflections from beneath the sediments,
- d) first-order multiples of the water bottom and sedimentary layers.

(Seismic traces are displayed above, autopower spectra below.)

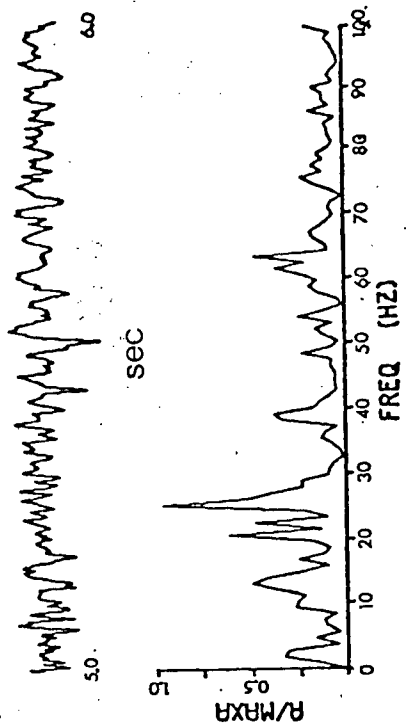
a)



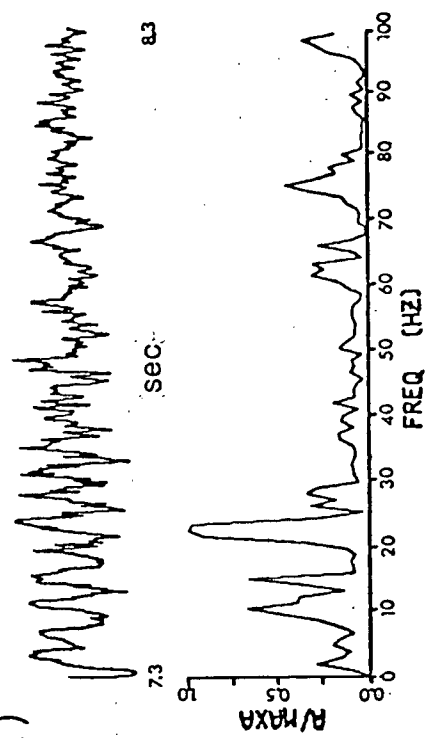
b)



c)



d)



a single reflection trace, on a set of six reflection traces and on a set of six refraction traces are displayed in Fig. 3.2. The diagrams of reflection data (Fig. 3.2a,b) show clearly that passbands of 2.5-30 Hz and 5-30 Hz enhance the seismic signals while maintaining their character. For narrower bands of frequencies, oscillatory effects are observed and the identification of the beginnings of seismic phases becomes difficult if not impossible. Similar effects are seen on the refraction traces. The best enhancement of the signals without additional ringing has been obtained with 0.5-25 Hz and 2.5-30 Hz filters. They give traces with clearly distinguishable refraction phases.

On the basis of the examples just shown and others, passbands of 2.5-30 Hz for reflection data and 0.5-25 Hz for refraction data were chosen and the filters were applied to the data.

3.3 Deconvolution

Deconvolution is used to improve the quality of seismograms with reverberation patterns. The desirable result from its application is sharper resolution of seismic arrivals, achieved by shaping a reverberation into a single spike or pulse.

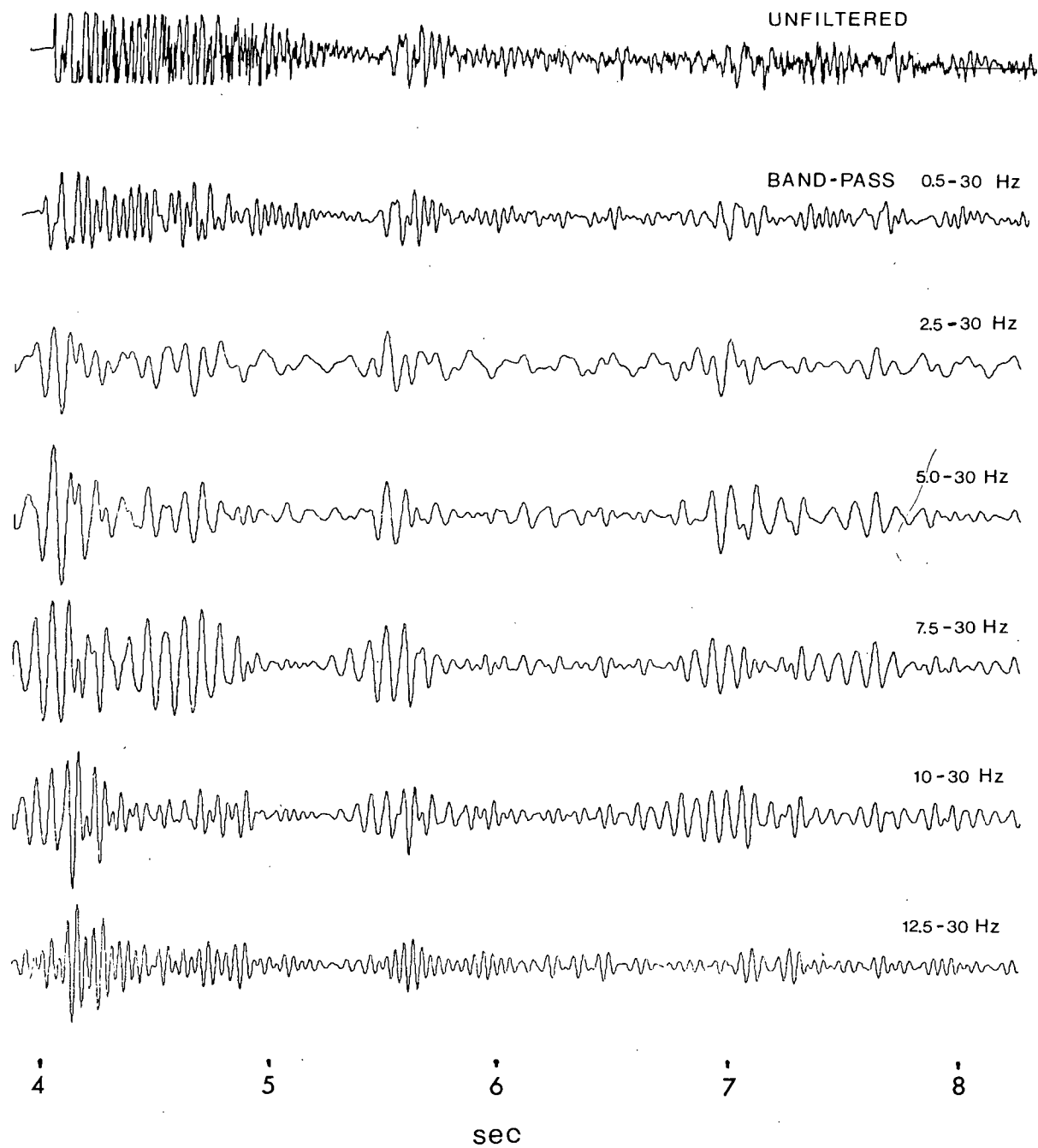
Figure 3.2 Examples of the Effect of Various Band-Pass Filters

a) A single reflection trace (showing the influence on reflection wavelet character and signal/noise ratio).

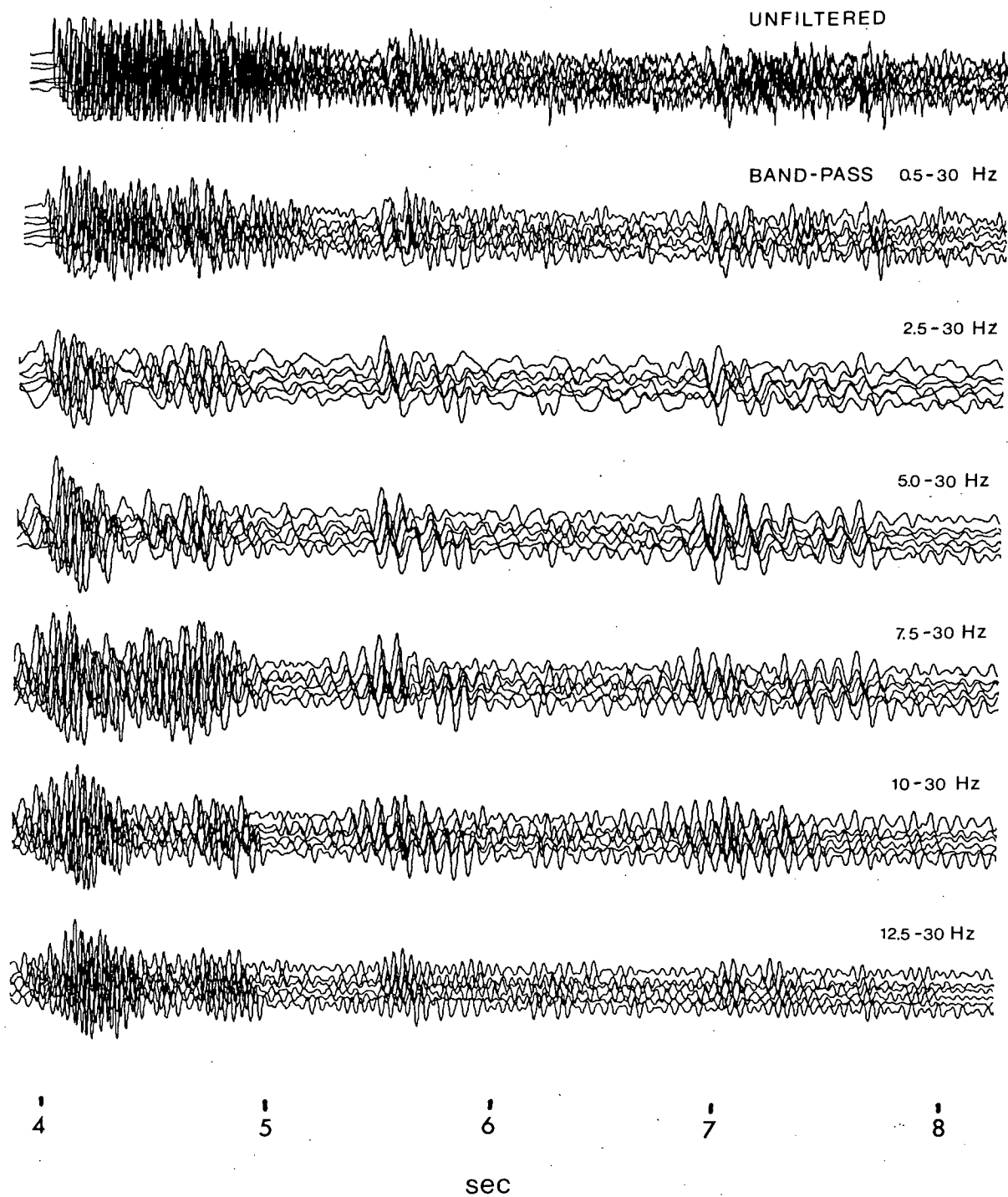
b) Six reflection traces (showing the change in quality of correlation across the traces).

c) Six refraction traces (showing the change in the amplitude and their correlation with the band-width). Note that as the lower limit of the passband increases, the traces for both reflection and refraction data become more oscillatory such that identification of phases becomes more difficult.

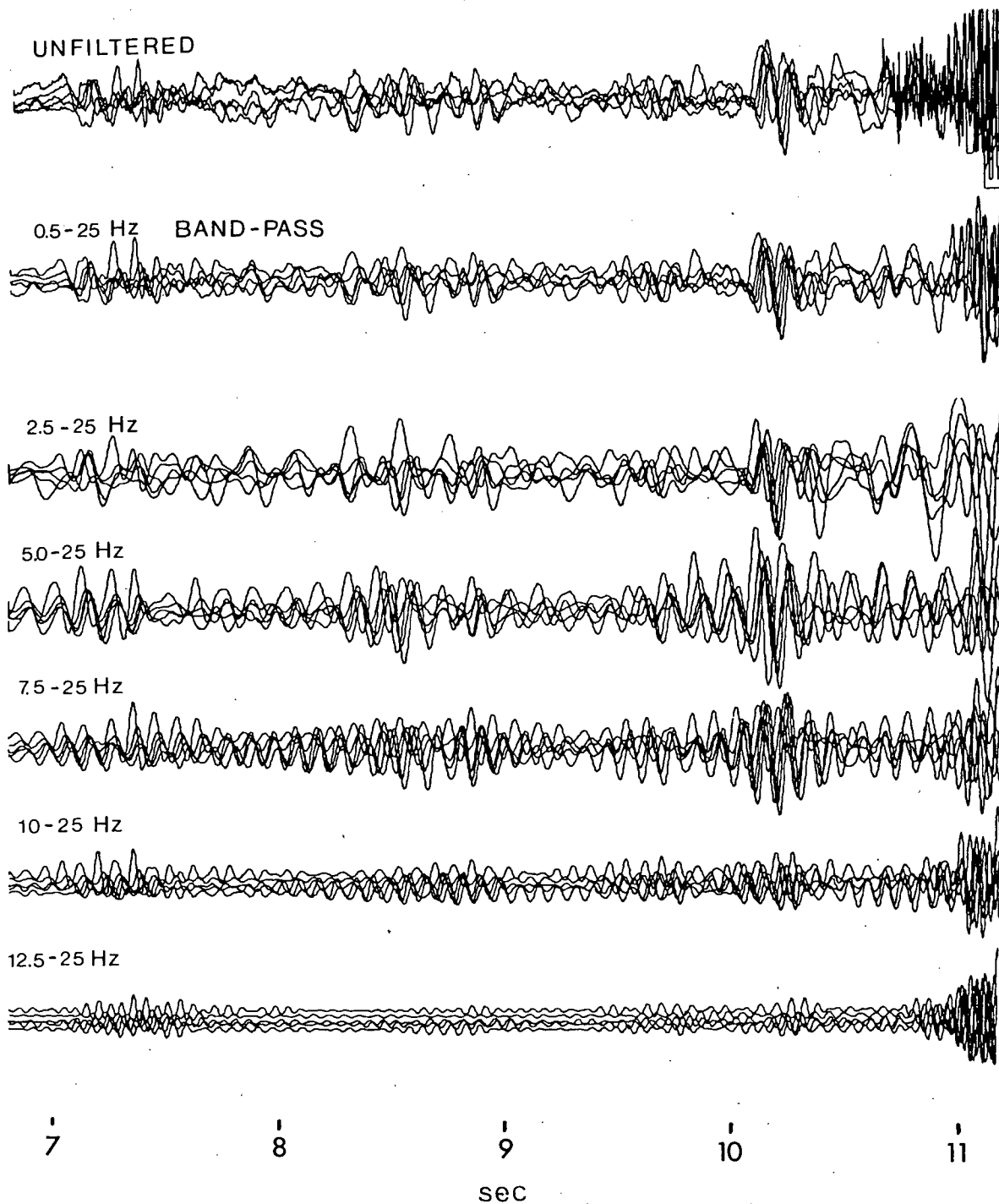
a)



b)



c)



It was decided to apply two different deconvolution techniques to the reflection data; one in the frequency domain and one in the time domain. In the frequency domain, spectral divisional deconvolution was chosen for its simplicity and because source wavelets of a good quality were available. In the time domain, spike deconvolution was chosen because it can be used to consider changes of the source wavelet with time.

SPECTRAL DIVISIONAL DECONVOLUTION

The time domain model for the j -th seismic trace is

$$S_j(t) = w(t) * r_j(t) + n_j(t) \quad (3.3-1)$$

where $w(t)$ is the source signature for the particular shot, $r_j(t)$ is the impulse response of the transmission path to the j -th hydrophone, $n_j(t)$ is a white noise sequence, and $*$ denotes convolution.

In the frequency domain a single seismic trace is described by

$$S(\omega) = W(\omega) \cdot R(\omega) + N(\omega) \quad (3.3-2)$$

where capital letters denote the Fourier transforms of the variables in (3.3-1). To obtain the estimated impulse response \tilde{R} , the spectrum of the seismic trace is divided by the spectrum of the source signature W

$$\tilde{R} = \frac{S}{W} = \frac{|W| \cdot R + W^* \cdot N}{|W|^2} \quad (3.3-3)$$

where W^* is the complex conjugate of W . As the amplitude of the source signature becomes small the factor multiplying the noise component becomes increasingly large. Therefore, to obtain an estimated impulse response \tilde{R} which converges to the impulse response R , it is essential to establish a minimum amplitude level for the source signature in order to limit the gain of the deconvolution in parts of the seismogram where the trace contains little or no information. This minimum source signature amplitude W_0 is termed the waterlevel (HelMBERGER and Wiggins, 1971).

For convenience a relative waterlevel TOL is introduced and defined as a fraction of the maximum source signature amplitude W_{max} : $TOL = W_0 / W_{max}$ (0-TOL-1). The estimate of impulse response \tilde{R} then becomes

$$\tilde{R} = \frac{|W|R + W \cdot N}{\max \{ |W|^2, (TOL \cdot W_{max})^2 \}} \quad (3.3-4)$$

Considering only the factor containing the impulse response R , we can see that as the relative waterlevel TOL approaches zero we obtain unrestricted deconvolution of the seismic trace S by the source signature W . As the parameter TOL approaches unity, the estimator is just a scale factor multiplied by the crosscorrelation of S and W (Clayton, 1975).

Unrestricted deconvolution attempts to remove all of the source effects from the seismogram, and the estimator R gives the best true impulse response. This type of estimator is best for resolving traveltimes. The crosscorrelation is the least-squares estimate of the arrival amplitude (Helmberger and Wiggins, 1971). This means that if the parameter TOL equals unity the best relative amplitude resolution is obtained. The waterlevel can therefore be used in determining the preferred trade-off between arrival time resolution and relative amplitude resolution. These considerations suggest that spectral divisional deconvolution of a seismic trace for a range of waterlevels should be attempted.

The effectiveness of spectral divisional deconvolution applied to the reflection data for different waterlevels TOL

is demonstrated in Fig. 3.3. A seismic reflection trace was deconvolved by a source signature which consists of the direct source wave arrival and the first bubble pulse as recorded for the particular shot. The source signature was first prefiltered for the same passband of frequencies as the seismic trace in order to avoid the introduction of higher frequencies into the deconvolved trace. Deconvolution was performed for five different waterlevels TOL of values from 0.01 to 1.0. In the figure, the deconvolved traces are compared with the filtered trace. In none of the cases do the deconvolved data show any significant improvement in quality.

The main reason that the data quality has not improved with the application of spectral divisional deconvolution is that the frequency content of the source signature drastically changes as it passes through the sediments and upper layers. Thus deconvolution using a source signature recorded in the water close to the source is not particularly effective. The application of a modified source signature was considered, but since the construction of its theoretical estimate without a detailed knowledge of the upper crustal structure is extremely difficult, this idea was not realized.

Another reason for negligible data improvement is the rather high noise level in the frequency domain relative to

Figure 3.3 Effects of the Spectral Divisional Deconvolution on a Reflection Trace

The filtered source signature (2.5-30 Hz) consists of a direct source wave arrival and the first bubble pulse. Six various waterlevels (TOL) were used for deconvolving the trace section containing deep crustal reflections and first-order multiples from the upper layers.

SOURCE WAVELET (FILTERED)



SEISMIC TRACE (FILTERED)



TOL = 1.00



= 0.40



= 0.20



= 0.10



= 0.01



7

8

9

10

T sec

the maximum spectral amplitude of the source signature. Naturally, if the waterlevel is placed above the noise level, most of the source signature is cut off and the effect of deconvolution is weak. If the waterlevel is placed below the noise level the effect of deconvolution is largely lost

SPIKE DECONVOLUTION

In spike deconvolution we look for an inverse filter which when applied to a seismic trace increases the resolution of seismic arrivals by shaping the source wavelet into a single spike. Such a filter is usually called a spike operator, and its coefficients are determined by the input source wavelet and the desired output of a unit spike.

Spike deconvolution was applied with two different source wavelets: first, the recorded source signature, and then, variable wavelets chosen from the seismic trace.

A) Spike Deconvolution with a Source Signature

Spike deconvolution using the recorded source wavelet was applied to the data in order to obtain a basis for comparison of the effectiveness of spike deconvolutions with constant and variable (time adaptive) wavelets. The spike operator was designed for the filtered (2.5-30 Hz) source wavelet from a given shot using Robinson's modified subroutine SPIKE (Robinson, 1967, p.79). The shaping quality of the operator was tested by its application to the source wavelet and the results are displayed in Fig. 3.4. The operator produced a near-ideal spike as the output as the figure shows.

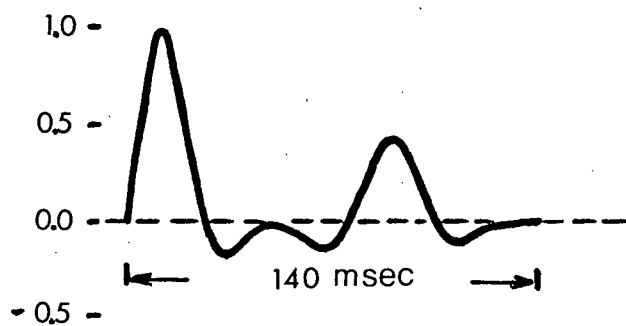
Fig. 3.5 illustrates the application of the operator to seismic traces. The deconvolved traces are displayed together with the unprocessed and filtered data in order to evaluate the effectiveness of deconvolution. The deconvolved data show some reduction in reverberation compared with the unprocessed data. However, the improvement in the arrival time resolution is not significant when compared with the bandpass filtered data. Consequently, a seismic model employing a variable source wavelet was considered.

Figure 3.4 Characteristics of the Shaping Operator for Spike Deconvolution

- a) Input - the prefiltered (2.5-30 Hz) source signature (for the 3 lb charge).
- b) Output - a unit spike delayed 53.2 msec (in the middle between the two maxima on the source wavelet).

(The parameters of the operator are: filter length=90, source wavelet length=50, length of the Parzen window=50, limit for the spike position=18. The lengths are given in samples; sampling interval is 2.8 msec.)

INPUT



OUTPUT

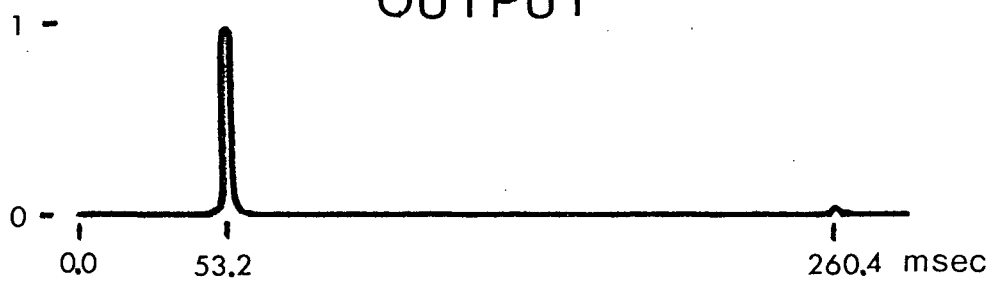


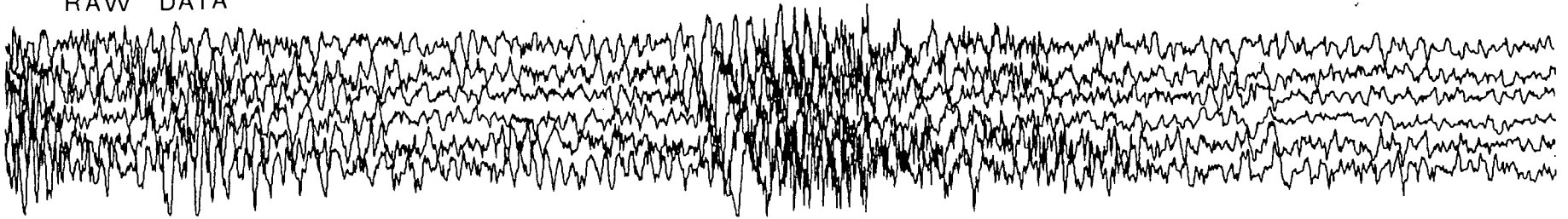
Figure 3.5 Example of the Application of Spike
Deconvolution to a Reflection Seismogram.

The signal resolution of the deconvolved section is compared with the resolution of the unfiltered and filtered traces.

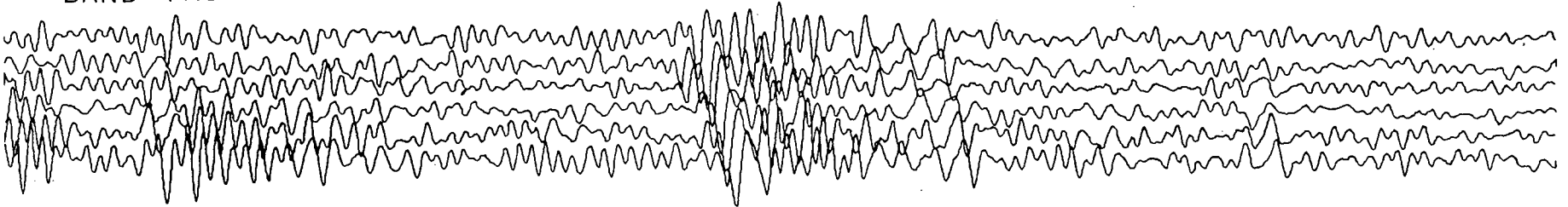
(The single trace used to exemplify spectral divisional deconvolution in Fig. 3.4 was one from this seismogram.)

SPIKE DECONVOLUTION

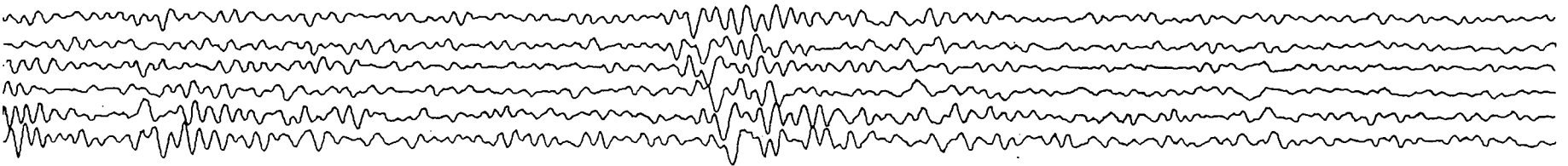
RAW DATA



BAND PASS FILTER 0.5-30 Hz



DECONVOLUTION WITH SOURCE



6

7

8

9

T sec

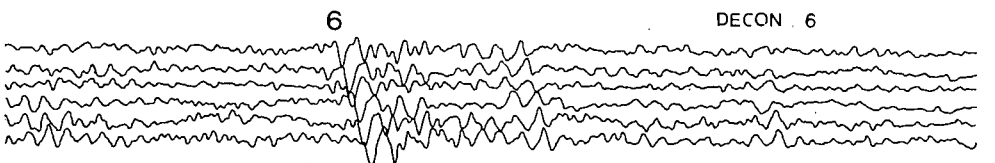
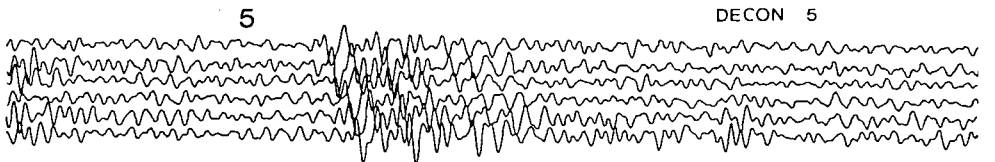
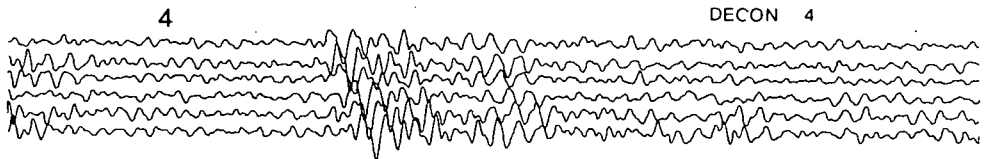
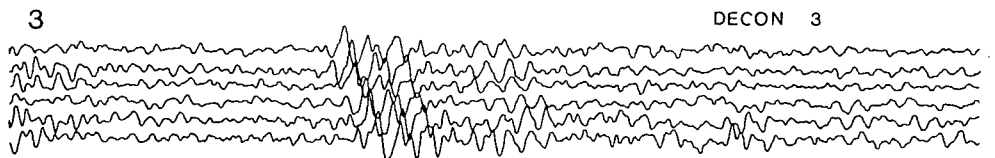
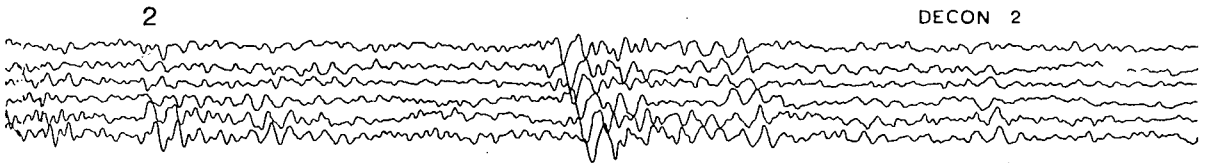
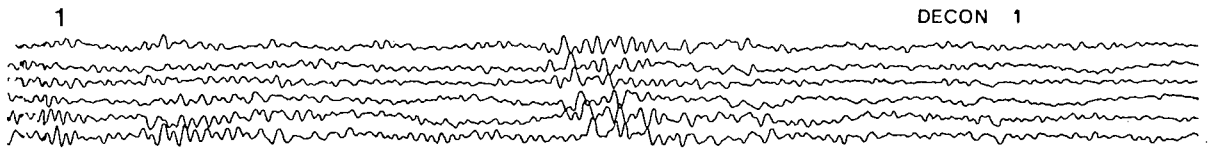
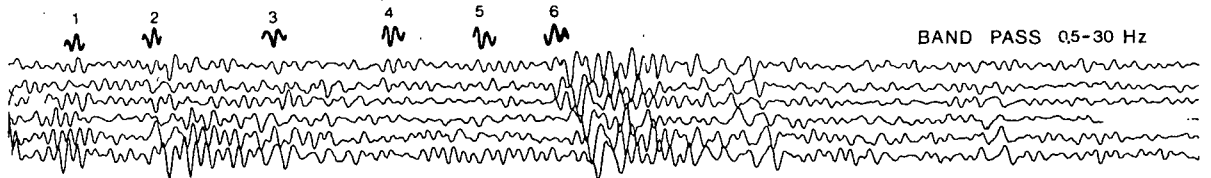
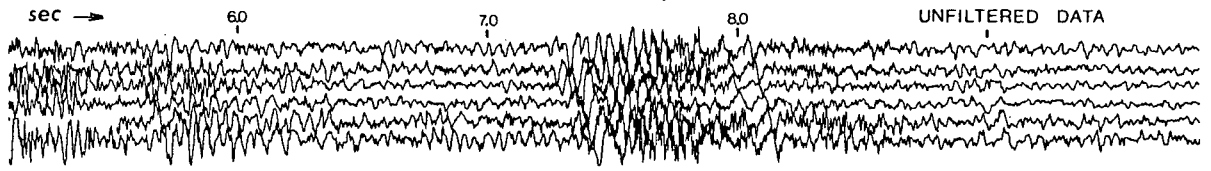
B) Spike Deconvolution with Variable Wavelet

For spike deconvolution with a variable wavelet, a segment of the seismic trace was used as the source wavelet. Such a wavelet results from two-way transmission of the source signature through the layers of the crust, and changes with each reflecting horizon. The variable wavelet is the most probable seismic phase picked along the seismogram within a particular time interval. Only those events are chosen which can be correlated over the record section or significant part of it (at least 3 shots). Thus for a given interval the correlatable phases are chosen, and for each of them a spike operator is designed. These are then individually applied to the seismic traces. Such a procedure is a simplified approach to more expensive time adaptive deconvolution in which the wavelet changes continuously with time as the operator is being applied along the trace.

The effects of the deconvolution on the data are displayed in Fig. 3.6. Six examples of deconvolution with different wavelets, chosen from the filtered reflection record, are shown. Analysis of the deconvolved traces reveals an improvement in the resolution of the seismograms for the interval from which the wavelet was chosen. In addition, there is a general improvement in the signal/noise

Figure 3.6 Example of the Application of Deconvolution with a Variable Wavelet to Seismograms

Six different wavelets picked along the uppermost trace of the bandpass filtered data were used. The location where a particular wavelet was picked and its shape are indicated. The numbers on subsequent deconvolved records show the time intervals corresponding to the choice of wavelet.



ratio.

Since the deep crustal reflections were expected in the interval before the first water bottom multiple arrival, an attempt to delineate seismic phases particularly in this interval was made. The application of spike deconvolution with variable wavelet indicated that time adaptive deconvolution would be the most appropriate method for such enhancement. It is possible that any reflection arrivals from deeper horizons, such as M-discontinuity and upper mantle layers, are obscured by the bottom multiple. To remove this multiple, predictive deconvolution (Peacock and Treitel, 1969) should be applied. However, for fiscal and time reasons this was not attempted as part of this research project.

3.4 Stacking of Refraction Data

Stacking is a signal enhancement technique which improves the signal/noise ratio and reduces the amount of data to be analysed while maintaining the seismic information. In order to stack multichannel data, summation along a predetermined lag trajectory is performed. The lag trajectory is defined by the paths of signals which are received at different distances. For refraction arrivals,

the trajectory is a straight line.

For stacking of refraction data, optimum stacking velocities for each seismic phase should be determined. This implies a time-varying velocity for stacking. As an alternative to such a difficult procedure, stacked traces using various stacking velocities corresponding to first and later seismic arrivals along the traces were computed. These showed little difference between them. This is a result of the fact that the six traces were recorded over a total distance of only 450 m and that the velocity contrast at the ocean bottom refracts all rays corresponding to head waves into near-vertical paths. Thus the stacking velocity to be used was not critical and so was chosen to correspond to that velocity determined from the first refraction arrivals. It was determined from the slope of the line connecting the first refraction arrivals which appeared most frequently.

The six refraction traces for each shot were stacked to give a single trace. Fig. 3.7 compares an unstacked refraction record section with the corresponding section of stacked traces. The seismic signals on the stacked traces are enhanced due to improvement in the signal/noise ratio. Seismic phase resolution is increased along each stacked trace. (As an example, note two distinct phases between 7 and 8 sec on the trace for shot 30 compared to a single train of amplitudes on the corresponding unstacked traces.)

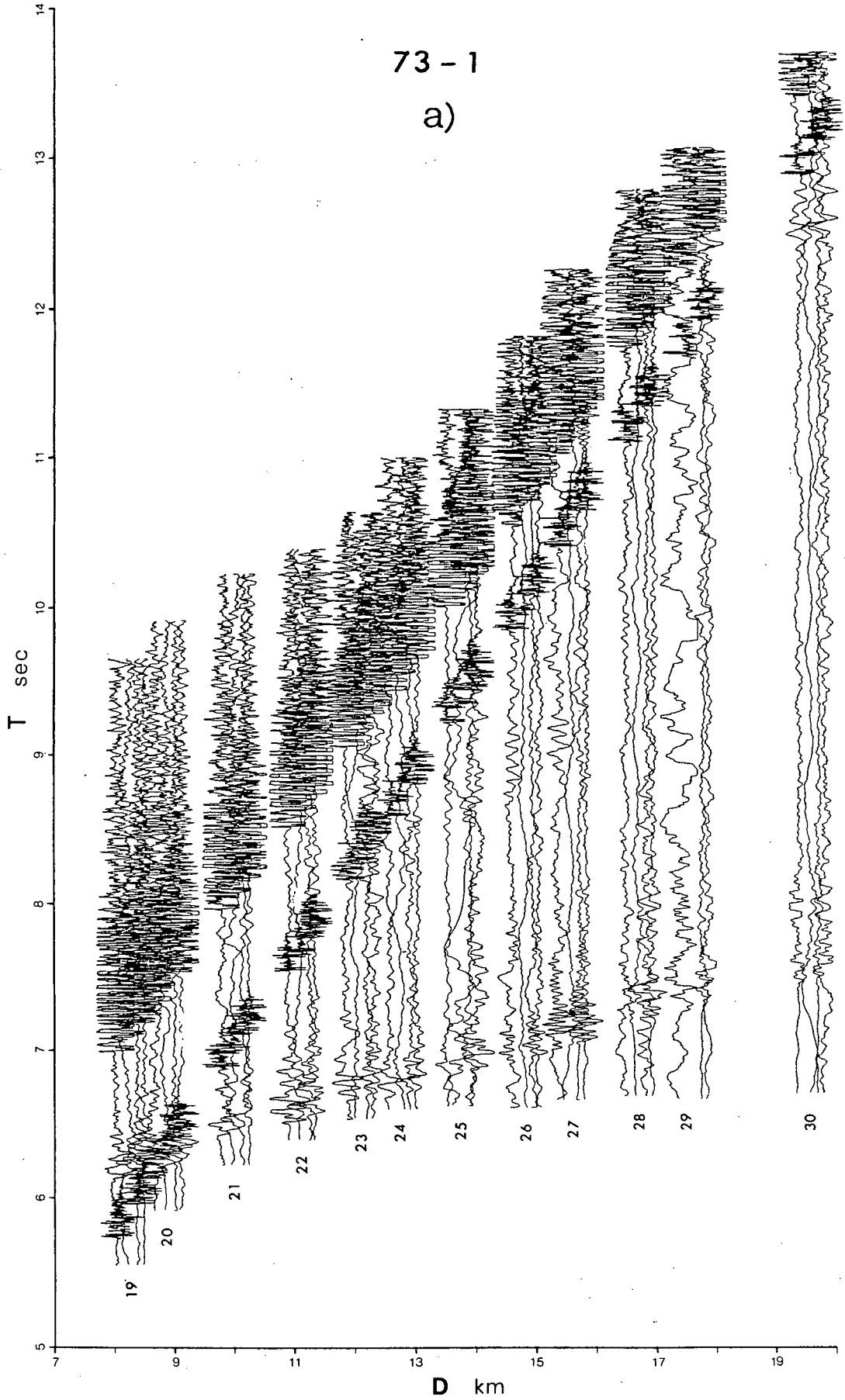
Figure 3.7 Unstacked and Stacked Refraction Record Sections from AREA 1

a) Unstacked section. The first refraction arrivals are seen between 6 and 8 sec. The short high frequency wave train consists of the direct arrivals; the large amplitude wave train arriving later are reflections from the water bottom and below. (Because of the high noise level only exemplary traces for each shot were displayed to be able to follow each trace on the section.)

b) Section of the stacked data with the stacking velocity of 4.5 km/sec (a typical velocity for basement). Six traces for each shot were stacked to give a single trace.

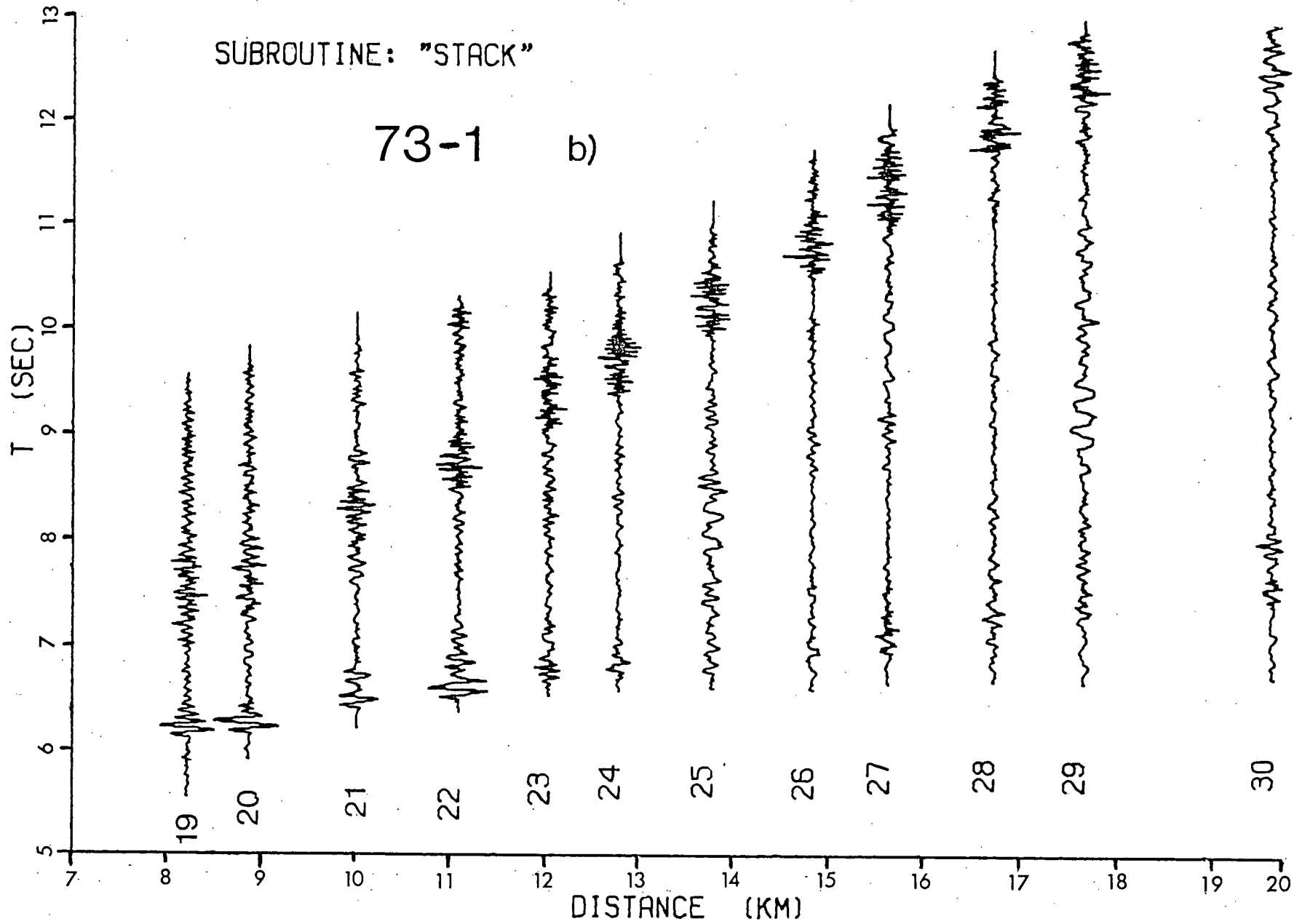
73 - 1

a)



SUBROUTINE: "STACK"

73-1 b)



However, because of greater intervals between stacked traces some of the refraction arrivals are more difficult to correlate across the seismic section. Therefore, both stacked and unstacked sections were used for further interpretation, depending on procedures being followed.

3.5 Velocity Analysis of Reflection Data

A computational method using velocity spectra was considered to determine the layer velocities from the reflection record sections of expanding profiles. A velocity spectrum is a graphical display of the reflection energy as a function of the normal incidence traveltime and the average root-mean-square (rms) velocity. The rms-velocity was defined by Dix (1955) as

$$\bar{V}_n^2 = \frac{\sum_1^n v_i^2 T_{0,i}}{\sum_1^n T_{0,i}} \quad (3.5-1)$$

where \bar{V}_n is the average rms-velocity from the surface down to the bottom of the n-th layer, v_i is the interval velocity of the i-th layer, and $T_{0,i}$ is the two-way normal incidence traveltime in the i-th layer. The velocity spectra enable us to measure the power of reflections arriving according to various paths determined by their time-distance

relationships.

Approximating the lag trajectory for the reflecting parts of expanding profiles by a hyperbola, the time-distance relationship can be expressed in the form

$$T_{x,n}^2 = T_{0,n}^2 + \frac{X^2}{V_{st}^2} \quad (3.5-2)$$

where $T_{x,n}$ is the two-way traveltime for a shot-to-receiver distance X , and the layer n , $T_{0,n}$ is the vertical two-way traveltime, and V_{st} is the stacking velocity. How much this stacking velocity differs from the true rms-velocity depends on the value of the spread-length/depth ratio. Al Chalabi (1973) has shown that for values less than 1 the discrepancy is less than 0.5%, and for values less than 2.0 it is less than 2%. In our case, since the depth of water was always more than 2 km, only the reflection arrivals from the first 4 km distance were used for determination of the velocities.

In order to display the reflection energy in the form of velocity spectra, measures of the coherency of the signal along hyperbolic paths defined by (3.5-2) are used. After the alignment of the input data with respect to a given hyperbolic delay pattern, a simple digital filter that would selectively pass events common to all traces is computed for each trace. Then, these are stacked together to give the best estimate of the input signal. The power of this

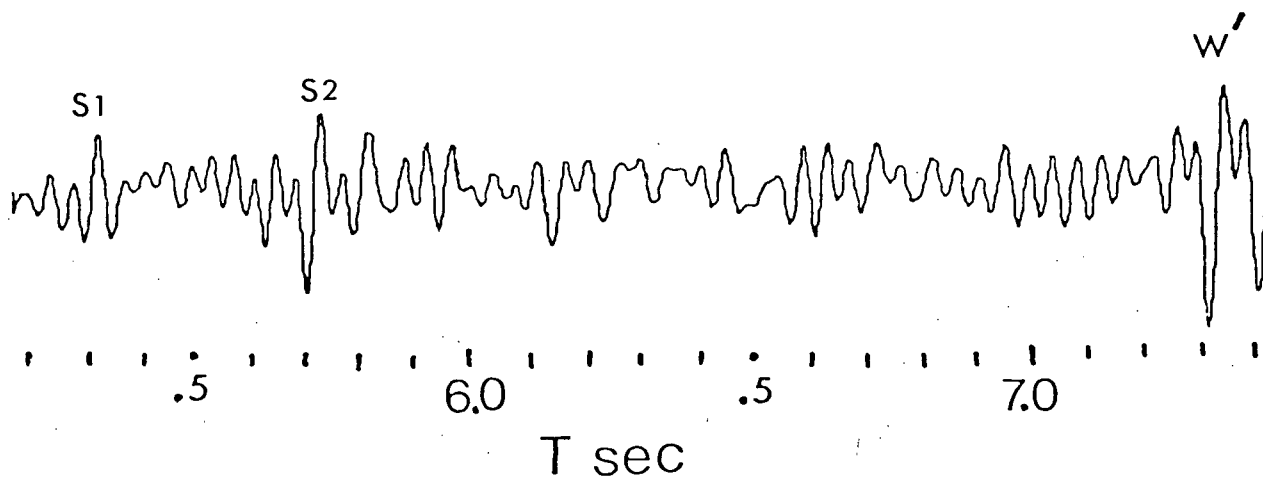
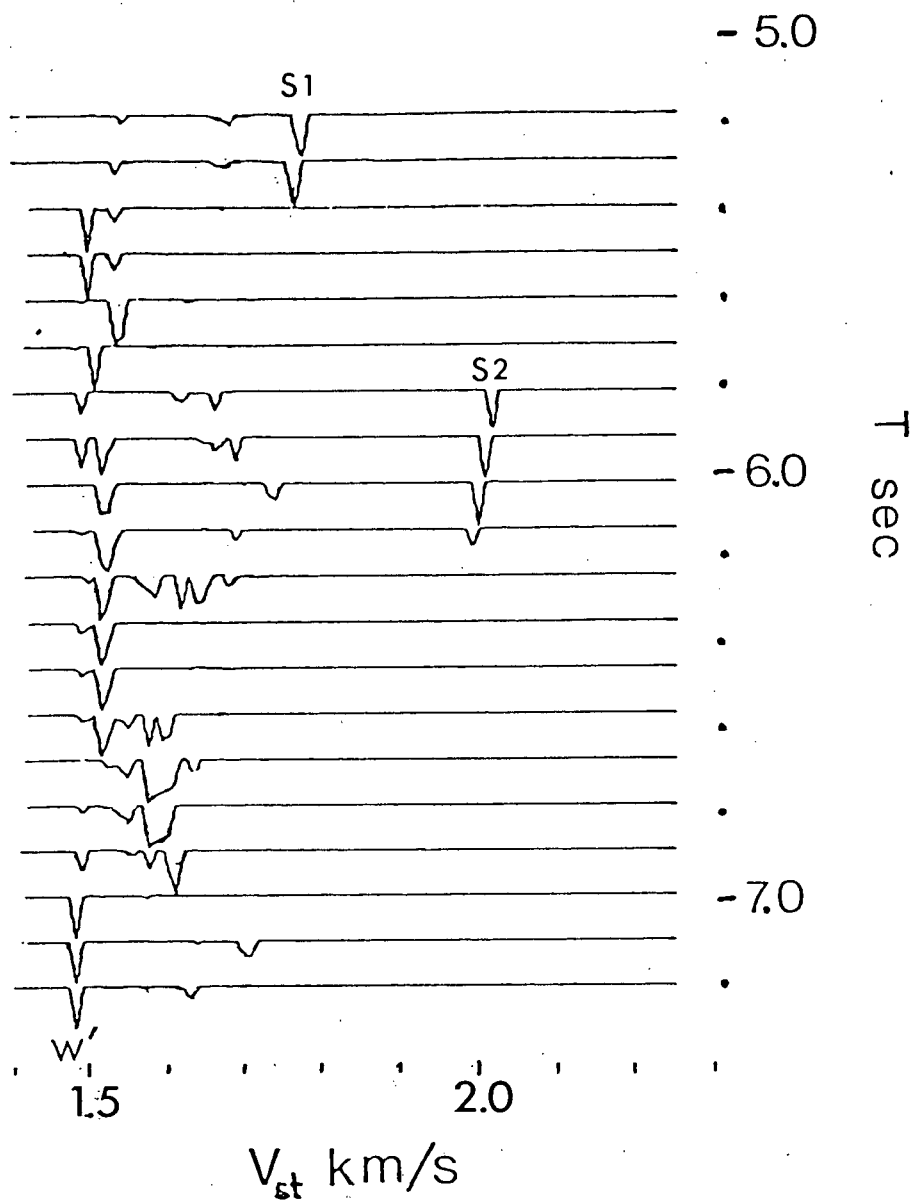
estimate is then computed within a specified time gate around the reference time and this power is displayed. In order to generate a velocity spectrum, the seismic traces are swept with various hyperbolas determined by the velocities in a chosen interval for the same reference time. Then another reference time point is chosen at a time interval equal to half the specified time gate and the procedure is repeated. The coherency measures express in a quantitative form the likeness of the data content among data channels. A computer program for deriving and displaying velocity spectra with the use of different measures of the coherency of signals was written. A fortran listing of the program is in the Appendix. Three different techniques for measurement of coherency along hyperbolic paths were applied: summation, unnormalized crosscorrelation and semblance coefficient. All three are time domain techniques and the latter two are well described by Neidel and Taner (1971). Summation is a coherency measure giving an estimate of total signal amplitude within a particular time gate. It is obtained by simple summing of the signal amplitudes or their powers within the gate. Unnormalized cross-correlation measure is equal to half the difference between the total energy and signal energy within the gate. Semblance coefficient is defined as the ratio of signal energy to total energy within the gate. The results obtained by their

use were compared. An advantage of semblance is that it requires a smaller dynamic range for the display of the total signal amplitude than summation or unnormalized cross-correlation, when signal/noise ratios remain greater than unity (Neidell and Taner, 1971). Since it also had the best resolution compared with the two other techniques, it was chosen for the generation of velocity spectra. To illustrate the use of the coherency measures as they were applied to our data, the characteristic parameters are given here: time gate 56 msec, time step 14 msec, minimum velocity 1.4 km/sec, maximum velocity 10 km, velocity step 0.1 km/sec.

The semblance was used at first for data from a single shot (6 seismic traces), and then for the first four neighbouring shots (24 seismic traces). The former one is displayed in Fig. 3.8. The computer program for displaying the velocity spectra was designed to increase the spectrum resolution by spiking the coherency measure amplitude. In spite of that the spectrum resolution in the figure is poor. The amplitudes have a tendency to spread along the velocity axis without showing a single peak maximum. This means that the measure of coherency does not have a sharp single maximum within the corresponding time gate. This is due to the small time differences between the ray-paths to the individual hydrophones (the layer depths were about 2500 m and more while the hydrophones were only 90 m apart). The

Figure 3.8 Velocity Spectrum for Six Seismic Reflection
Traces of the Profile 73-5

The spectrum is shown at the top. It was obtained using semblance coefficient as the measure of coherency of the signal across six seismic traces recorded at distances near 2.5 km. One of the traces is displayed at the bottom of the figure. The section between 5 and 7.5 sec (two-way) traveltime was chosen because deep crustal reflections arrive in this interval. The seismic arrivals S1 and S2, and the first water bottom multiple W' from the trace appear clearly in the spectrum. The remaining peaks in the spectrum are mostly deformed and do not give velocities which could be associated with the deep crustal reflections.



results obtained by applying the semblance to a group of shots did not show the necessary consistency. The inaccuracy in determination of the origin times for individual shots (10-20 msec) limited the effectiveness of the crosscorrelation procedure.

Since the computer derived spectra are not sensitive to individual seismic traces (displaying the signal coherency of the stack) and their velocity resolution was poor for the kind of data we had, it was abandoned. A simpler method of travelttime squared versus distance squared (T^2-X^2) graphs (Dix, 1955) was adopted for velocity analysis and interpretation of the reflection data. The method is explained and presented together with the interpretation of the data in the following chapter.

4 INTERPRETATION

4.1 Methods of Interpretation

In order to obtain an initial model of the oceanic crust in each area of recording, seismic refraction arrivals were first interpreted. For this, both traveltime and amplitude information were used by application of traveltime plots and synthetic seismograms. After establishing the initial refraction models, the reflection data were interpreted. Layer velocities and thicknesses were computed using T^2-X^2 lines with application of the least-squares method. Finally, detailed velocity-depth models based on the reflection and refraction data are presented and their geological implications are given.

TRAVELTIME INTERPRETATION - REFRACTION DATA

The simplest method used for the interpretation of marine refraction data is the slope-intercept method (Ewing, 1963) which uses traveltime plots. The method is

based on a seismic model consisting of homogeneous horizontal layers where with increasing depth each subsequent layer has a higher velocity. Because of the non-applicability in certain situations of these assumptions the slope-intercept method sometimes may lead to artificial velocity-depth models.

The traveltime plots used to derive the initial velocity-depth models were constructed from refraction arrival picks made on computer plotted seismograms. The maximum error in timing of the arrival picks was about 15 msec due to the low signal/noise ratio on some traces. Therefore, together with the error associated with the origin times, the estimated maximum traveltime error was about 35 msec.

An example of a traveltime-distance plot is given in Fig. 4.1. The straight lines are least square fits to the refraction arrival points. The reciprocal of the slope for each line is the refraction velocity of the corresponding layer; the time intercept determines the layer thickness. The velocity-depth models based on these parameters were then used as initial models for the generation of synthetic seismograms consistent with the observed traveltime curves and amplitudes.

TRAVELTIME AND AMPLITUDE INTERPRETATION-REFRACTION DATA

The interpretation of seismic body waves consists of finding a range of velocity-depth models which would match the observed traveltime and amplitude information. The number of models which are consistent with the traveltimes of seismic arrivals is generally quite large (McMechan and Wiggins, 1972; Wiggins and Helmberger, 1973; Bessonova et al., 1974). However, the number is considerably reduced by the requirement of their consistency with the observed amplitudes (Helmberger and Wiggins, 1971; Wiggins and Helmberger, 1973; Fuchs and Muller, 1971).

The computer programs used for derivation of synthetic seismograms in this work are based on the disc ray theory introduced by Wiggins (1976). The method was derived from quantized ray theory (Wiggins and Madrid, 1974), and named disc ray theory (DRT) because the model of wave propagation is given in terms of planar discs guided by rays.

In order to generate synthetic seismograms matching both traveltime and amplitude information the initial velocity-depth models were expressed in terms of ray parameter versus epicentral distance (p - Δ) curves. These were derived with the use of a computer routine called MDLPLT by Wiggins. Using a specified velocity-depth model and a digitized source wavelet as input, the program

generates traveltimes curves, p - Δ curves and synthetic seismograms as the output. To test for consistency, the computed traveltimes curves were compared with the observed ones. The p - Δ values were then used as input for the computer program called HRGLTZ, also by Wiggins.

For the interpretation a trial-and-error procedure was followed. From the initial p - Δ curve, traveltimes curves and synthetic seismograms were generated using HRGLTZ and compared with the observed data. If necessary, the p - Δ curves were modified to match the amplitudes and the calculation repeated until the synthetic seismograms were consistent with the recorded data. Since both traveltimes and amplitudes were to be matched, a trade-off between the two was sometimes necessary. Examples of a set of stacked seismograms and of a synthetic record section are shown in Fig. 4.3 and Fig. 4.9. The resultant velocity-depth models derived from the refraction data were used as a check on the models obtained from the interpretation of the reflection data.

TRAVELTIME INTERPRETATION - REFLECTION DATA

If seismic traces are displayed according to their distances, reflection arrivals from common reflectors appear along particular hyperbolic paths. When plotted as a traveltime squared versus distance squared (T^2-X^2) graph, they give straight lines of different slopes and intercepts. The reciprocals of the slopes determine the average rms-velocities from the surface to the bottom of a particular reflector, and the intercepts determine the normal incidence arrival times and hence the depth to the reflectors (Dix, 1955). It should be mentioned that, since the time arrivals on the record section are picked visually, the T^2-X^2 method is a subjective one and its accuracy largely depends on the interpreter's ability to recognize and correlate the reflection arrivals on seismograms. From the average (surface to reflector) rms-velocities and intercept times determined from the T^2-X^2 graphs, the true rms-velocities and thicknesses of individual layers can be calculated.

Let the average rms-velocity from the surface down to the top of the k -th layer be V_{k-1} . The corresponding normal incidence two-way traveltime is T_{k-1} . From the surface to the bottom of the k -th layer they are V_k and T_k respectively. Then according to the expression (3.5-1) the interval rms-

velocity for the k-th layer is given by

$$V_k^2 = \frac{\bar{V}_k^2 T_k - \bar{V}_{k-1}^2 T_{k-1}}{T_k - T_{k-1}} \quad (4.1-1)$$

The detailed velocity-depth models obtained from the reflection data are based on such analyses.

4.2 Velocity-depth Models

The data from AREA 1 were analysed first in order to compare the results with a previously known refraction model. AREA 3 was approached next because the quality of the reflection data was best and the crustal structure in the area was presumably more normal than that of AREA 2. Therefore, interpretation was expected to be more straightforward. After acquiring experience from these interpretations, the data from the more tectonically complex AREA 2 were analysed and interpreted.

AREA 1

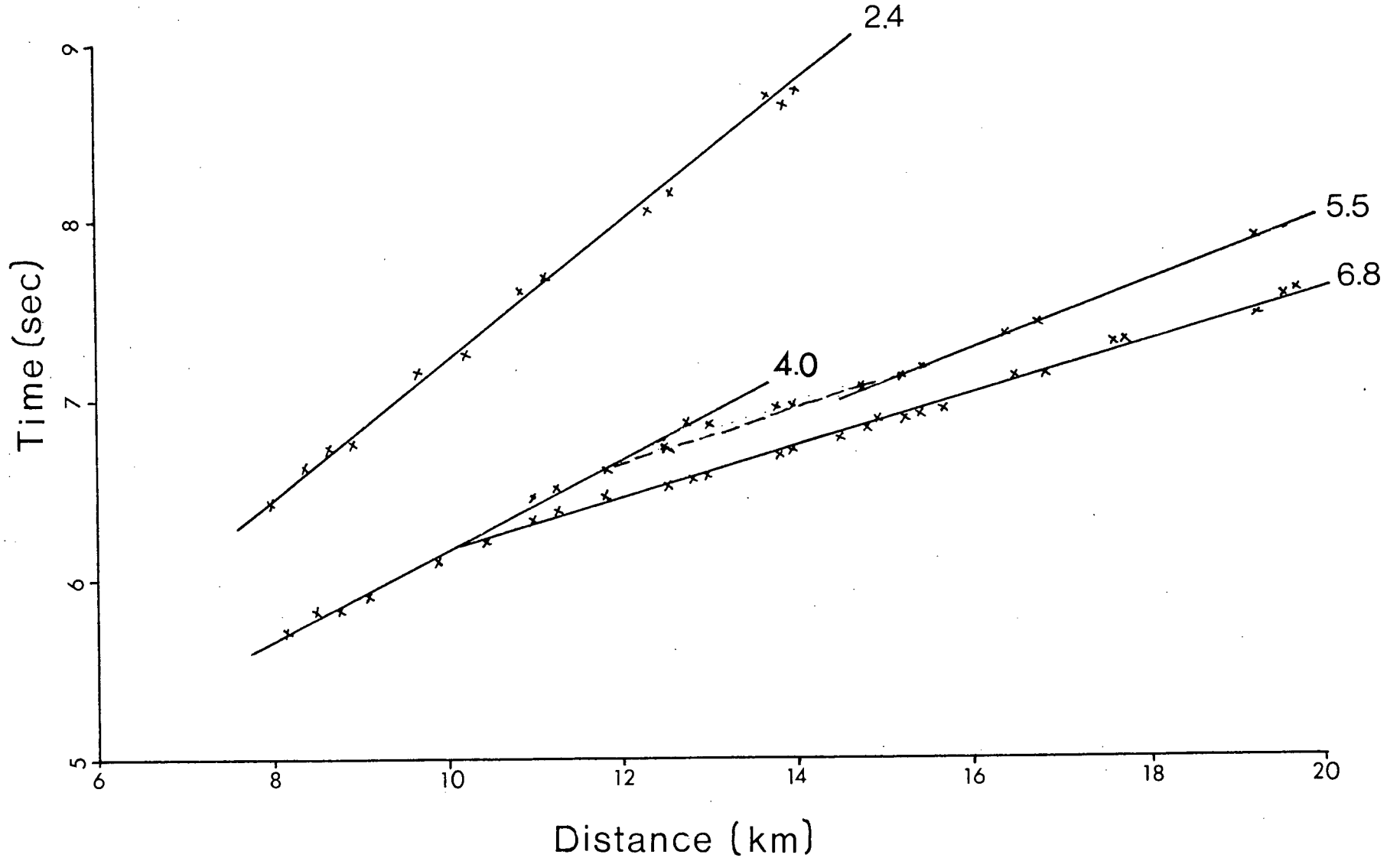
Since the reflection data from AREA 1 were of poor quality, only the refraction part of the expanding profile was interpreted; the record section is shown in Fig. 3.7. A travelttime plot based on the analysis of individual traces was used for the interpretation and the resulting velocity-depth model compared with the model of Keen and Barrett (1971) from the 'HUDSON 70' seismic survey in the area (Fig. 2.4a).

The analysis of the travelttime plot (Fig. 4.1) shows that: 1) the refractions from the sediments were never observed as first arrivals; 2) the refraction arrivals from the basement give a curve with two branches of velocities 4.0 and 5.5 km/sec, the refractions of velocity 4.0 km/sec appeared as first arrivals over a short distance interval (8-10 km); 3) the refractions from the oceanic layer appeared as first arrivals for most of the length of profile (from 10 to 20 km) and gave the velocity of 6.8 km/sec; 4) the profile was too short to observe upper mantle refractions. In general, to distinguish the phases of the first arrivals from those arriving immediately after was difficult. In particular to distinguish the oceanic layer arrivals from the basement refractions for distances from 10 to 17 km was a problem. Their clear separation could be

Figure 4.1 Traveltime - Distance Plot of the Refraction Profile
73-1 from AREA 1

The lines correspond to individual refracting horizons. The associated velocities are given in km/sec at their ends. Line with the velocity 2.4 km/sec corresponds to the sediments, lines with velocities of 4.0 and 5.5 km/sec to the upper and lower part of the basement, and line with the velocity of 6.8 km/sec to the oceanic layer. (The lines are least-square fits to the observed arrival times.)

73-1



followed only near the end of profile (from 17 to 20 km). There is a possibility of a velocity gradient in the basement layer which is indicated by a dashed line connecting the branches of the basement traveltime curve between 12 and 15 km.

The velocity-depth model based on this traveltime plot is compared with the 'HUDSON 70' model in Table 1. The symbols V and H in the table, are velocity (km/sec) and layer thickness (km) respectively. The errors given include the timing errors (from picking the individual arrivals) and the standard deviations (from the line fits to the picked points).

TABLE 1

Layer	'ENDEAVOUR 73'		'HUDSON 70'	
	V	H	V	H
Sediment	2.4±.2	0.6±.2	2.3**	0.5
Basement	4.7*	2.4	4.5*	1.6-2.4
a	4.0±.2	1.1±.3		
b	5.5±.2	1.5±.4		
Oceanic	6.8±.2		6.7-7.0	4.7*

*Indicates an average value, ** an assumed value.

The mean value of 4.5 km/sec for the basement velocity in 'HUDSON 70' model assumes a velocity gradient for the layer from 4.0 to 5.5 km/sec. In our case, assuming that there is a velocity gradient (between 4.0 and 5.5 km/sec) in

the basement layer, we have obtained a mean velocity of 4.7 km/sec. The average value for the thickness of the oceanic layer in 'HUDSON 70' model as presented here does not consider an anomalous value of 8.5 km recorded at the north station on one of the profiles. This station was the furthest from our profile. The thickness of the oceanic layer could not be determined in our model because the profile was not long enough to observe mantle refractions.

In conclusion, in spite of the small amount and poor quality of the recorded data, the velocity-depth model of AREA 1 shows good agreement with the 'HUDSON 70' model of Keen and Barrett (1971).

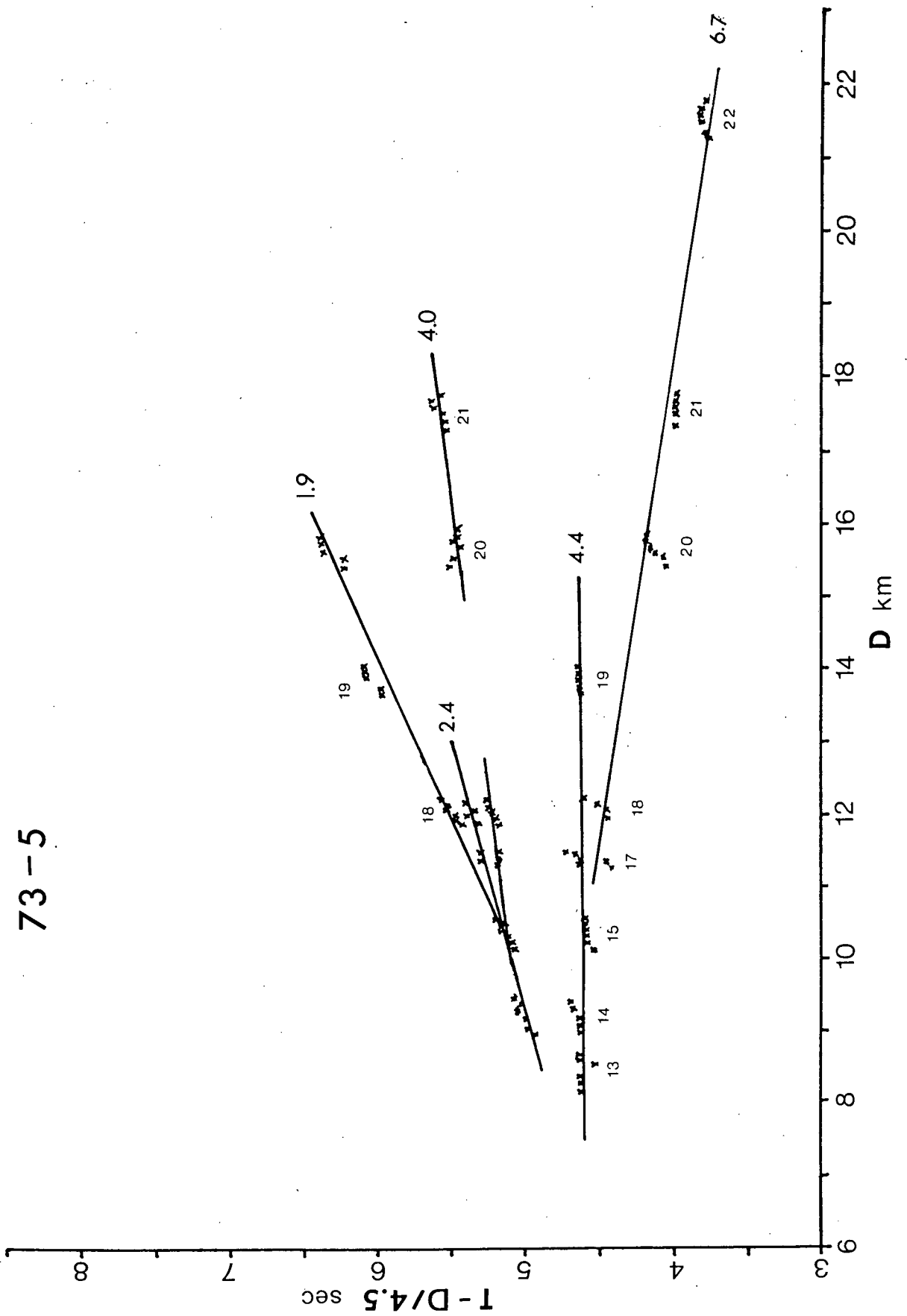
AREA 3

The initial velocity-depth model for AREA 3 in the northern Cascadia Basin was based on the interpretation of the refraction part of the expanding profile 73-5 shown in Fig. 2.8b. From the analysis of individual seismic traces a travelttime-distance plot was constructed (Fig. 4.2). It shows that 1) the refractions from the sediments were not observed as first arrivals; as secondary arrivals they indicate a possibility of two distinguishable sedimentary layers with velocities of 1.9 and 2.4 km/sec; 2) the

Figure 4.2 Reduced Traveltime - Distance Plot of the Refraction Profile 73-5 from AREA 3

A typical velocity of 4.5 km/sec for basement layer was used to reduce the traveltimes. The small numbers beside the data points are the shot numbers. The associated velocities in km/sec are given at the end of each line.

73-5



refraction arrivals with the velocity of 4.0 km/sec did not appear as first arrivals but are clearly distinguishable on shots 18, 20 and 21; 3) the refractions giving the velocity of 4.4 km/sec basement showed as first arrivals only over a short distance interval between 8 and 11 km; 4) the refractions from the oceanic layer appeared as first arrivals at a distances of about 16 km and could be followed to the end of the profile at the distance of 22 km; 5) the profile was not long enough to observe the refractions from the M-discontinuity.

From the slopes and intercepts of the travelttime lines, the velocities and depths of the layers were determined and the initial velocity-depth model is presented in Table 2.

TABLE 2

Layer description		V	H
Water		1.5	2.5
Sediment	a	1.9	1.3
	b	2.4	0.7
Basement	a	4.0	0.7
	b	4.4	1.7
Oceanic		6.7	

The symbols V and H in the table are velocity (km/sec) and thickness (km) respectively. This initial velocity-depth model was used for the generation of synthetic seismograms.

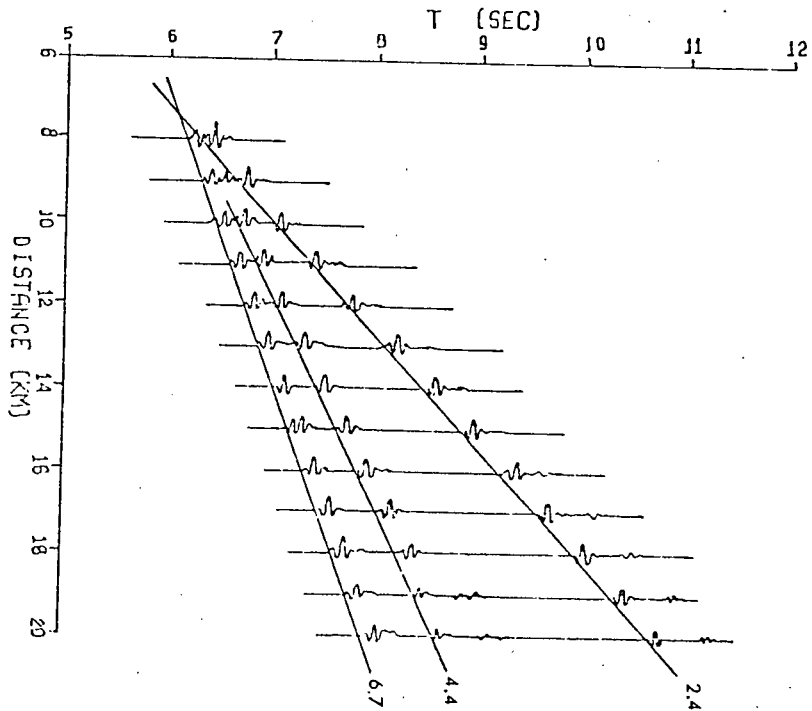
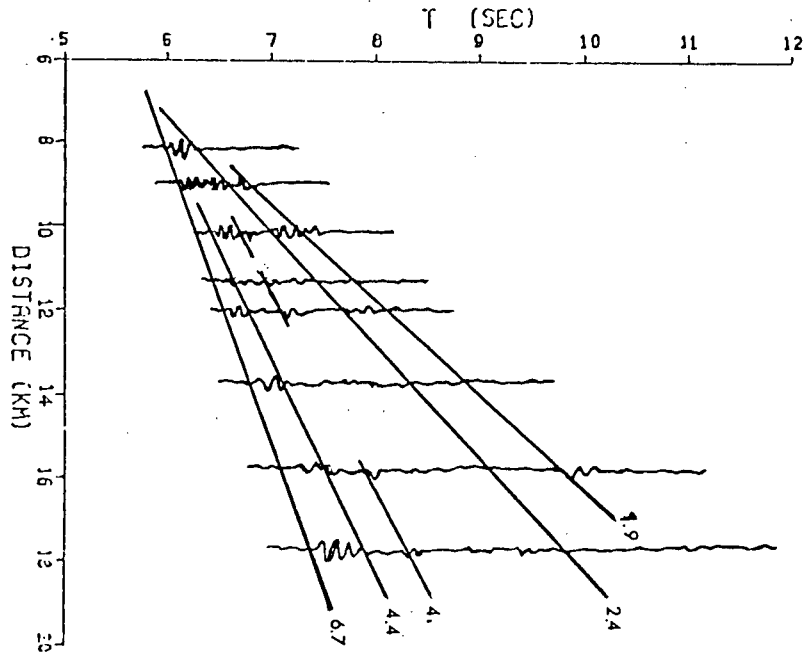
The section of the synthetic seismograms is compared with the stacked recorded data in Fig. 4.3. The refraction arrivals with the velocities of 2.4 km/sec (lower sediments), 4.4 km/sec (basement) and 6.7 km/sec (oceanic layer) are observed on both sections. The upper sediment arrivals with the velocity of 1.9 km/sec and the refractions from the transition between the sediments and the basement do not appear on the synthetic seismograms. The former could be explained by a possibility that there is a small velocity gradient in the sediments (slight changes in the amplitudes caused by such gradient would be difficult to observe on small amplitudes.) The latter could be explained similarly by a small velocity gradient in the upper part of the basement. Another possible explanation is that the velocity corresponds to an irregular transition layer with an average thickness less than the limit of the HRGLTZ program resolution for the given velocity (4.0 km/sec) and the input wavelet frequency (12 Hz). The results of attempts to generate these arrivals would indicate this. When the layer was modelled 0.7 km thick (value calculated from the traveltimes plot), it was not possible to match the generated refractions from the oceanic layer with those recorded. The match of these was achieved only when the transition was modelled as a thin layer (0.3 km). However, such a thin layer did not give any observable refractions on the

Figure 4.3 Comparison of the Observed and Synthetic Seismograms
Sections Of Refraction Profile 73-5

Left - record section of stacked seismograms.

Right - record section of synthetic seismograms.

(As discussed in the text, the arrivals with velocities of 1.9 km/sec and 4.0 km/sec from the section of stacked seismograms could not be included in the section of synthetic seismograms.)



synthetic seismograms.

Fig. 4.4 shows the record section of the filtered reflection data from the expanding profile 73-5, and Fig. 4.5 the record section of the filtered data from the near-vertical incidence reflection profile 73-6. Coherent seismic arrivals from individual reflecting horizons can be distinguished and correlated on parts of either or both profiles.

A series of sedimentary reflections arrives within the time interval of about 1.7 sec (two-way) traveltime after the first water bottom reflection. The first identifiable reflections from within the sediments are from the reflecting horizon A. This reflector can be followed clearly along the section 73-6 and is characterized by a sudden change in both frequency and amplitude. Following the continuity of this horizon on the expanding profile 73-5 is difficult because the amplitudes in this time interval were often distorted due to the high gain settings of the amplifiers as mentioned before. The arrivals from reflecting horizon B on the expanding profile are easy to identify along the section. The reflecting horizon C can be followed clearly on section 73-5, but its identification on section 73-6 is more difficult. Horizons D and E which show on the near-vertical incidence reflection seismograms on both sections are impossible to follow beyond the distance of 3 km.

Figure 4.4 Record Section of the Expanding Reflection Profile
73-5 from AREA 3

The water depth was 2.5 km. The data were bandpass filtered (2.5-30 Hz). The letters designate reflecting horizons: W- reflection from the water bottom, A to C- reflections from sedimentary horizons, D to G- reflections from the top of the basement and beneath. The primed letters designate first-order multiples of these reflections. (Note the emergence of the refracted waves as first arrivals between 8 and 10 km.)

73 - 5

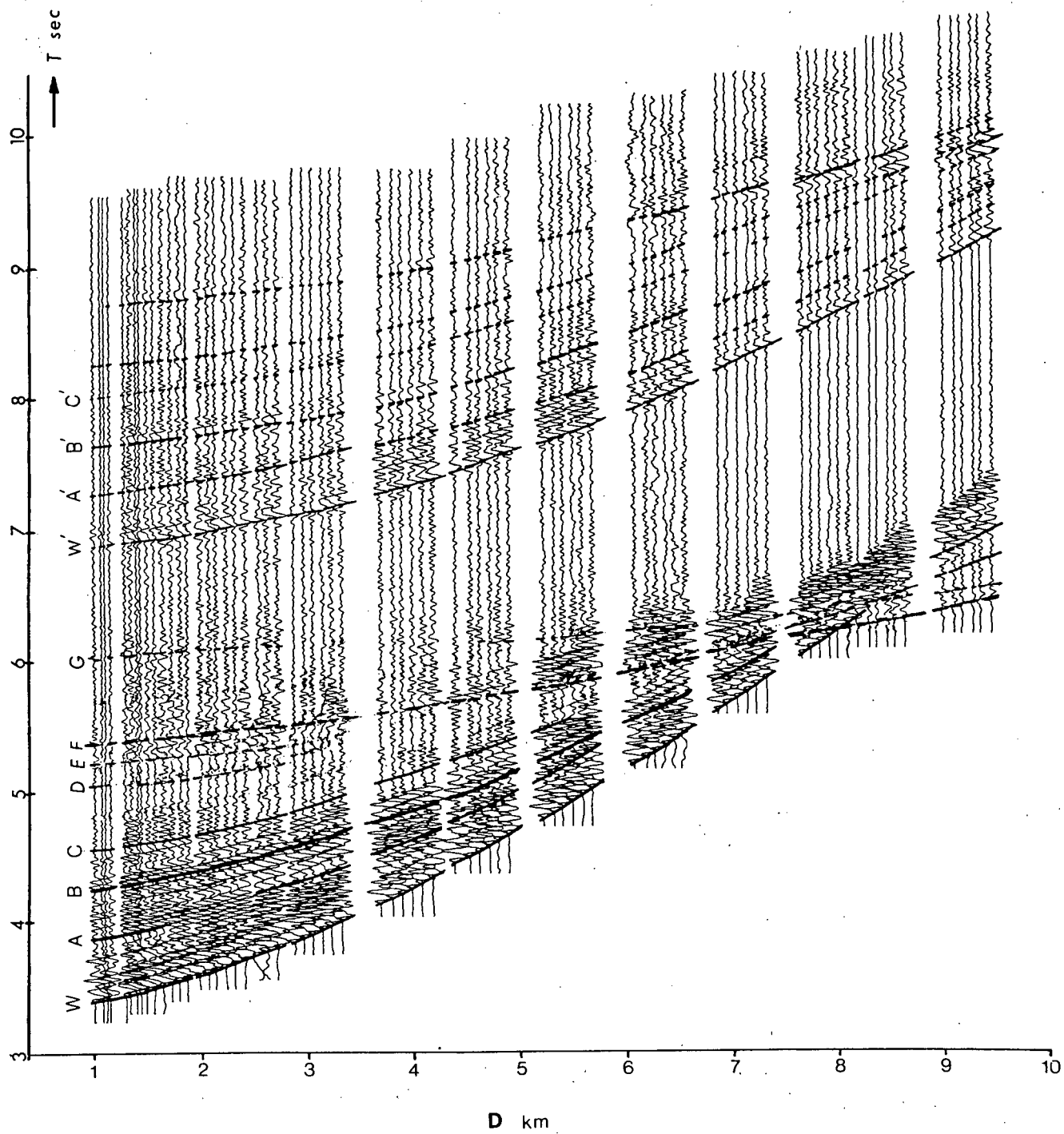
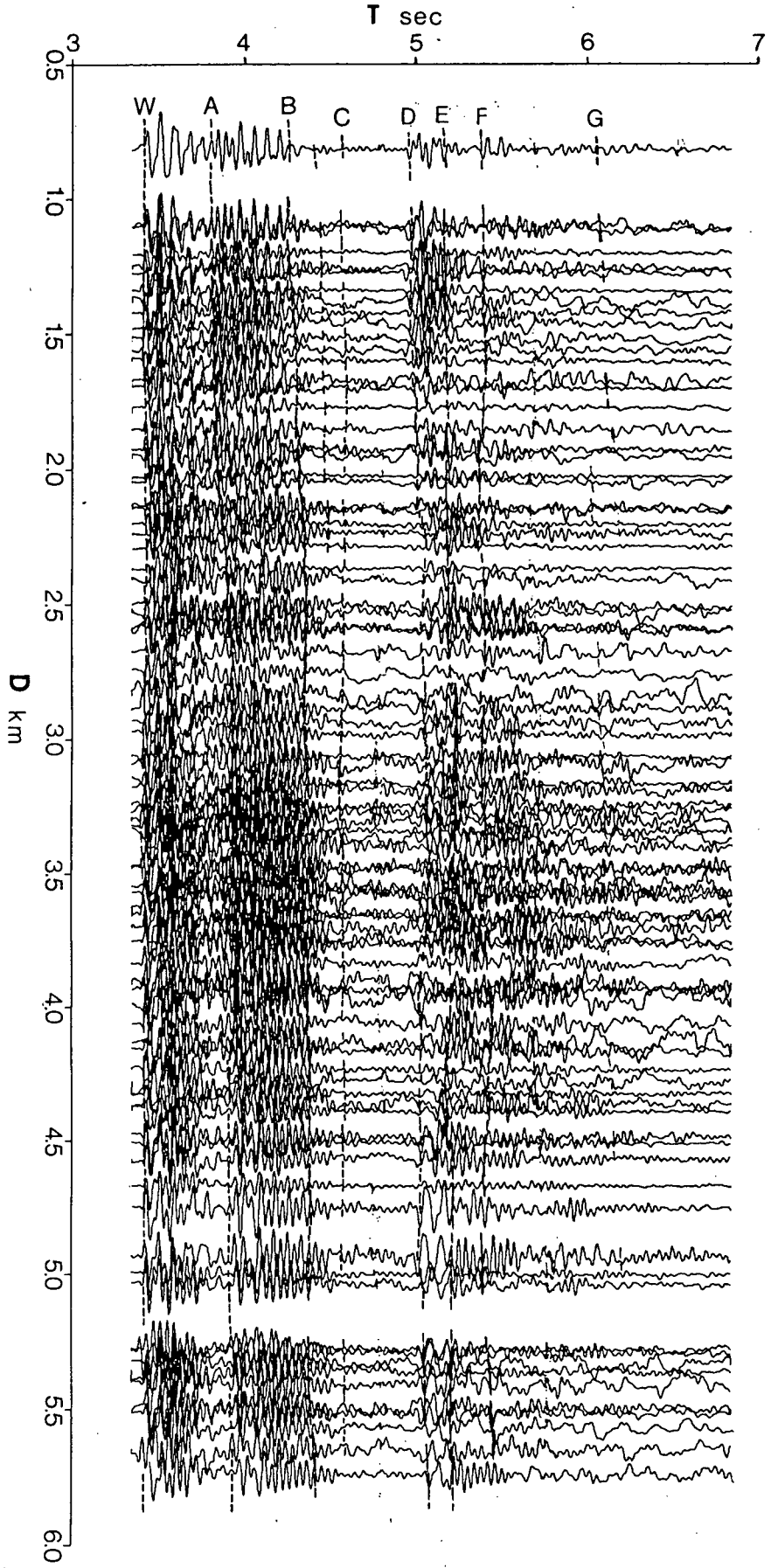


Figure 4.5 Record Section of the Quasi-continuous Subcritical Profile 73-6 from AREA 3

The letters designate the same primary reflections identified on the expanding profile 73-5 in Fig. 4.4. (The individual arrivals are discussed in detail in the text.)



73-6

Arrivals from horizon F, which appear in the interval of possible basement reflections, are clear on section 73-6 and can be correlated to the end of the expanding profile, although they are less clear on 73-6. Horizon G gives reflection arrivals which can be distinguished on the near-vertical incidence seismograms, but it is difficult to identify them on the wide-angle seismograms, particularly for the distances between 3 and about 5 km. After that they appear again and in the interval from 7 to 9 km they arrive almost simultaneously with other reflection phases and cannot be distinguished from them. The reflection arrivals from this horizon appear in the time interval where the oceanic layer reflections could be expected. They also seem to correlate with the refractions from the oceanic layer which follow closely the first (basement) arrivals at the end of the expanding profile.

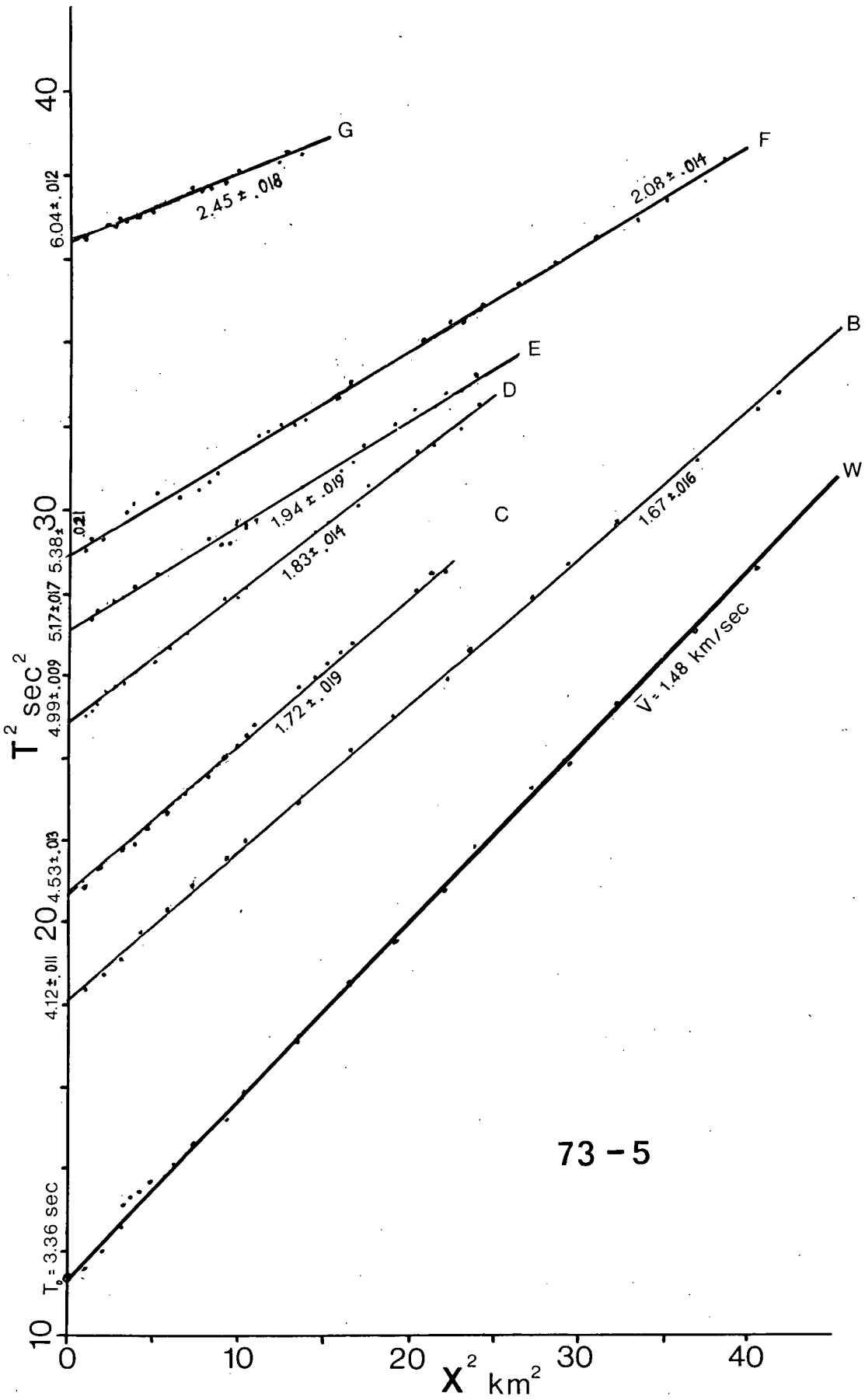
Also, first-order multiples of the reflections from the same horizons can be easily distinguished on the expanding seismic record section 73-5. The filtering effect of multiple paths through layers makes the phases even more distinguishable, however the amplitudes are attenuated. These multiple reflection arrivals and their correlation with the first reflections were not analysed, although they might be used in the interpretation to confirm the results

A T^2-X^2 graph for the reflection arrivals of profile 73-5 was constructed to determine the average rms-velocities of the layers. From the average velocities and intercept times, the interval velocities and thicknesses of individual layers were computed with the use of the least-square method. Fig. 4.6 shows straight line fits corresponding to the reflection arrivals along hyperbolic trajectories on the expanding profile section in Fig. 4.4. The most reliable information should be obtained from the first part of the curves (to about 9 km²), where the hyperbolic approximation of lag trajectories is most accurate.

The values of the interval velocities and layer thicknesses derived from the T^2-X^2 graph are presented in Table 3 of Fig. 4.7. As well, the interval velocities of the upper crust layers determined from the seismic recording in the southern Cascadia Basin near 44°N (Seely et al., 1974) are entered in the table. They compare well with our values. The figure also shows a comparison of the reflection and the refraction velocity-depth models for AREA 3 in the northern Cascadia Basin. The models agree well for the sedimentary sequence. Since it was not possible to correlate the arrivals from the uppermost reflecting horizon A on the expanding profile, its interval velocity was assumed to be that of the refraction model for the upper sediments. The sequence of the reflection horizons A, B and C could be

Figure 4.6 T²-X² Graph for the Expanding Reflection Profile
73-5

The individual reflectors are designated by capital letters corresponding to the same reflectors on the record section in Fig.4.4. The arrival points were picked visually. The rms average velocities (km/sec) and intercept times (sec) were computed using the least-square method. The former are given along the lines and the latter along the ordinate. Both are accompanied by their associated standard deviations.



73-5

Figure 4.7 Velocity - Depth Model for AREA 3

Symbols V and H in Table 3, indicate layer velocity (km/sec) and thickness (km) respectively. Symbol V' indicates layer velocity recorded in the southern part of the Cascadia Basin near 44°N (Seely et al., 1974). The solid line shows the refraction model, the dashed line the reflection model. The letters designate the bottoms of individual reflecting horizons and correspond to the reflections observed in Fig. 4.4 and 4.5.

VELOCITY - DEPTH
MODEL

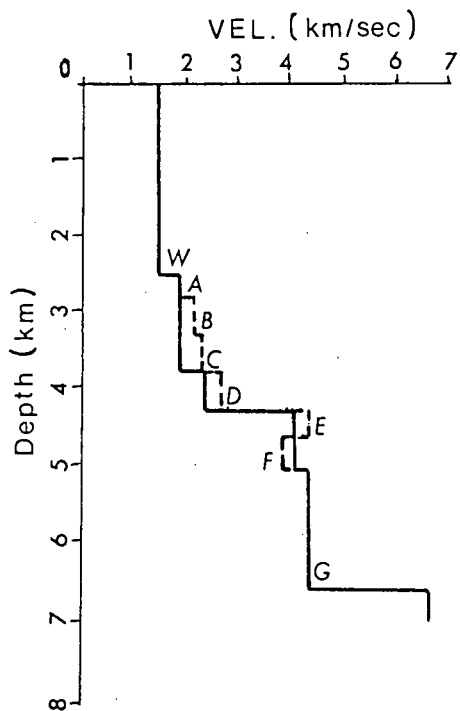


TABLE 3

Reflecting horizon	V	H	V'
W	1.48	2.5	
A	1.90*	.30*	1.83
B	2.21	.50	2.13
C	2.33	.48	
D	2.63	.60	2.68
E	4.56	.41	
F	3.78	.40	3.96
G	4.43	1.5	

*Indicates an estimated value.

modelled on the refraction model by a velocity gradient from 1.9 to 2.4 km/sec in the upper sediments. The tops of the reflecting horizons D and E are at the same depth as the tops of the corresponding layers on the refraction model. The transition between the sediments and the basement (previously suggested in the analysis of the refraction traveltime curves) has two distinct layers in the reflection model; a high velocity layer (4.56 km/sec) at the top and a low velocity layer (3.78 km/sec) at the bottom. (The velocity of 3.78 km/sec compares with the velocity of 3.96 km/sec, the highest velocity recorded for the sediments in the Southern Cascadia Basin.) The top of the basement layer is at the same depth on both models. As well, the velocity and thickness of the basement as determined from the reflections and refractions are the same. The deepest reflections in the model are those arriving from the top of the oceanic layer.

In conclusion, the comparison of both models shows that the velocity structure determined from the reflection information is quite detailed yet agrees with the velocity structures obtained from the refraction data.

AREA 2

Three seismic profiles were recorded in AREA 2 : two parallel reversed expanding profiles 15 and 18 km long, and a quasi-continuous near-vertical incidence reflection cross-profile 36 km long (Fig. 2.4b). A reduced traveltime-distance plot based on the analysis of seismograms from the reversed profiles is shown in Fig. 4.8. Four clearly distinguishable layers with associated velocities of 1.8, 2.1, 3.0 and 4.2 km/sec were observed on seismograms from both profiles. Refraction arrivals giving a velocity of 6.8 km/sec were observed at the end of the SE profile. Only refractions from the basement and the oceanic layer were observed as first arrivals on the record section. Seismic arrivals giving a velocity of 3.4 km/sec appeared on the SE profile.

The initial refraction velocity-depth model was calculated using the traveltime curves of Fig. 4.8 and it is presented in Table 4 on the next page. The symbols V and H in the table are velocity (km/sec) and layer thicknesses (km) respectively. The refraction model shows that the overall thickness of sediments is nearly constant along the reversed profile. Refraction arrivals having a phase velocity of 3.4 km/sec might correspond to a high velocity sediment layer lying on the top of the basement.

Figure 4.8 Reduced Traveltime-Distance Plot of the Two Reversed Refraction Profiles 73-2,3 from AREA 2

The traveltime is reduced with the velocity 4.5 km/sec. The numbers give the velocities (km/sec) derived from the slopes of traveltime lines. Crosses refer to data points for profile 73-2 and circles refer to data points for profile 73-3.

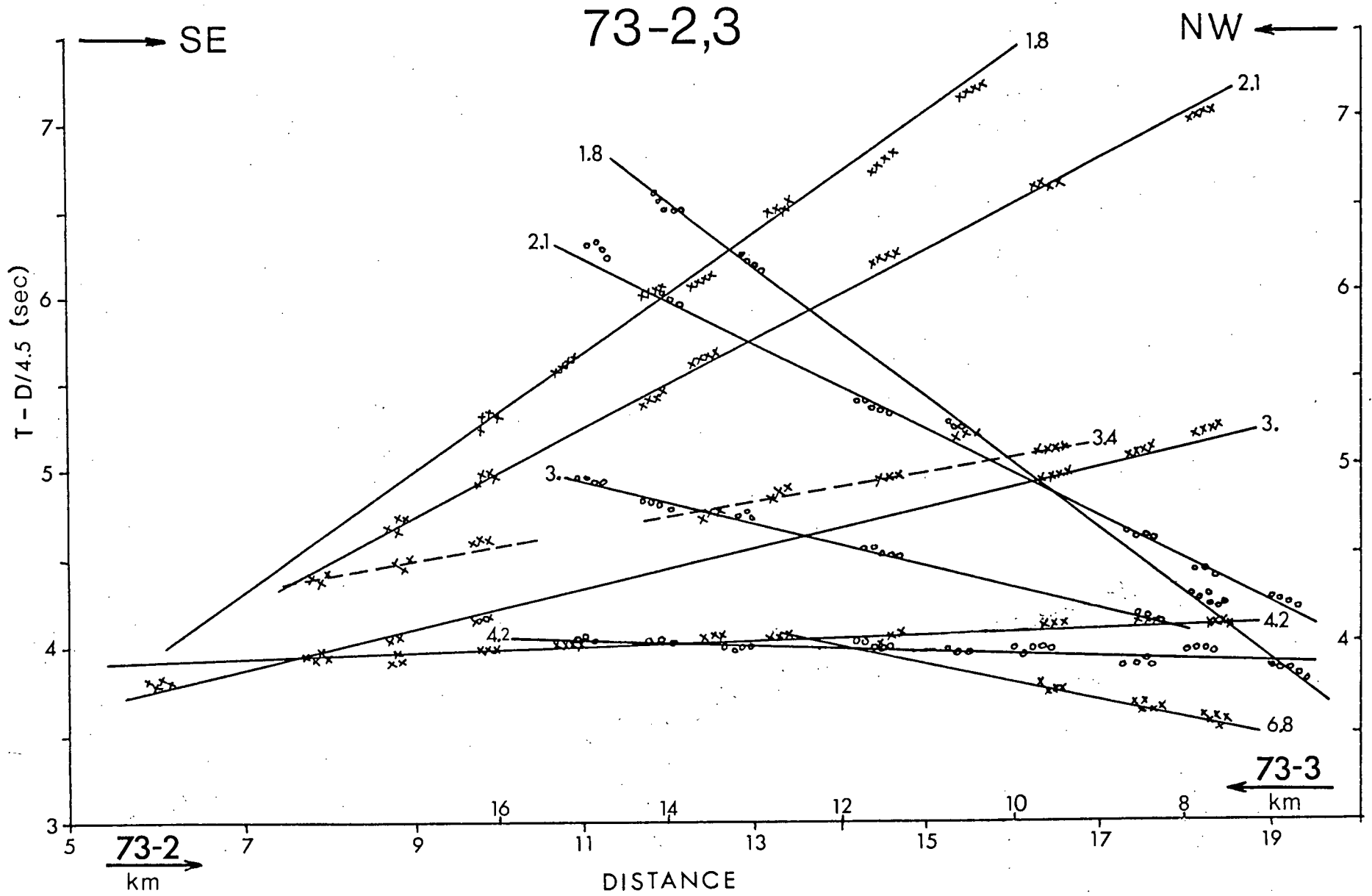


TABLE 4

Layer description	V	NW-station H	SE-station H
Water	1.5	2.0	2.0
Sediment			
a	1.8	0.7	0.5
b	2.1	0.8	0.6
c	3.0	0.7	0.9
d	3.4		0.4
Basement	4.2	2.2	2.1
Oceanic	6.8		

Its thickness is only 0.4 km and it was observed only on the SE profile. The basement is situated at the depth of 2.4 km below the sea bottom and its thickness is about 2.1 km. The oceanic layer has a velocity of 6.8 km, but its thickness could not be determined since the profiles were not long enough to obtain refraction arrivals from the M-discontinuity.

This initial refraction model was used for the generation of synthetic seismograms using HRGLTZ computer program. All seismic arrivals could be modelled with the synthetic seismograms except the arrivals with velocity of 3.4 km/sec. The layer with this velocity was too thin to be modelled for the given input wavelet. The section of synthetic seismograms is compared with the section of stacked observed seismograms in Fig. 4.9. The initial refraction model of Table 4 was further used to check the model obtained from the analysis of the reflection data.

The expanding reflection profile 73-2 is displayed in Fig. 4.10. The quality of the data is poor and correlation

**Figure 4.9 Comparison of the Observed and Synthetic
Seismograms of the Refraction Profile 73-2**

Left- record section of the observed seismograms.

Right- record section of synthetic seismograms.

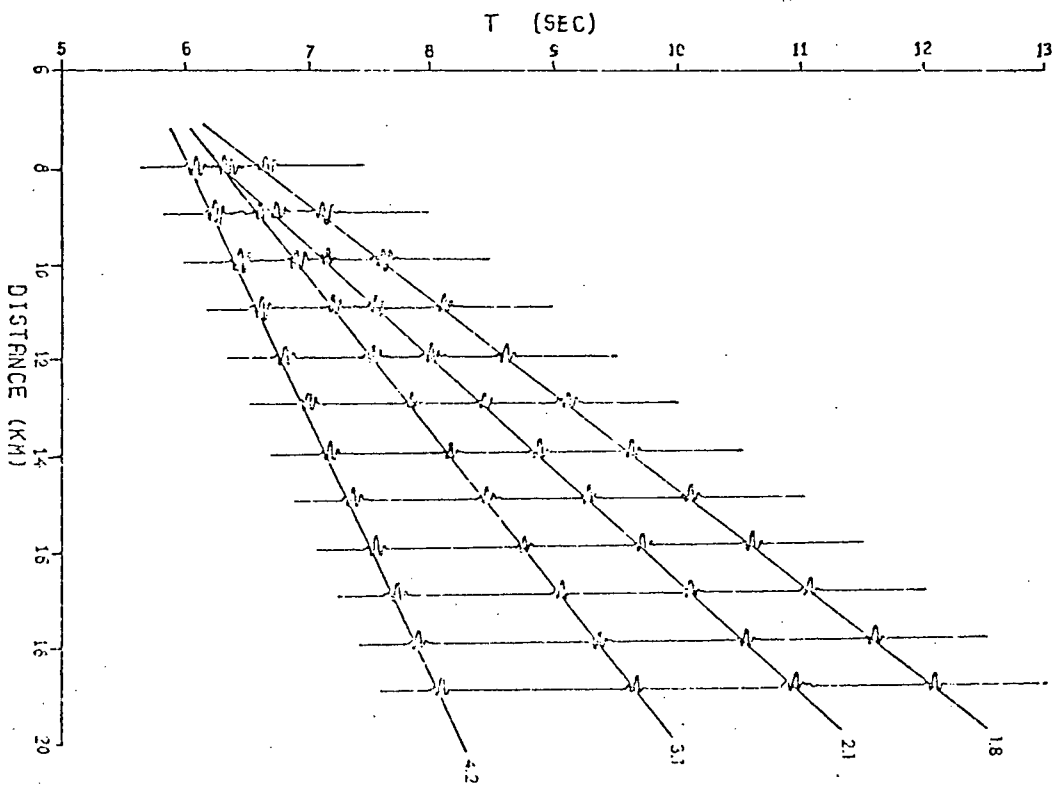
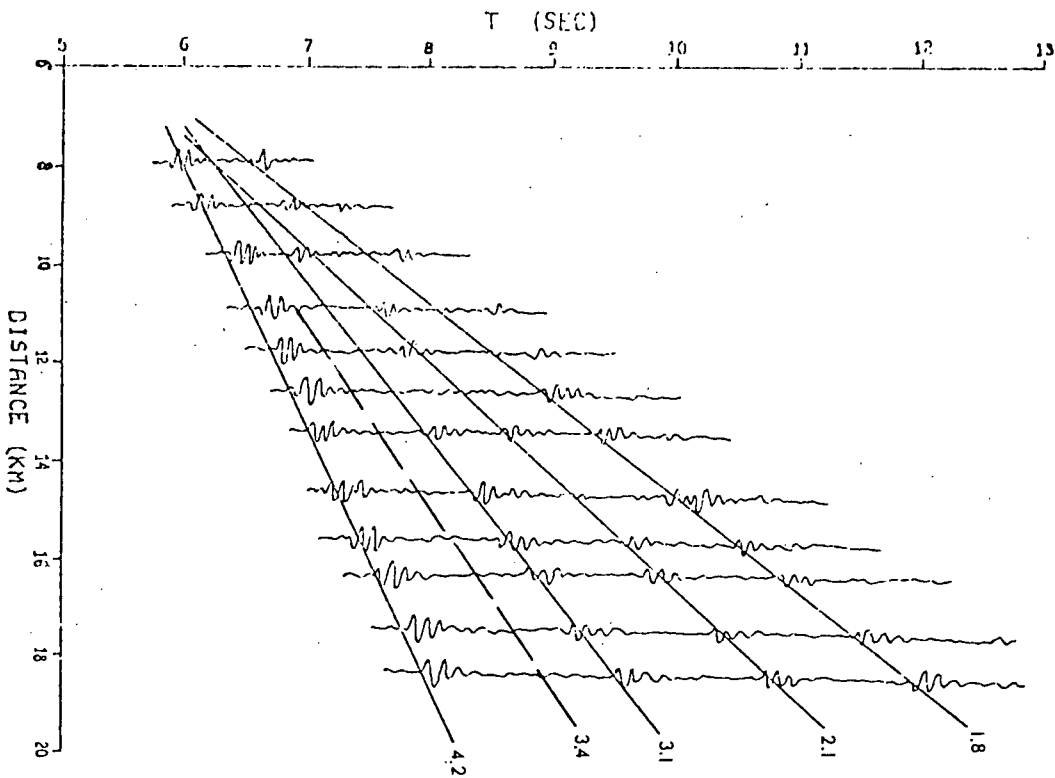
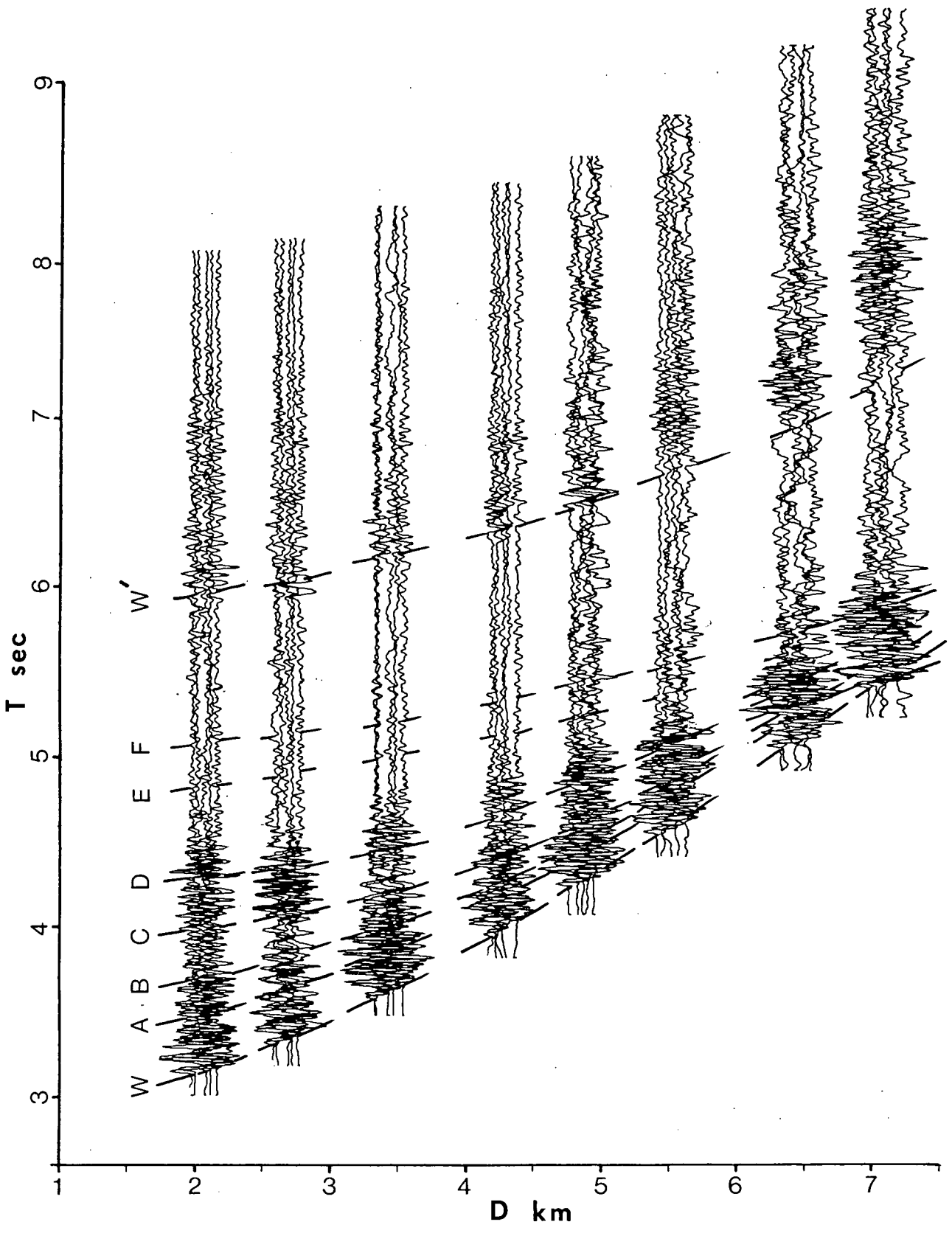


Figure 4.10 Record Section of the Expanding Reflection Profile
73-2 from AREA 2

The letters indicate arrivals from the individual horizons. (They are not intended to be correlated with the horizons of AREA 3.) With the possible exception of horizon F, all other reflections are from within sediments. W' is the first-order multiple of the water bottom reflection.

73-2



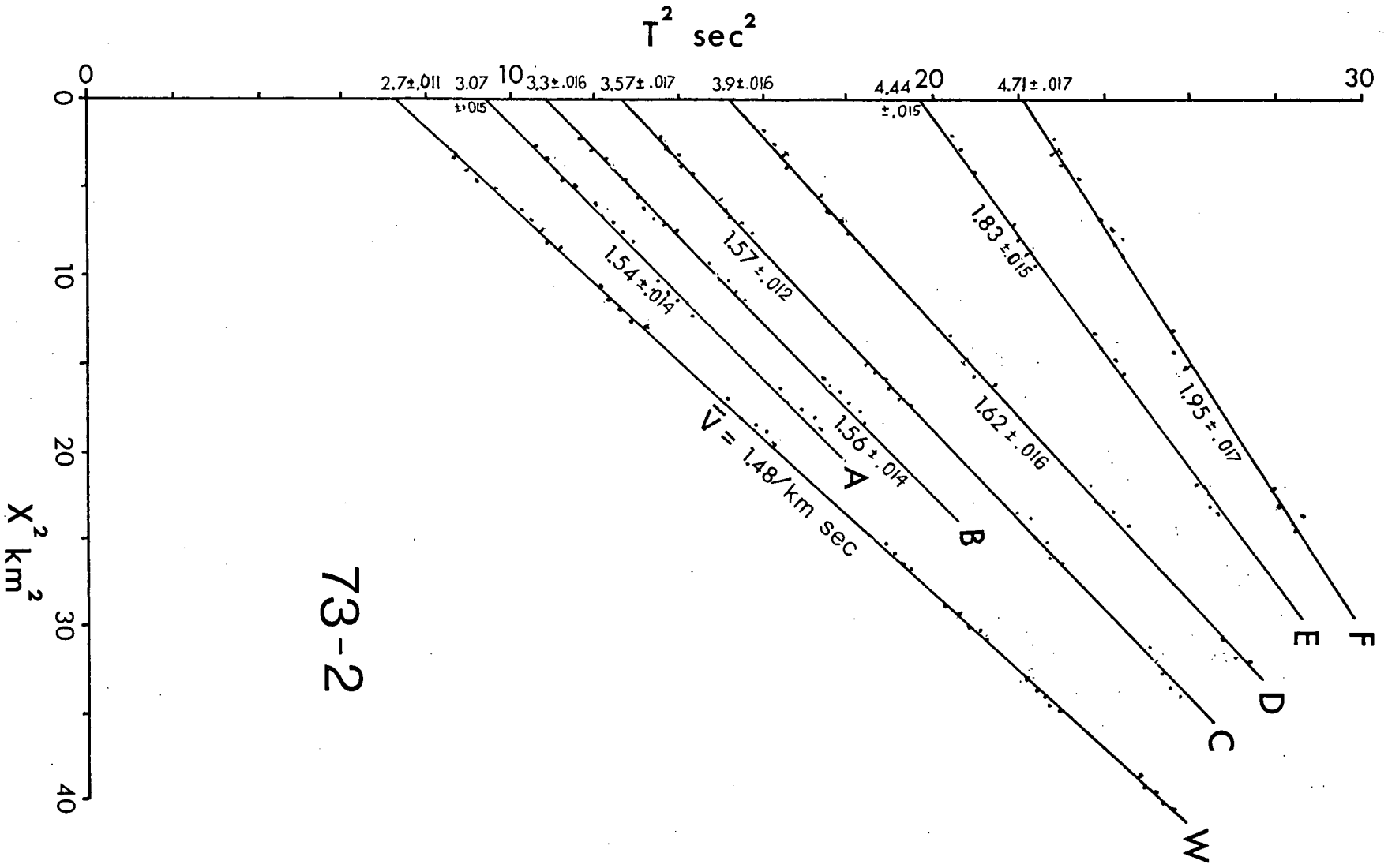
of individual seismic phases along the whole profile is extremely difficult. The quality of the reflection record section of the reversed expanding profile was even worse and the section was not used in the interpretation. (Bad weather conditions during recording in this area severely limited the quality of the reflections.) In Fig. 4.11, reflection arrivals from horizons C and D can be easily identified for near-vertical incidence reflection distances. To identify and correlate the phases from the other horizons required a detailed analysis of individual seismograms. The overall error in picking the arrivals was about ± 25 msec. The corresponding T^2-X^2 graph is shown in Fig. 4.11. The slopes and intercepts of the line fits corresponding to the picked arrivals were computed directly with the use of the least-square method.

The comparison of the reflection and the refraction velocity-depth models for AREA 2 is shown in Fig. 4.12. The agreement between the models is excellent. The refraction velocities of 1.9 and 2.4 km/sec average the velocities of horizons A and B, and C and D. The average velocity for the upper sediments, derived from the reflection model, is 1.99 km/sec. The velocities and thicknesses of the lower sediment refractors and of the reflecting horizons are almost identical. They give an average velocity of about 3.1 km/sec for the lower sediments. There are two low velocity layers

Figure 4.11 T^2-X^2 Graph for the Expanding Reflection Profile 73-

2

The letters designate lines corresponding to the reflectors on the record section in Fig. 10. The rms average velocities (km/sec) and the intercept times (sec), both accompanied by their associated standard deviations, are given along the lines and the ordinate respectively. (The lines are least-square fits to the observed data points.)



73-2

Figure 4.12 Velocity-Depth Model from the Bottom of the Continental Slope in AREA 2

In the diagram, the solid line shows the refraction model, the dotted line the reflection model. The letters designate the bottoms of the individual layers. In Table 5, the symbols V and H indicate layer velocity (km/sec) and thickness (km) respectively.

VELOCITY - DEPTH
MODEL

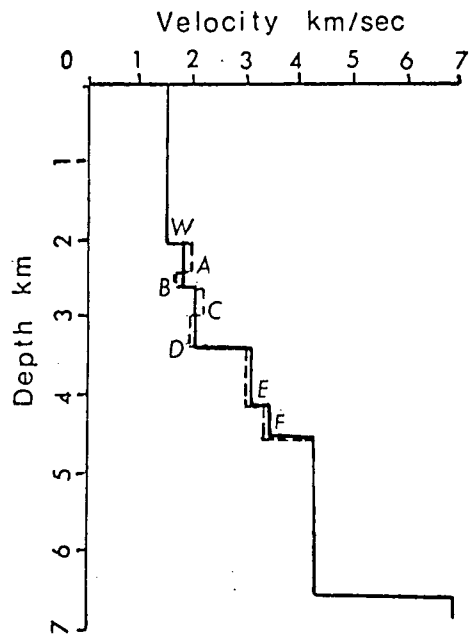


TABLE 5

Reflecting horizon	V	H
W	1.48	2.0
A	1.92	.35
B	1.74	.20
C	2.25	.31
D	2.04	.34
E	2.92	.79
F	3.34	.45

within the upper sediments, horizon B with the velocity of 1.72 km/sec and horizon D with the velocity 2.04 km/sec. Both are situated below the horizons of higher velocity. There is a pronounced change in the velocity (0.9 km/sec) at the boundary between the upper and lower sediments. The deepest reflections observed are from the top of the basement.

The quasi-continuous near-vertical incidence reflection profile 73-6, which crosses the reversed profile at right angles is displayed in Fig. 4.13. The reflection arrivals observed on the expanding profile 73-5 can be identified on seismograms of the profile 73-6 from the bottom of the continental slope. To follow the arrivals from individual layers going up the slope is extremely difficult because of the increased number of multiples interfering with the reflection arrivals. The layer velocities derived from the expanding reflection profile at the bottom of the slope were used to convert the traveltime section to a depth-varying structural model of the continental slope in AREA 2. This model is presented together with CSP line 37 of the Geological Survey of Canada in Fig. 4.14. The relative location of the DSS profile and CSP line no. 37 recorded in 1973 is shown in Fig. 2.4b. The CSP profile indicates the presence of a number of horizontally stratified reflection horizons within the sediments. The DSS model suggests six

Figure 4.13 Quasi-continuous Subcritical Reflection Profile 73-4 from Along the Continental Slope in AREA 2

The reflection arrivals correlate with the arrivals on the expanding reflection profile 73-2, for which the location is shown, and are designated by the same letters. W is the first water bottom reflection, W', W'' and W''' are the multiples. (Because of the number of multiples the correlation of individual reflectors along the record section is difficult, some places impossible. In spite of that, an attempt has been made.)

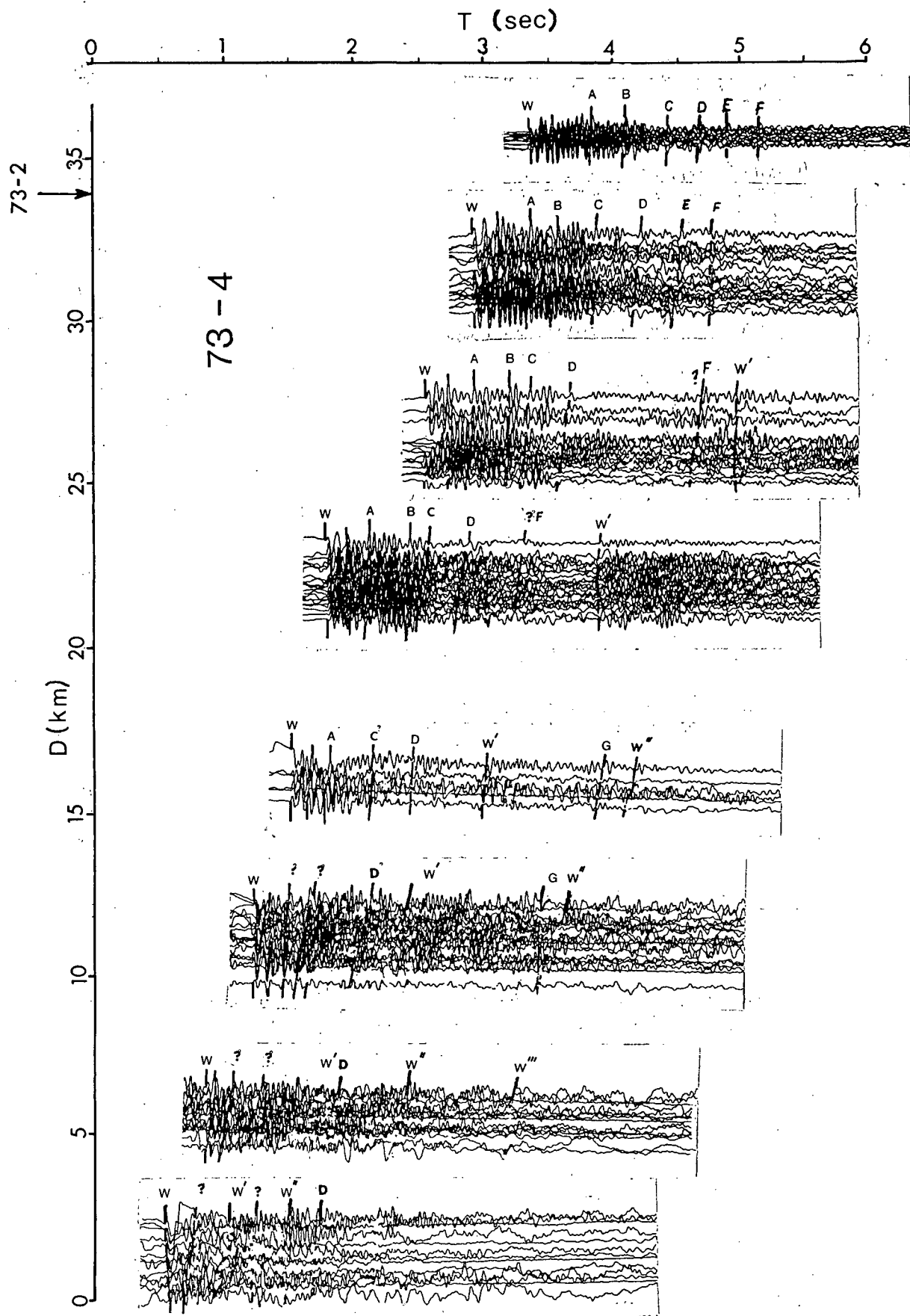
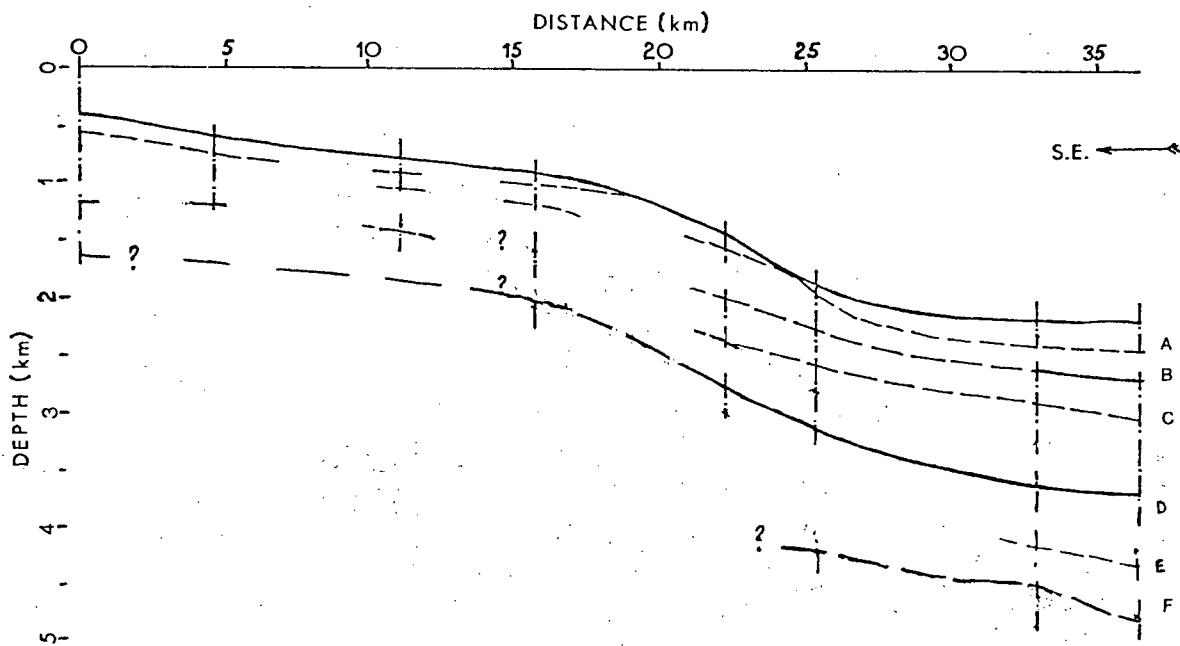
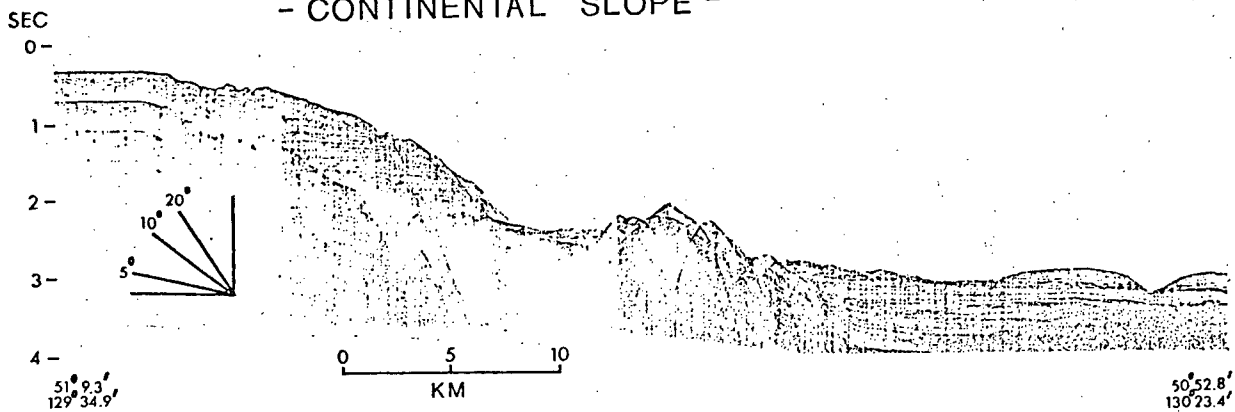


Figure 4.14 Comparison of the Velocity Structure Model of Sediments from the Continental Slope with the CSP Profile

The letters in the model designate the reflecting horizons. Their corresponding velocities are presented in Table 5 of Fig. 4.11. The CSP profile is part of Line 37 recorded by the Geological Survey of Canada. (The relative location of the two profiles is shown in Fig. 2.4b.)

QUEEN CHARLOTTE SOUND

- CONTINENTAL SLOPE -



such horizons with various velocities. There is an indication of rising or thickening of the basement with the rise of the continental slope it should be emphasized that the velocity structure presented in Fig. 4.14 is very tentative. In spite of this, it does yield some additional information about the approximate thicknesses of the sediment layers observed on the CSP profile.

4.3 Discussion of the Results

The interpretation of the data depends on the methods of analysis and the amount and quality of the data. The standard techniques of interpretation, such as fitting traveltime curves for the refraction data, and T^2-X^2 graphs for the reflection records, determined the final velocity-depth models.

The synthetic seismogram amplitude analysis of the refraction data did not give any additional information. The refraction profiles were too short for substantial amplitude variation. The computer programs used to generate the synthetic seismograms were near their limits of resolution (for the given input wavelet) when some of the thin crustal layers were modelled, and did not show the corresponding arrivals. The synthetics did confirm the reality of the

basic refracting layers obtained from the observed traveltime curves. The models in all three areas extend only to the top of the oceanic layer. The expanding profiles were too short to observe M-discontinuity refractions. All of the final refraction velocity-depth models are credible in spite of the poor quality of the data in some areas. The poorest records were obtained from AREA 1, but since a previously published seismic model agreed well with the presented interpretation, the results were considered adequate.

A modern method of velocity analysis using computer derived velocity spectra was applied to the reflection data, but it proved to be unsuccessful for reasons mentioned in section 3.5. However, the simpler T^2-X^2 method was adequate for reflection data of the type and quality obtained in this thesis. The seismic phases were mostly determined with accuracy ± 10 msec. An exception was AREA 2 where the error was about ± 25 msec. For the deepest reflector observed in the area (reflector F of the velocity 3.34 km/sec), this amounts to 40 m, a value near the limits of resolution of the recording.

4.4 Relation to Regional Geology

The continental margin of Western Canada lies within a tectonically active part of the earth's crust which includes the triple junction of the Pacific, American and Juan de Fuca plates. Typical for the area is: 1) faulting parallel to the continental margin; 2) changes in the character of the continental shelf from north to south across the triple junction; 3) marginal basins to the west of the continental slope; 4) quaternary volcanism at the base of the continental slope; 5) and interaction of tectonic deformation and Pleistocene glaciation.

The margin is divisible into three tectonic regions (Chase et al., 1975): a northern region from Dixon Entrance to Queen Charlotte Sound (characterized by strike-slip faulting); a central region from Queen Charlotte Sound to Brooks Peninsula on Vancouver Island (characterized by faulting and folding); and a southern region from Brooks Peninsula to Juan de Fuca Strait (characterized by slow subduction).

Each of the areas of the DSS recording (Fig. 1.1) was situated in one of the tectonic regions. AREA 1 is west of the Queen Charlotte Trough in the northern region; AREA 2 is west of the central part of Queen Charlotte Sound, in the central tectonic region; AREA 3 is in the northern part of

Cascadia Basin, in the southern tectonic region.

AREA 1 served only as a convenient area for the testing of the DSS technique and was not of particular geological interest to us. Since the recorded data from the area did not yield any new information, the geology of the area will not be discussed in the thesis. The geophysical characteristics of the area are given by Keen and Barrett (1971); the overall geology of the tectonic region is discussed by Chase et al. (1975).

AREA 2 is situated at the base of the continental slope between J. Tuzo Wilson Knolls (to the north) and the southern canyon of Queen Charlotte Sound (to the southeast). Recent findings of young volcanic material (Tiffin, 1974, GSC Report of Activities) at the J. Tuzo Wilson Knolls prove that there is volcanic activity in the area. The southern canyon is the largest trough in Queen Charlotte Sound. It cuts the continental slope thus providing a channel for transportation of the sediments from across the sound to the base of the slope. The age of the sediments in Queen Charlotte Sound ranges from Pleistocene (Luternauer, 1972) through Upper and Lower Pliocene to Miocene (wildcats Harlequin and Osprey of Shell Canada Ltd.; Shouldice, 1971). Geology of the adjacent areas indicates that AREA 2 could have been subjected to two different geological processes, volcanism and Pleistocene glaciation.

The velocity-depth model for the base of the continental slope in AREA 2 (Fig. 4.12) shows six horizons within the sediments. The upper sediments (average velocity of 2.0 km/sec, 1.2 km thick) comprise a sequence of layers with alternately high and low velocity. The thickness of individual layers is almost uniform (about 300 m). The alteration of the layer velocities indicates probably two different depositional processes. The velocity alteration together with the regularity in the layer thicknesses indicate that the two processes took place alternately and occurred with approximately the same time period. It is suggested that the deposition of the sediments in AREA 2 occurred during Pleistocene times. During the advances, coarser sediments pushed by a glacier across the sound were deposited, whereas during retreats, deposition of finer sediments took place.

The lower sediments (average velocity 3.1 km/sec, thickness 1.2 km) are formed by two high velocity layers. Their velocities indicate that they are highly compacted dewatered sediments (Nafe and Drake, 1957). The basement which lies 4.4 km beneath the sea floor is 2.3 km thick and has a velocity of 4.2 km/sec, suggesting it is volcanic. Substantial deformation of the basement was not observed. The underlying oceanic layer has velocity of 6.8 km/sec. (both velocities, for the basement and for the oceanic

layer, were determined from the refraction recording.)

AREA 3 is located at the foot of the continental slope in the northern Cascadia Basin. The basin is a wedge of sediments thickening toward the continental slope and overlying the basaltic layer of the southeastern flank of Juan de Fuca Ridge (Chase et al., 1975). Sediments of Cascadia Basin merge with those of Tofino Basin through a zone of folding beneath the continental slope. The volcanic basement, which is exposed along the crest of Juan de Fuca Ridge, dips gently eastward and disappears beneath the slope (Barr, 1974). Its age increases towards the continental slope. AREA 3 belongs to a region of magnetic anomaly 3 (Heirtzler scale) which indicates the age of between 4 and 5 myr (Barr, 1974).

The velocity-depth model of AREA 3 (Fig. 4.7) shows a sequence of sedimentary layers totalling 1.9 km in thickness. Velocities increase almost uniformly with depth and range from 1.9 to 2.63 km/sec. This indicates that the process of sedimentation in the area is a regular deposition with subsequent compaction. Sediment is supplied via Vancouver Channel, which extends south from the southern end of Winona Basin, and via canyons cutting the slope between Kyuquoit Uplift and Nitinat fan (Carson, 1973). An interesting feature in the model is the occurrence of a transition in velocity between the sediments and the

basement: a high velocity layer (4.56 km/sec) overlies a low velocity layer (3.78 km/sec), which in turn overlies the high velocity basement layer (4.43 km/sec). The high velocity for the upper layer (4.56 km/sec) indicates that the layer is made of basalt. The lower velocity of the layer beneath suggests that the layer is composed of compacted sediments, possibly including basaltic debris. A layer with a similar velocity (3.96 km/sec) was recognized in the southern part of Cascadia Basin near 44°N (Seely et al., 1974). From magnetic anomalies, one deduces that 5 myr ago the present AREA 3 was in the process of formation at Juan de Fuca Ridge. The origin of the interbedding of the basalt with compacted sediments would be explained by contemporaneous sedimentation and volcanism at the ridge crest. Contemporaneity has been observed at the crest of the northern end of Juan de Fuca Ridge. Barr and Chase (1974) show that faulting and differential uplift at the crest of the ridge formed valleys which were subsequently filled with turbidites. The volcanic basement in AREA 3 with velocity of 4.43 km/sec, is situated at the depth of 2.7 km beneath the sea floor. It is 1.5 km thick and lies over the oceanic layer with velocity of 6.7 km/sec (determined from refraction measurements).

5 CONCLUSIONS

In this thesis project a marine DSS technique useful for detailed structural studies of the oceanic crust was established. The technique unites the advantages of the more standard methods of marine seismic recording, such as refraction and CSP profiling, and is an inexpensive compromise to the multichannel methods used in the oil industry.

The technique is simple in its design (using an array of individual hydrophones), easily adaptable to changes (the number of the hydrophones can be increased up to eleven), and flexible in its application. With the same equipment, it can be used for near-vertical incidence reflection recording, wide-angle reflection recording, and refraction recording.

The feasibility of the technique was studied by testing the DSS procedure at sea in three tectonically different areas: AREA 1 - west of the Queen Charlotte Islands, AREA 2 - at the continental slope off Queen Charlotte Sound, and AREA 3 - in the northern Cascadia Basin west of Vancouver Island. The data were recorded digitally in the frequency range from 0.8 to 100 Hz. The quality of the data varied with the area of recording, but in general the signal/noise ratio was poor.

The analysis of the recorded data has demonstrated that the penetration of the DSS technique and the signal/noise ratio depends greatly on the thickness and structural quality of the sedimentary layer. In regions with little or no sediments, most of the signal energy is reflected from the uppermost layer, the seismograms are 'noisy' and yield seismic information which is extremely difficult to extract. Such an area of recording was AREA 1 where identification of any reflections from beneath the thin layer of sediments was impossible since their amplitudes were small and obscured by the noise. The deepest penetration is achieved in regions where the density of the sediments increases gradually with depth and 'soft' (low density) sediments are at the top (only a small part of the energy is reflected from the first layers and more energy is available for transmission deeper into the section). Such an area of recording was AREA 3 where the deepest reflections observed were from the depth of 4.19 km beneath the sea bottom (from the top of the oceanic layer). In the regions with velocity reversals in the sediments, the penetration of the signal decreases. Such an area was AREA 2 where the deepest reflections observed were from the depth of 2.44 km beneath the sea bottom (from the top of the basement). From the frequency content of individual reflection arrivals, the resolution power of the technique for reflections within the sedimentary sequence is

calculated to be about 25 msec (frequency 20 Hz), and for the deeper reflections about 40 msec (frequency 12 Hz). (It should be noted that the parameters, such as penetration and resolution, which specify the feasibility of the established technique for detailed studies of the deep crustal structure are based on the analysis of the first data recorded with this technique during testing. The results depended greatly on the poor quality and small amount of the data. In the meantime, data of much better quality have been acquired during following cruises, however they have not been analysed yet.)

To investigate the possibility of identifying finer structure and/or deeper reflections than those already observed, various methods of data processing and analysis were studied. They can be divided into two groups, stacking techniques and deconvolution techniques. Stacking techniques (such as velocity spectra analysis and stacking of reflection data) require accurate knowledge of the absolute origin times and satisfaction of the CDP condition. However, neither of the requirements can be well satisfied with the established technique. Deconvolution techniques do not have these restrictions on the data and therefore were more convenient for the application. The results obtained with deconvolution using variable wavelet indicated that time adaptive deconvolution should be applied to the data in the

interval before the first water bottom multiple arrival. For the identification of the deep reflections obscured by the first-order water bottom and upper layers multiples, these should be first removed and then time adaptive deconvolution used also in this interval.

Within the bounds of the determined signal penetration and resolution, detailed velocity-depth models of the upper and middle part of the oceanic crust have been derived for two regions in which no such information existed previously. Geological interpretation of the models contributed to the understanding of the geology of the areas. Velocity reversals within the sediments in AREA 2 indicate the effects of Pleistocene glaciation on the deposition of the sediments below the continental slope off the Queen Charlotte Sound. A velocity reversal within the upper part of the basement in AREA 3 indicates the occurrence of interbedding of the volcanic basement with sediments at the top of the basement. The formation correlates with the geological processes observed recently at the crest of the near by Juan de Fuca Ridge.

The main contribution of this thesis is that it established an inexpensive marine recording technique and analysis procedures which can be used for detailed investigation of the crust in such a tectonically interesting area as the west coast of Canada. No such

similar technique convenient for detailed seismic study of the oceanic crust has been used in this area before. The marine DSS program provides additional information about geological structures and assists our understanding of the complex tectonic features off the coast of British Columbia. This local application is complementary to the use of other techniques by marine geoscientists. This was demonstrated during 1974 when the DSS system was used successfully for investigations over Explorer Ridge (Malecek, 1976), a region where a marine geological study is currently in progress. The following year 1975, extensive DSS profiling was undertaken in Winona Basin, a deep water sedimentary basin of both tectonic and economic interest. Good quality reflections from within the sediments and deeper have been identified (Clowes, personal communication, 1976).

Thus the seismic system which was developed in this thesis project has already proven its worth on subsequent cruises and further use of it is planned for the future. The analysis procedures discussed in this work provide a foundation for extracting the maximum information from the marine data which has been and will be recorded.

REFERENCES

- Al-Chalabi, M., 1973. Series approximation in velocity and traveltime computations. *Geophys. Prosp.*, 21, 784-795.
- Aric von K., 1968. Reflexionsseismische Messungen im Skagerrak. *Zeitschrift f. Geophysik*, 34, 223-226.
- Aric von K., H. Hirschleber, H. Menzel and W. Weigel, 1970. Über die Struktur der Grossen Meteor-Bank nach Seismischen Ergebnissen. 'Meteor'-Forschungsergebnisse, Reihe C, 3, 48-64.
- Barr, S.M., 1974. Structure and tectonics of the continental slope west of southern Vancouver Island. *Can. J. Earth Sci.*, 11, 1187-1199.
- Barr, S.M., and R.L. Chase, 1974. Geology of the northern end of Juan de Fuca Ridge and sea floor spreading. *Can. J. Earth Sci.*, 11, 1384-1406.
- Bessonova, S.M., V.M. Fishman, V.Z. Ryaboyi and G.A. Sitnikova, 1974. The tau method for inversion of traveltimes - I. Deep seismic sounding data. *Geophys. J. R. astr. Soc.*, 36, 377-398.

Braile, L.W., and R.B. Smith, 1975. Guide to the interpretation of crustal refraction profiles.

Geophys. J. R. astr. Soc., 40, 145-176.

Carmichael, D.G., A. Hubbard, K. McCamy, and W. McDonald, 1973. A recording ocean bottom seismograph.

J. Geophys. Res., 78, 8748-8750.

Carson, B., 1973. Acoustic stratigraphy, structure, and history of Quaternary deposition in Cascadia Basin.

Deep-sea Res., 20, 387-396.

Červený V., and R. Ravindra, 1971. Theory of seismic head waves. University of Toronto Press, p.147.

Chase, T. E., H. W. Menard and J. Mammerickx, 1970. Bathymetry of the North Pacific (Chart no. 4), Scripps Institute of Oceanography, Calif.

Clayton, R. W., 1975. The deconvolution of teleseismic recordings. Unpublished M.Sc. thesis, University of British Columbia.

Chase, R. L., D. L. Tiffin, and J. W. Murray, 1975. The Western Canadian continental margin. In: Canada's continental

margins and offshore petroleum exploration; Canadian Society of Petroleum Geologists (Publ.),
Calgary, Alberta.

Dix, C.H., 1955. Seismic velocities from surface measurements. *Geophysics*, 20, 68-86.

Ewing, J.I., 1963. Elementary theory of seismic refraction and reflection measurements. In: The Sea, vol. 3, M.N.Hill (Ed.), Interscience, New York.

Ewing, J.I., and J.E.Nafe, 1963. The unconsolidated sediments. In: The Sea, vol. 3, M.N.Hill, (Ed.), Interscience, New York.

Ewing, J.I., and R. Houtz, 1969. Mantle reflections in air-gun sonobuoy profiles. *J.Geophys.Res.*, 74, 6706-6719.

Ewing, M., 1963. Submarine geophysics. *Trans.Amer.Geophys.Union*, 44 (2), 351-354.

Francis, T.G., and I.I.Porter, 1973. Median valley seismology: The mid-Atlantic ridge near 45°N. *Geophys.J.R.astr.Soc.*, 34, 279-311.

Fuchs, K., and G. Muller, 1971. Computation of synthetic seismograms with the reflectivity method and comparison with observations. *Geophys. J. R. astr. Soc.*, 23, 417-433.

Hammond, A. L., 1975. Minerals and plate tectonics: A conceptual revolution. *Science*, 189, 779-781.

HelMBERGER, D. V., 1968. The crust-mantle transition in the Bering Sea. *Bull. Seismol. Soc. Amer.*, 58, 179-214.
Science, 189, 779-781.

HelMBERGER, D. V., and G. B. MORRIS, 1969. A travel time and amplitude interpretation of a marine refraction profile: Primary waves. *J. Geophys. Res.*, 74, 483-494.

HelMBERGER, D. V., and G. B. MORRIS, 1970. A travel time and amplitude interpretation of a marine refraction profile: Transformed shear waves.
Bull. Seism. Soc. Amer., 60, 593-600.

HelMBERGER, D. V., and R. A. WIGGINS, 1971. Upper mantle structure of the Midwestern United States.
J. Geophys. Res., 76, 3229-3271.

Hersey, J. B., 1963. Continuous reflection profiling. In: The

Sea, vol.3, M.N.Hill, (Ed.), Interscience, New York, 73-84.

Hill, M.N., 1952. Seismic refraction shooting in an area of the eastern Atlantic.

Phil.Trans.Roy.Soc., London, A244, 561-596.

Houtz, R.E., J.I.Ewing, and X.LePichon, 1968. Velocities of deep sea sediments from sonobuoy data.

J.Geophys.Res., 73, 2615-2641.

Hussong, D.M., A.A.Nowroozi, M.E.Odegard, and G.H.Sutton, 1969. Crustal structure under an ocean bottom seismometer using explosive sources. Eos Trans.A.G.U., 50, 644.

Kanasewich, E.R., 1973. Time sequence analysis in geophysics. The University of Alberta Press, Edmonton, 170-201.

Keen, C.E., and D.L.Barrett, 1971. A measurement of seismic anisotropy in the northeast Pacific. Can.J.Earth Sci., 8, 1056-1064.

Kramer, F.S., R.A.Peterson, and W.C.Walter, 1968. Seismic energy sources handbook, 1968. United Geophysical Corporation, p.57.

Le Pichon, X., J. I. Ewing, and R. E. Houtz, 1968. Deep-sea sediment velocity determination while reflection profiling. *J. Geophys. Res.*, 73, 2597-2614.

Limond, W. Q., P. Patriat, F. Gray and G. Grau, 1972. Mantle reflections in the Bay of Biscay. *Earth Planet Sci. Letters*, 15, 361-366.

Lister, C. R. B., and B. T. R. Lewis, 1974. An ocean bottom seismometer suitable for arrays. *Eos Trans. A.G.U.*, 55, 357.

Luternauer, J. L., 1972. Patterns of the sedimentation in Queen Charlotte Sound, British Columbia. Unpublished Ph.D. thesis, University of British Columbia.

Malecek, S. J., 1976. A marine deep seismic sounding survey in the region of Explorer Ridge. Unpublished M.Sc. thesis, University of British Columbia.

Maynard, G. L., G. H. Sutton, and D. M. Hussong, 1969. Seismic observations in the Solomon Islands and Darwin rise regions using repetitive sources. *Eos Trans. AGU*, 50, p. 206.

- Maynard, G.H., 1970. Crustal layer of seismic velocity 6.9 to 7.6 kilometers per second under the deep oceans. *Science*, 168, 120-121.
- McMechan, G.A., and R.A. Wiggins, 1972. Depth limits in body wave inversions. *Geophys. J. R. astr. Soc.*, 28, 459-473.
- Minkley, B.G., R.L.K. Tripe, and D.A. Healey, 1970. Oceanographic observations at Ocean Station P (50°N, 145°W) 27 June to 25 September 1969. Tech. Report, Fisheries Research Board Canada, 184-222.
- Nafe, J.L., and C.L. Drake, 1957. Variation with depth in shallow and deep water marine sediments of porosity, density and the velocities of compressional and shear waves. *Geophysics*, 22, 523-552.
- Neidell, N.S., and M.T. Taner, 1971. Semblance and other coherency measures for multichannel data. *Geophysics*, 36, 482-497.
- O'Brien, P.N.S., 1960. Seismic energy from explosions. *Geophys. J. R. astr. Soc.*, 3, 29-44.
- Officer, C.B., J.I. Ewing, J.F. Hennion, D.G. Harkrider, and

- D.E. Miller, 1959. Geophysical investigations in the eastern Caribbean. *Phys. Chem. Earth*, 3, 17-109.
- Orcutt, J., B. Kennett, L. Dorman, and W. Prothero, 1975. A low velocity zone underlying a fast spreading rise crest. *Nature*, 256, 475-476.
- Orcutt, J., B. Kennett, and L. Dorman, 1976. Structure of the East Pacific Rise from an ocean bottom seismometer survey.
- Peacock, K.L. And S. Treitel, 1969. Predictive deconvolution: Theory and practice. *Geophysics*, 34, 155-169.
- Perkins, W., 1970. Deep crustal reflections on land and at sea. Ph.D. thesis, Princeton University.
- Prothero, W.A. 1974. A short period ocean bottom seismograph. *Bull. Seism. Soc. Am.*, 64, 1251-1262.
- Raitt, R.W., 1952. Oceanographic instrumentation. *Nat. Res. Council Pub.*, 309, 70.
- Raitt, R.W., G.G. Shor, Jr., G.B. Morris, and H.K. Kirk, 1971. Mantle anisotropy in the Pacific Ocean. *Tectonophysics*, 12, 173-

186.

Robinson, E.A., 1967. Multichannel time series analysis with digital computer programs. Hodden-Day, San Francisco.

Seely, D.R., P.R. Vail, and G.G. Walton, 1974. Trench slope model. In: The Geology of Continental Margins. C.A. Burk and C.L. Drake (Ed.), New York, 249-260.

Shor, G.G., Jr., 1963. Refraction and reflection techniques and procedures. In: The Sea, vol. 3, M.N.Hill, Ed., Interscience, New York, 20-38.

Shor, G.G., Jr., and F.W. Raitt, 1969. Explosion seismic refraction studies of the crust and upper mantle in the Pacific and Indian Oceans. A.G.U. Monogr., no. 13, 225-230.

Shouldice, D.H., 1971. Geology of the western Canadian continental shelf. Can. J. Earth Sci., 11, 1187-1199.

Shor, G.G., H.W. Menard, and R.W. Raitt, 1970. Structure of the Pacific Basin. In: The Sea, vol. 4, M.N.Hill (Ed.), New York, 3-27.

- Sutton, G.H., G.L. Maynard, and D.M. Hussong, 1971. Widespread occurrences of a high velocity basalt layer in the Pacific crust found with repetitive sources and sonobuoys. Amer. Geophys. Union Monogr., 14, 193-209.
- Taner, M.T., and F. Koehler, 1969. Velocity spectra - Digital computer derivation and applications of velocity functions. Geophysics, 34, 859-881.
- Tiffin, D.L., and D. Seeman, 1975. Bathymetric map of the continental margin of Western Canada. Open file map, Geol. Surv. of Canada.
- Watkins, J.S., J.L. Worzel, M.H. Houston, M. Ewing, and J.B. Sinton, 1975. Deep seismic reflection results from the Gulf of Mexico; Part I. Science, 187, 834-836.
- Whitmarsh, R.B., 1971. Seismic anisotropy of the uppermost mantle absent beneath the east flank of the Reykjanes ridge. Bull. Sess. Soc. Amer., 61, 1351-1368.
- Wielandt, E., 1975. Generation of seismic waves by underwater explosions. Geophys. J. R. astr. Soc., 40, 421-439.
- Wiggins, R.A., and D.V. Helmberger, 1973. Upper mantle structure

of the western United States. J.Geophys.Res.,78,1869-1879.

Wiggins,R.A.,and J.A.Madrid,1974. Body wave amplitude calculations. Geophys.J.R.astr.Soc.,37,423-433.

Wiggins,R.A.,1976. Body wave amplitude calculations II. Geophys.J.R.astr.Soc., (submitted for publication).

Zverev,S.M.,1967. Problems in deep seismic sounding. New York: Consultants Bureau,p166.

Zverev,S.M.,1970. Problems in seismic studies of the oceanic crust. Izvestiya, Earth Physics,4,49-64, (transl.).

APPENDIX

FORTRAN SOURCE LISTING
OF THE VELOCITY SPECTRUM COMPUTER PROGRAM

The velocity spectrum program is designed to derive and display velocity spectra of the seismic reflection data. The logic of the program follows the procedure described in chapter 3.5. Three subroutines are called from the main program. Subroutine RETAP reads seismic data from a tape into the array A. Subroutine SUMMAX (summation), UNNOCR (unnormalized crosscorrelation) or SEMBLA (semblance coefficient) is called to compute the signal coherency of the data. Subroutine ELVESP plots the derived velocity spectrum. The principle of each of the measures of signal coherency is presented in section 3.5. The mathematical expressions on which the subroutines SUMMAX, UNNOCR and SEMBLA are based were derived and discussed by Taner and Koehler (1969).

```

DIMENSION A(20,384.0),PLTA(20,1000),STCK(1100)
DIMENSION V(1000),VSQ(1000),VOPT(30),VOPT2(30),COHM(1000)
DIMENSION TDIST(60),DIST(60),DISTSQ(60),RSTART(10),NH(10)
DIMENSION T(60),KT(60)
READ(5,1000)T1,GT,DT,NGI,V1,V2,DV
READ(5,1100)NSH
PFAD(5,1100)(NH(I),I=1,NSH)
READ(5,3000)(RSTART(I),I=1,NSH)
M=0
DO 3 I=1,NSH
3 M=M+NH(I)
READ(5,4000)(TDIST(I),I=1,M)
SI=0.0028
NV=IFIX((V2-V1)/DV+0.5)+1
NG=IFIX(GT/DT+0.5)+1
GT2=GT/2.0
NG2=(GT2/SI+0.5)
IF(NGI-1)11,11,12
11 T2=T1+GT
GO TO 13
12 T1=T1+GT2/2.0
T2=T1+FLCAL(NGI)*GT2
13 CONTINUE
WRITE(6,777)
WRITE(6,666)M,NG,NGI
WRITE(6,777)
WRITE(6,2000)T1,T2,V1,V2,GT,DT,DV
DO 1 I=1,M
1 DIST(I)=TDIST(I)*1.48
WRITE(6,777)
WRITE(6,5000)(DIST(I),I=1,M)
WRITE(6,777)
MM=M-1
II=NGI-1
DO 2 IX=1,MM
2 DISTSQ(IX)=DIST(IX+1)**2-DIST(IX)**2
CALL BETAP(A,NSH)
T(1)=T1
V(1)=V1
DO 4 IV=1,NV
VSQ(IV)=V(IV)**2
V(IV+1)=V(IV)+DV
4 CONTINUE
KDT=IFIX(DT/SI)
NSTART=IFIX((T1-RSTART(1))/SI+0.5)+1
NEND=IFIX((T2-RSTART(1))/SI+0.5)+1
NS=NEND-NSTART
WRITE(6,777)
WRITE(6,222)NSTART,NEND
222 FORMAT('NSTART=',I5,5X,'NEND=',I5)
TIN1=T1
TIN2=T1+GT
NH(1)=NH(1)-1
DO 10 IT=1,NGI
WRITE(6,777)

```

```

WRITE(6,6100)TIN1,TIN2
WRITE(6,777)
COHMAX=0.0
IQ=0
DO 20 IV=1,NV
  IC=1
  DO 80 IN=1,NSF
    KT(1)=IFIX((T(1)-RSTART(IN))/SI+0.5)+1
    N=NH(IN)
    DO 30 IX=1,N
      IC=IC+1
      T(IC)=SQRT(T(IC-1)**2+DISTSQ(IC-1)/VSO(IV))
      KT(IC)=IFIX((T(IC)-RSTART(IN))/SI+0.5)+1
30  CONTINUE
80  CONTINUE
    JE(IV,EQ,1) GO TO 88
    CALL SUMMAX(A,KT,KDT,M,NG,COH)
    COH(IV)=COH
    IF(COH(IV).GT.COHMAX) IO=IV
    IF(COH(IV).GT.COHMAX) COHMAX=COH(IV)
    GO TO 20
88  COH(1)=0.0
20  CONTINUE
    DO 40 IV=1,NV
      COH(IV)=COH(IV)/COHMAX
40  CONTINUE
    WRITE(6,777)
    WRITE(6,9000)IC,V(IC)
    IK=IC
    CH=COH(IK)
    VC1=V(IK)
    SUB=0.1
41  COHMAX=COH(IK)-SUB
    COH(IK)=COH(IK)-SUB-0.01
    DO 45 IV=1,NV
      IF(COH(IV).GE.COHMAX) IO=IV
      IF(COH(IV).GE.COHMAX) COHMAX=COH(IV)
45  CONTINUE
    VC2=V(IC)
    JE(VC2,EQ,VC1) GO TO 46
    GO TO 41
46  CONTINUE
    COH(IK)=CH
    WRITE(6,777)
    WRITE(6,9000)IO,V(IO)
    WRITE(6,8100)
    DO 50 IV=1,NV
      IF(IV.GE.NV-4) GO TO 36
      FUB=0.15
      SMX=0.0
      DO 33 I=1,5
        IK=I-1
33  SMX=SMX+COH(IV+IK)
      CAV=SMX/5.0
      IF(COH(IV).GT.(CAV-RUB).AND.COH(IV).LT.(CAV+RUB)) COH(IV)=0.0

```

```

36 CONTINUE
  WRITE(6,8000)IV,COHM(IV)
  PLTA(IT,IV)=COHM(IV)
50 CONTINUE
  IF(IT.EQ.NT) GO TO 10
  TIN1=TIN1+GT2
  TIN2=TIN2+GT2
  T(1)=T(1)+GT2
10 CONTINUE
  ORD=C.21
  YST=1.5
  CALL PLVESP(PLTA,NGI,NV,YST,ORD)
  CALL PLOTND
666 FORMAT('M=',I2,2X,'NG=',I2,2X,'NGI=',I2)
777 FORMAT(' ')
1000 FORMAT(F5.2,2F6.3,I3,2F6.2,F5.2)
1100 FORMAT(30I2)
2000 FORMAT('T1=',F5.2,2X,'T2=',F5.2,2X,'V1=',F5.2,2X,'V2=',F5.2,2X,'TI
  *MF GATE=',F6.3,2X,'TIME STEP=',F6.3,2X,'VELOSTEP=',F6.3)
3000 FORMAT(10F7.3)
4000 FORMAT((30X,6F7.3,8X))
5000 FORMAT('DIST(KM)',I3,17F7.2,/, (9X,17F7.2,/))
6000 FORMAT('KT(I)=' ,I3,19I6)
6100 FORMAT(40X,'INTERVAL T= (' ,F4.2,'-',F4.2,') SEC')
7000 FORMAT(9X,19I6,/, (11X,19I6,/))
8000 FORMAT(5X,I3,3X,F6.3)
8100 FORMAT(11X,'COHM')
9000 FORMAT(48X,'V(',I2,')=' ,F5.2)
  STOP
  END

```

C

SUBROUTINE RETAP(A,NSH)

C

DIMENSION DATON(96),A(20,3840)

INTEGER*2 LEN

1000 FORMAT(3I3)

2000 FORMAT('FILE NO. ',I3,' IS ANALYSED')

16 READ(5,1000,END=1008)NFSK,NP SK,NPEC

NF=NFSK

MFSK=80-NPEC

NPTS=NPEC*96

CALL SKIP(NFSK,NRSK,1)

DO 60 J=1,NSH

NF=NF+1

DO 61 NCH=1,6

DO 63 J=1,NREC

II=I-1

CALL READ(DATON,LEN,0,LNUM,1,&1008)

DO 64 K=1,96

64 A(NCH,II*96+K)=DATON(K)

63 CONTINUE

IF(NCH.EQ.6) GO TO 61

CALL SKIP(0,MRSK,1)

61 CONTINUE

WRITE(6,2000)NF

IF(J.EQ.NSH) GO TO 60

CALL SKIP(1,NFSK,1)

60 CONTINUE

1008 RETURN

END

SUBROUTINE SUMMAX(A,KT,KDT,M,NG,COH)

DIMENSION A(20,3840),KT(60),P(20)

N=5

PMAX=0.0

DO 1 J=1,NG

P(J)=0.0

DO 2 I=1,M

K=KT(I)

P(J)=P(J)+A(I,K)

2 CONTINUE

P(J)=ABS(P(J)**N)

IF(P(J).GT.PMAX) PMAX=P(J)

IF(J.EQ.NG) GO TO 1

DO 10 J=1,M

10 KT(I)=KT(I)+KDT

1 CONTINUE

DO 20 I=1,M

20 KT(I)=KT(I)-(NG-1)*KDT

COH=PMAX

IF(COH.LE.0.0) COH=0.01

RETURN

END

SUBROUTINE SEMBLA(A,KT,KDT,M,NG,CCH)

C

DIMENSION A(20,3840),KT(60),P(20),Q(20)

NAH=0.0

DCL=0.0

DO 1 J=1,NG

P(J)=0.0

Q(J)=0.0

DO 2 I=1,M

K=KT(I)

P(J)=P(J)+A(I,K)

Q(J)=Q(J)+A(I,K)**2

2 CCNTINUE

P(J)=P(J)**2

NAH=NAH+P(J)

DCL=DCL+Q(J)

IF(J.EQ.NG) GO TO 1

DO 10 I=1,M

10 KT(I)=KT(I)+KDT

1 CCNTINUE

DO 20 I=1,M

20 KT(I)=KT(I)-(NG-1)*KDT

SC=NAH/M*DCL

CCH=(M*SC-1)/(M-1)

IF(CCH.LE.0.0) CCH=0.01

RETURN

END

SUBROUTINE UNNCCR(A,KT,KDT,M,NG,COH)

DIMENSION A(20,3840),KT(60),P(20),Q(20)

UNC=0.0

DO 1 J=1,NG

P(J)=0.0

Q(J)=0.0

DO 2 I=1,M

K=KT(I)

P(J)=P(J)+A(I,K)

Q(J)=Q(J)+A(I,K)**2

2 CONTINUE

P(J)=P(J)**2

UNC=UNC+(P(J)-Q(J))

IF(J.EQ.NG) GO TO 1

DO 10 I=1,M

10 KT(I)=KT(I)+KDT

1 CONTINUE

DO 20 I=1,M

20 KT(I)=KT(I)-(NG-1)*KDT

COH=UNC*0.5

IF(COH.LE.0.0) COH=0.01

RETURN

END

C
C
SUBROUTINE PLVESP(PLTA,NGI,NV,YST,CFD)

DIMENSION PLTA(20,1000)

SC=5.0

DY=0.03

XO=-ORD

DO 1 I=1,NGI

CALL PLOT(XO+ORD,YST,3)

Y=YST-DY

DO 2 JJ=1,NV

Y=Y+DY

X=PLTA(I,JJ)/SC+XO+ORD

CALL PLOT(X,Y,2)

2 CONTINUE

XO=XO+ORD

1 CONTINUE

RETURN

END